Heat tracing in the variably saturated shallow subsurface

Landon James Szasz Halloran
BSc (Hons), MSc

A thesis in fulfilment of the requirements for the degree of
Doctor of Philosophy

School of Civil and Environmental Engineering
Faculty of Engineering

March 2016 · Sydney · Australia

PLEASE TYPE

THE UNIVERSITY OF NEW SOUTH WALES
Thesis/Dissertation Sheet

Surname or Family name: **Halloran**

First name: **Landon** Other name/s: **James Szasz**

Abbreviation for degree as given in the University calendar: **PhD**

School: **Civil and Environmental Engineering** Faculty: **Engineering**

Title: **Heat tracing in the variably saturated subsurface**

Abstract 350 words maximum: (PLEASE TYPE)

Temperature and soil moisture are two of the most important parameters that affect a wide variety of ecological, geochemical, and hydrological processes in the shallow subsurface. By understanding and exploiting the coupled physics of heat transport and water content, temperature can be used as a proxy for soil moisture measurement in variably saturated conditions. This dissertation develops and refines novel temperature-based hydrogeophysical methods while expanding the applicability of heat-tracing to unsaturated conditions. To this end, a comprehensive review of existing research into heat-tracing in the vadose zone is presented. Thermo-hydraulic physics of vadose zone porous media, field-based and numerical methods, thermal regime studies, and both active and passive heat tracing methods are reviewed. Several knowledge gaps and opportunities that exist in its application to unsaturated conditions are identified.

Two novel methodologies related to heat-tracing are developed. The first, a matrix method, delineates contrasting subsurface conditions and compares existing saturated zone velocity heat-tracing methods. The method is applied to both coiled fibre-optic distributed temperature sensing (FO-DTS) measurements and finite element (FE) model output. These are used to illustrate the thermal signature of common subsurface conditions as well as to assess the reciprocal relationship between sensor spacing and noise in water flux estimates. Next, a semi-analytical vadose zone heat tracing model and associated methodology, based on the full advection-conduction-dispersion equation coupled with an established empirical thermal conductivity-saturation model, are derived for the calculation of soil moisture profiles. The method exploits measurements of ambient temperature profiles in the subsurface and is shown to predict soil moisture profiles accurately under certain limits on percolation rate or saturation level.

Finally, the subsurface thermal regime of an estuarine inter-tidal zone is investigated. In this highly transient and variably saturated zone, analytical heat-tracing methods are not applicable and common electromagnetic probes can fail due to high salinity. Measured FO-DTS temperature profiles and a fully coupled thermo-hydraulic FE model are used to evaluate the relative propagation depths of tidal and diurnal signals and to quantify the importance of variably unsaturated conditions for heat transport.

"I hereby declare that this submission is my own work and to the best of my knowledge it contains no materials previously published or written by another person, or substantial proportions of material which have been accepted for the award of any other degree or diploma at UNSW or any other educational institution, except where due acknowledgement is made in the thesis. Any contribution made to the research by others, with whom I have worked at UNSW or elsewhere, is explicitly acknowledged in the thesis. I also declare that the intellectual content of this thesis is the product of my own work, except to the extent that assistance from others in the project's design and conception or in style, presentation and linguistic expression is acknowledged."

Signed,

on the date
18-Mar-2016.

COPYRIGHT STATEMENT

'I hereby grant the University of New South Wales or its agents the right to archive and to make available my thesis or dissertation in whole or part in the University libraries in all forms of media, now or here after known, subject to the provisions of the Copyright Act 1968. I retain all proprietary rights, such as patent rights. I also retain the right to use in future works (such as articles or books) all or part of this thesis or dissertation.
I also authorise University Microfilms to use the 350 word abstract of my thesis in Dissertation Abstract International (this is applicable to doctoral theses only).
I have either used no substantial portions of copyright material in my thesis or I have obtained permission to use copyright material; where permission has not been granted I have applied/will apply for a partial restriction of the digital copy of my thesis or dissertation.'

Signed . ……………………………………………

Date 26-May-2016 ……………………………………………………………………

AUTHENTICITY STATEMENT

'I certify that the Library deposit digital copy is a direct equivalent of the final officially approved version of my thesis. No emendation of content has occurred and if there are any minor variations in formatting, they are the result of the conversion to digital format.'

Signed ……………………………………………

Date 26-May-2016 ……………………………………………………………………

ORIGINALITY STATEMENT

'I hereby declare that this submission is my own work and to the best of my knowledge it contains no materials previously published or written by another person, or substantial proportions of material which have been accepted for the award of any other degree or diploma at UNSW or any other educational institution, except where due acknowledgement is made in the thesis. Any contribution made to the research by others, with whom I have worked at UNSW or elsewhere, is explicitly acknowledged in the thesis. I also declare that the intellectual content of this thesis is the product of my own work, except to the extent that assistance from others in the project's design and conception or in style, presentation and linguistic expression is acknowledged.'

Signed ……………………………………………..............

Date 26-May-2016 ……………………………………………..............

Supervisors:
Dr. Martin S. Andersen and Dr. Gabriel C. Rau

Co-supervisors:
Prof. R. Ian Acworth and Dr. Hamid Roshan

À Névée.

Que ta vie soit toujours remplie de merveilles.

ABSTRACT

Temperature and soil moisture are two of the most important parameters that affect a wide variety of ecological, geochemical, and hydrological processes in the shallow subsurface. By understanding and exploiting the coupled physics of heat transport and water content, temperature can be used as a proxy for soil moisture measurement in variably saturated conditions. This dissertation develops and refines novel temperature-based hydrogeophysical methods while expanding the applicability of heat-tracing to unsaturated conditions. To this end, a comprehensive review of existing research into heat-tracing in the vadose zone is presented. Thermo-hydraulic physics of vadose zone porous media, field-based and numerical methods, thermal regime studies, and both active and passive heat tracing methods are reviewed. Several knowledge gaps and opportunities that exist in its application to unsaturated conditions are identified.

Two novel methodologies related to heat-tracing are developed. The first, a matrix method, delineates contrasting subsurface conditions and compares existing saturated zone velocity heat-tracing methods. The method is applied to both coiled fibre-optic distributed temperature sensing (FO-DTS) measurements and finite element (FE) model output. These are used to illustrate the thermal signature of common subsurface conditions as well as to assess the reciprocal relationship between sensor spacing and noise in water flux estimates. Next, a semi-analytical vadose zone heat tracing model and associated methodology, based on the full advection-conduction-dispersion equation coupled with an established empirical thermal conductivity-saturation model, are derived for the calculation of soil moisture profiles. The method exploits measurements of ambient temperature profiles in the subsurface and is shown to predict soil moisture profiles accurately under certain limits on percolation rate or saturation level.

Finally, the subsurface thermal regime of an estuarine inter-tidal zone is

investigated. In this highly transient and variably saturated zone, analytical heat-tracing methods are not applicable and common electromagnetic probes can fail due to high salinity. Measured FO-DTS temperature profiles and a fully coupled thermo-hydraulic FE model are used to evaluate the relative propagation depths of tidal and diurnal signals and to quantify the importance of variably unsaturated conditions for heat transport.

CONTENTS

LIST OF FIGURES

LIST OF TABLES

ACKNOWLEDGEMENTS

First and foremost, I'd like to thank my supervisory team: supervisors Dr. Martin Andersen and Dr. Gabriel Rau, and co-supervisors Dr. Hamid Roshan and Prof. Ian Acworth. Martin has been very encouraging since the day of my arrival in Australia. His extensive geoscience knowledge and his open and approachable demeanour have had an overwhelmingly positive influence on me and my research. Gabriel has always given very useful and clever input and has been supportive of my ideas. His expertise, guidance, and positivity have been vital to the completion of this thesis. Hamid has provided a lot of technical know-how and his advice has had a great impact. Ian is the father of the UNSW Connected Waters Initiative Research Centre and I, among others, owe him a great deal of gratitude for his advocacy of, and passion for, groundwater research.

Other staff and students at the Water Research Lab have also provided valuable input and assistance. The technical assistance and advice of Dr. Mark Cuthbert, Evan Jensen, Dr. Richard Crane, Dr. Ander Guinea, and Dayna McGeeney, among many others, has aided me during my PhD. It has been an overwhelmingly positive experience to be part of the dynamic research environment at the WRL.

My parents, Laurel Szasz and Joe Halloran, and my sister, Afton Halloran, have been supportive as always. Their encouragement and love sent from afar are sources of inspiration and strength.

Enfin, la dernière mais non la moindre, ma conjointe (et bientôt ma femme), Marianne Laurin, a accepté de déménager à 16000 km de son Québec natal pour que je puisse poursuivre mon doctorat à l'UNSW. Ce fut une épreuve que nous avons traversé glorieusement ensemble. Elle a toujours été là pour moi et sans son amour et son soutien je n'aurais pas réussi ce coup! Cette aventure en Australie, et l'aventure d'être parents de notre belle petite Névée qui vient de commencer, me remémore que je veux passer la reste de ma vie à ses côtés.

RESEARCH OUTPUT

Peer-reviewed journal articles

- *Chapter 5 of this thesis:*
  L.J.S. Halloran, M.S. Andersen, and G.C. Rau (in preparation). "Heat transport dynamics in a tidally-driven variably saturated streambed."

- *Chapter 2 of this thesis:*
  L.J.S. Halloran, G.C. Rau & M.S. Andersen (under review). "Heat as a tracer to quantify processes and properties in the vadose zone: A review," *Earth-Science Reviews*.

- *Chapter 3 of this thesis:*
  L.J.S. Halloran, H. Roshan, G.C. Rau, M.S. Andersen, and I. Acworth (2016). "Improved spatial delineation of streambed properties and water fluxes using distributed temperature sensing," *Hydrological Processes*. doi:10.1002/hyp.10806

- *Chapter 4 of this thesis:*
  L.J.S. Halloran, H. Roshan, G.C. Rau, and M.S. Andersen (2016). "Semi-analytical model for the calculation of water saturation levels from passive temperature measurements in near-surface sediments," *Advances in Water Resources*, **89**, pp. 67-79. doi:10.1016/j.advwatres.2016.01.007

- G.C. Rau, M.O. Cuthbert, A.M. McCallum, **L.J.S. Halloran**, and M.S. Andersen (2015). "Assessing the accuracy of 1-D analytical heat tracing for estimating near-surface sediment thermal diffusivity and water flux under transient conditions," *Journal of Geophysical Research: Earth Surface* **120**(8), pp. 1551-1573. doi:10.1002/2015JF003466

Conference presentations and posters

- **L.J.S Halloran**, M.S. Andersen, G.C. Rau, H. Roshan, I. Acworth (2015). "Natural temperature variations and soil moisture content in the vadose zone," Poster at: *Australian Groundwater Conference*, Nov. 2015; Canberra, ACT, Australia. doi:10.13140/RG.2.1.4545.7363
- **L.J.S. Halloran**, H. Roshan, G.C. Rau, M.O. Cuthbert, M.S. Andersen, I. Acworth (2015). "Soil moisture content estimation from passive temperature measurements," Poster at: *EGU General Assembly*, April 2015; Vienna, Austria.
- **L.J.S. Halloran**, H. Roshan, M.S. Andersen, R.I. Acworth (2013). "Passive surface water-groundwater interaction investigation with coiled distributed temperature sensing: a new analytical approach," Presentation at: *American Geophysical Union Fall Meeting*, 9-13 Dec. 2013; San Francisco, CA, USA. doi:10.13140/RG.2.1.4699.4401
- **L.J.S. Halloran**, H. Roshan, G. Rau, A. McCallum, M.S. Andersen, I. Acworth (2013). "Effects of floods and groundwater pumping on hyporheic flows measured by coiled fibre-optic distributed temperature sensing," Presentation at: *40th International Association of Hydrogeologists Congress*, 16-20 Sept. 2013; Perth, WA, Australia.
- M.S. Andersen, H. Rutlidge, S. Eberhard, **L. Halloran**, B. Nielsen, G. Rau, C. Li, A. Salma, J. Chen, C. Moll, C. Murphy, M. Cuthbert, A. Baker (2015). "Mapping groundwater discharge and water chemistry in a perennial stream in northern New South Wales," Presentation at: *Australian Groundwater Conference*, Nov. 2015; Canberra, ACT, Australia.
- H. Rutlidge, M.S. Andersen, S. Eberhard, **L. Halloran**, B. Nielsen, G. Rau, C. Li, A. Salma, J. Chen, C. Moll, C. Murphy, M. Cuthbert, A. Baker (2015). "Organic matter content and redox chemistry at upwelling and downwelling hyporheic zones," Presentation at: *Australian Groundwater Conference*, Nov. 2015; Canberra, ACT, Australia.
- H. Rutlidge, M. Andersen, G. Rau, M. Cuthbert, P. Graham, N. Unland, H. Hofmann, B. Gilfeddder, A. Atkinson, I. Cartwright, **L. Halloran**, A.

Baker (2014). "Use of Fluorescence in Conjunction with Radon Activity to Monitor Groundwater-Surface Water Interactions in a System Under Stress," Presentation at: *Goldschmidt California*, June 2014; Sacramento, CA, USA.

- H. Roshan, M. Young, M.S. Andersen, **L. Halloran**, A.M. McCallum, G.C. Rau, R.I. Acworth (2013). "Evaluating thermal response of Fiber Optic Distributed Temperature Sensing," Poster presented at: *40th International Association of Hydrogeologists Congress*, 16-20 Sept. 2013; Perth, WA, Australia.

ACRONYMS

AHD	Australian height datum
AHFO	active heating fibre-optics
DHR	dynamic harmonic regression
DTFT	discrete time Fourier transform
DTS	(fibre-optic) distributed temperature sensing
EC	electrical conductivity
FE	finite element
FO	fibre-optic
FO-DTS	fibre-optic distributed temperature sensing
GPS	global positioning satellite
GW	groundwater
GW-SW	groundwater–surface water
NSW	New South Wales, Australia
OM	optical multi-mode
PVC	polyvinyl chloride
RMS	root mean squared
RPM	rotations per minute
STP	standard temperature and pressure
SW	surface water
SWRC	soil water retention curve
TDR	time-domain reflectometry
TDT	time-domain transmissometry
UZ	unsaturated zone
VZ	vadose zone

Tab. 0.1: Acronyms used in this thesis

1. INTRODUCTION

1.1 Overview and motivation

This doctoral thesis advances knowledge in two connected themes: heat-as-a-tracer and the variably saturated subsurface. These two topics have been and continue to be the focus of a wide range of investigations by researchers in the areas of hydrogeology and hydrogeophysics. "Heat-as-a-tracer" refers to the use of temperature as a proxy for gaining insight into, or measuring, a quantity or physical process in the subsurface. Temperature measurements, generally recorded as multiple point time-series, are combined with an understanding of thermal and hydraulic physics in order to estimate quantities such as groundwater flow rates (Chapter 3) or soil moisture content (Chapter 4). The term "variably saturated subsurface" refers to the shallow subsurface zone where the pore space may not be completely filled with water. This is also known as the vadose zone or unsaturated zone, although "variably saturated" makes explicit that, here, moisture content may be temporally and spatially variable, and includes full saturation as a special case.

Temperature and water saturation (or, equivalently, soil moisture content) both have strong effects on many shallow subsurface processes of biological, geochemical and hydrological interest. In addition to transport phenomena, these include microbial activity (e.g., Russell et al., 2012), soil respiration (e.g., Lloyd and Taylor, 1994), chemical volatilisation (e.g., Cohen and Ryan, 1989), and agricultural production (e.g., Ramakrishna et al., 2006). Soil moisture content in the vadose zone strongly affects phenomena such as nitrification and ecosystem diversity (Vereecken et al., 2008) and thus there is strong interest in its quantification over time and depth. This motivation is further discussed in Chapter 2. Furthermore, the physics that govern thermal and hydraulic processes in variably saturated porous media exhibit a degree of interdependence that can be studied to evaluate the thermal regime of a hydrogeologic system or, if well constrained, exploited to perform indirect measurements of physical processes or quantities.

As soil moisture is a variable that is critical for answering many ecological, agricultural, and other scientific and management-related questions, a wide range of research on soil moisture measurement techniques has been undertaken (e.g., Stafford, 1988, Robinson et al., 2008). These range in application from field scale (e.g., neutron probes) to global (e.g., satellite-based measurements). The method employed must be suited to the temporal and spatial scale of the processes investigated.

Heat-tracing is a research theme that has seen widespread interest since the early 2000's (see the reviews of Anderson, 2005, Constantz, 2008, Rau et al., 2014). The majority of research has focused on surface water-groundwater interactions in the saturated zone and the development of new methods to estimate vertical exchange fluxes and thermal diffusivity. In general, heat-tracing methods use temperature measurements over space and time, as well as some material properties, as inputs. Groundwater percolation and, in the case of unsaturated conditions, variable soil moisture content affect conductive and advective heat transport. Thus, temperature records can be used to understand and quantify hydraulic processes in the subsurface.

1.2 Structure of this thesis

Each of the main chapters (Chapters 2–5) in this thesis are adapted from manuscripts (a full list of research output is available on page xxix). These chapters are currently in preparation for submission (Chapter 5), undergoing peer-review (Chapter 2), or have been published in leading peer-reviewed water resources journals (Chapters 3 and 4) by the author of this thesis. Publication details are also noted at the beginning of each chapter. The body of work comprised by this thesis combines extensive consideration of previous work (Chapter 2), lab techniques (Chapter 5), field measurements (Chapters 3–5), numerical models (Chapters 3–5), and analytical model development (Chapter 4).

To introduce and describe advances and knowledge gaps on the topic, a comprehensive review of previous research pertaining to heat-tracing in the variably saturated subsurface is presented in Chapter 2. The relevant physics governing thermal and hydraulic phenomena in variably saturated porous media are detailed. As the water saturation dependence of thermal conductivity is of particular importance for heat transport, several empirical models are discussed. The limited number of previous studies on unsaturated zone thermal regimes are examined and the opportunity for further research is noted. Research groups have developed temperature-based models and methods for estimating soil moisture. While a plethora of research has been carried out on method development for saturated zone heat and water fluxes (e.g., Hatch et al., 2006, McCallum et al., 2012, Vandersteen et al., 2015), research into heat-tracing for soil moisture estimation is still at a relatively preliminary stage. Both active-heating and passive methods are reviewed in Section 2.3. Active heating methods frequently utilise fibre-optic distributed temperature sensing (FO-DTS) and can, to an extent, be considered as an extension of the heat pulse probes that are used extensively in soil research. Passive methods such as that developed here in Chapter 4, rely on natural temperature variations induced by diurnal and seasonal climate cycles. Practical considerations regarding temperature probes, FO-DTS, and relevant numerical modelling packages are explored in depth. Finally, prospects for future research are discussed, and the need for effective heat-tracing methods in the unsaturated zone and for further thermal regime studies with variable saturation are noted.

In Chapter 3, a methodology for the interpretation of subsurface temperature records with fine vertical resolution, such as those recorded by coiled FO-DTS installations, is developed and tested. This methodology makes use of pair-by-pair calculations from temperature records to produce a detailed matrix that maximises the spatial information. This matrix provides a visual representation of depth-dependent thermal properties and water fluxes in a shallow subsurface system and can be employed to evaluate different heat-tracing methods and sensor spacing effects, as well as to identify the presence of lateral flow or layers with contrasting thermal properties. The method is investigated by applying it to a detailed coiled FO-DTS dataset measured during a field application and also to the output of numerical models. The field dataset is used to compare three common heat-tracing methods: the amplitude- and phase- based methods of Hatch et al. (2006) and the method of McCallum et al. (2012). Furthermore, the trade-off between vertical resolution and noise effects in field installations of vertical temperature probe arrays for heat-tracing is explored. Numerical data from fully coupled thermo-hydraulic finite element models are used to evaluate the signature imparted to the matrix visualisation by three common subsurface conditions: contrasting layers, lateral flow, and unsaturated conditions. The characteristic effects of contrasting layers and lateral flow on the matrices are noted. Finally, the effect of the presence of unsaturated conditions on established heat-tracing methods is investigated and the need for specialised unsaturated zone heat-tracing methods is demonstrated.

Having observed the potential for heat-tracing in the unsaturated zone, a novel unsaturated zone heat-tracing model is developed in Chapter 4. Two forms of the model are derived through the synthesis of three equations: 1) the full advection-convection-dispersion equation, 2) the empirical thermal conductivity model of Côté and Konrad (2005), and 3) a temporally sinusoidal temperature equation. The developed model takes into account vertical water flux and non-uniform thermal conductivity in the unsaturated zone, two important physical aspects that prior studies have largely avoided. A physically relevant subset of the parameter space of the model is visualised and the model is tested on output from numerical models similar to those discussed in Chapter 3. Multiple implementation variations are tested in order to determine the optimal form of the semi-analytical model. A sequential implementation, wherein a reference saturation value is updated at each vertical step, of one form of the model is found to accurately predict a saturation-depth profile to within 2% error. This methodology is then combined with a velocity estimation method to test the limits of the model in transient conditions. Percolation rates up to 20 cm/day are tested and accurate calculation of saturation profiles is confirmed for percolation rates up to $\sim$10 cm/day and for lower saturation levels.

The developed heat-tracing method of Chapter 4, like all passive methods that based their calculations on amplitude and phase, utilises the dominant diurnal temperature oscillation. This is a limitation in highly transient systems where non-stationary components dominate subsurface temperature behaviour (Rau et al., 2015). In Chapter 5, one such variably saturated system is considered in detail. An investigation of the thermal regime of a tidally-affected and variably saturated sandy streambed (Korogoro Creek in Hat Head, NSW, Australia) is carried out using multiple field measurements including coiled FO-DTS temperature profiles installed in a transect. Through frequency-domain analysis of this data, the relative penetration depths of diurnal and tidal thermal signals are constrained. The thermal and hydraulic properties of the subsurface are measured using a variety of techniques including evaluation of the soil water retention curve using a centrifuge method (Šimunek and Nimmo, 2005). Passive heat-tracing methods fail in highly transient systems and electromagnetic probes have limitations in high salinity conditions. Thus, a finite element modelling approach is used to evaluate soil moisture and temperature throughout the domain of interest by coupling Richards' equation (Richards, 1931) for flow in variably saturated conditions with porous media thermal physics. The modelled saturation is then used to quantify the thermal regime by refining heat balance calculations. This approach demonstrates that when unsaturated conditions are present, even intermittently, heat flux calculations, as well as any temperature or moisture-dependent ecological or geochemical applications, need to be adjusted appropriately.

Through considered review of previous research, development and testing of new approaches, and analysis of environmental data, this thesis advances knowledge of the coupled nature of heat and water saturation in the earth's shallow subsurface. By providing tools and knowledge to make full use of heat-as-a-tracer in the variably saturated subsurface, the methods and investigations detailed in this thesis will form the foundation for a range of future research and applications.

2. REVIEW OF HEAT-TRACING IN VARIABLY SATURATED CONDITIONS

This chapter is currently under review for publication as a journal article:
L.J.S. Halloran, G.C. Rau & M.S. Andersen (under review). "Heat as a tracer to quantify processes and properties in the vadose zone: A review," *Earth-Science Reviews*.

Abstract

Soil moisture and temperature are arguably some of the most important controls for a wide variety of geochemical and ecological processes in the vadose zone (VZ). Soil moisture is highly variable both spatially and temporally, and methods to measure it on various scales have been the subject of much activity. Recently, geoscientists have been increasingly interested in measuring temperature as a proxy for hydraulic quantities and parameters, including soil moisture. Here, we discuss the motivation, primary concepts, equipment, and fundamental thermal and hydraulic models related to heat and water transport in variably saturated porous media. A large variety of methods for heat tracing including both passive and active-heating methodologies are detailed. Heat tracing methods offer the capacity to measure soil moisture on a scale from $\sim$1 cm up to several km using temperature, a parameter whose measurement in VZ studies is often required anyway due to its effect on many subsurface processes. Furthermore, heat-tracing methods are not affected by high salinity pore water that can limit electromagnetic soil moisture methods. We also review coupled thermo-hydro VZ modelling software and VZ thermal regime studies and identify knowledge gaps. With the intention to serve as an introduction to VZ heat-tracing, this review consolidates recent advances and outlines potential themes for future research.

2.1 Introduction

Moisture content and temperature act as strong controls on a wide variety of ecological and geochemical processes. Consequently, both are of great interest to researchers investigating the vadose zone (also known as the unsaturated zone). Although moisture in the vadose zone (VZ) represents only $\sim$0.05% of the global freshwater balance (Dingman, 2002), variable saturation occurs in $\sim$87% of the global land cover (Latham et al., 2014). Temporal and spatial variations of soil moisture have pronounced effects on ecology. Anthropogenic and climatic effects on hydrological conditions can affect soil moisture distributions and consequently natural ecosystems or crops. Similarly, many chemical and physical processes are dependent on temperature, often non-linearly. Because accurate knowledge of soil moisture and, in many cases, temperature is crucial for studies and applications in agronomy (e.g., Brandt, 1992, Bolten et al., 2010), geochemistry (e.g., Rousseau et al., 2004, Robinson et al., 2009), and hydrogeology (e.g., Vereecken et al., 2010, Stewart et al., 2013), the thermodynamics of the vadose zone and, specifically, the use of temperature to quantify moisture content is of interest to a broad and interdisciplinary audience.

The importance of soil moisture and its various measurement methods have been discussed in depth by many (e.g., Stafford, 1988, Blöschl and Sivapalan, 1995, Mahmood, 1996, Western et al., 2002, Vereecken et al., 2008, Robinson et al., 2008). Vereecken et al. (2008) presented a review of the value of soil moisture measurements on field and catchment scales, while Robinson et al. (2008) reviewed watershed-scale (defined as 0.1–80 km^2) soil moisture measurement methods. Different research and management questions require soil moisture information on a wide variety of temporal and spatial scales, ranging from minute-duration and centimetre scale to a yearly, 10,000 km^2 scale. Because no single method is suitable for all applications, it is important to choose an appropriate approach.

The most direct and conceptually simple of the many methods for soil moisture measurement is the thermogravimetric measurement, wherein a sediment sample is weighed before and after oven drying to determine the weight that is lost due to evaporation. However, this necessitates disturbance of the sediments and delivers only a point-in-space and point-in-time measurement.

All other methods involve some form of indirect measurement of water content. For instance, the relatively large neutron scattering cross-section of hydrogen atoms in water molecules can be exploited to infer moisture content. Invasive mobile neutron probes containing a radiation source and detector have been widely used to measure soil moisture (Bell, 1987, Chanasyk and Naeth, 1996), although their usage is generally subject to regulation. More recently, neutrons originating from collisions with cosmic rays have been used to measure soil moisture integrated on the $\sim$100 m scale (Zreda et al., 2008), most notably in the COSMOS network (Zreda et al., 2012, Rosolem et al., 2013, Franz et al., 2013). Ground penetrating radar (Daniels et al., 1988, Huisman et al., 2003, Lunt et al., 2005) represents another set of methodologies for measuring soil moisture on the $>$1 m scale. The method exploits the soil moisture dependence of dielectric permittivity, which affects the phase and amplitude of reflected and transmitted electromagnetic waves. Time-domain reflectometry (TDR) and transmissometry (TDT) probes (Robinson et al., 2003, Vereecken et al., 2008) use the reflected or transmitted signals, which depend on soil dielectric properties, from electromagnetic pulses to infer soil moisture and are useful for small-scale measurements. Ground-reflected global positioning satellite (GPS) signals have also been used as soil moisture proxies for the top $\sim$5 cm of the subsurface (e.g., Larson et al., 2008, Chew et al., 2014). Finally, the *Soil Moisture and Ocean Salinity* (SMOS) (Kerr et al., 2001) and *Soil Moisture Active Passive* (SMAP) (Entekhabi et al., 2010) missions have mapped soil moisture globally to $\sim$35 km and $\sim$10 km resolution, respectively, using interferometry and taking advantage of the moisture-dependence of microwave emissivity. All methods, with exception of direct weighing of samples, capitalise upon the quantifiable effects that moisture content has on the transmission of atomic particles electromagnetic waves or, in the case of this review, thermal energy.

All methods have caveats and limitations in their applicability. Electromagnetic methods, for example, are effected by salinity, which can limit applications in coastal zones or dryland regions of high salinity, while neutron probes require on-board radioactive material. On the other hand, temperature offers the advantage of being an extremely robust parameter that is easily measured with high precision and resolution. Furthermore, temperature measurements are often required for other analyses. The thermal methods discussed in this review extend soil moisture measurement capabilities to smaller spatial and temporal scales.

Since the early publication of foundational studies (e.g., Constantz et al., 2003a), heat-tracing has seen rapid uptake by researchers interested in surface water-groundwater (SW-GW) exchange and other hydrogeological processes. Reviews on heat-as-a-tracer for groundwater flow and SW-GW exchange (Anderson, 2005, Constantz, 2008, Rau et al., 2014), as well as a review of deep subsurface flow geothermal heat-tracing (Saar, 2011), have provided in-depth summaries of progress made in heat-tracing methods and applications, albeit only for saturated conditions.

Vadose zone heat-tracing is a rapidly accelerating domain of research this chapter seeks to review. Prior to 2006, only 7 articles indexed in the Scopus database containing "vadose" or "unsaturated" and "heat-tracing" or "heat-as-a-tracer" were published. However, from 2006 to 2010, 16 articles were published and from 2011 to 2015, 104 articles were published, which indicates that VZ heat-tracing is a rapidly developing domain of research within hydrogeology and hydrogeophysics. Firstly, details of the relevant physics are presented. Variable saturation introduces another level of non-linear complexity into the equations that govern heat transport in porous media. While some of the physics describing heat and moisture transport can be described analytically, other parameters, most notably thermal conductivity, require empirical models. Secondly, we present a comprehensive review of methods applicable to heat-tracing in the VZ. A discussion of both active heating and passive methods is undertaken. Thirdly, we discuss thermal regime studies that have been carried out in the variably saturated subsurface. Fourthly, a brief overview of the temperature measurement methods used in heat-tracing is offered, much of which is equally applicable to the saturated zone with simplifications. We also review numerical studies of heat transport in the variably saturated subsurface and associated software packages. Finally, the current knowledge gaps and areas for future research in VZ heat-tracing are outlined.

2.2 *Water and heat transport in the vadose zone*

Much research has been dedicated to the mechanics and deformation of porous materials and their coupling with thermal and fluid flow processes (e.g.,

Symbol	Definition	units
α	Van Genuchten constitutive relation constant	m^{-1}
θ	volumetric water content	–
θ_r	residual liquid volume fraction	–
ϵ	porosity	–
ρ	density	$kg\ m^{-3}$
ϕ	phase of temperature oscillation	radians
ω	angular velocity	radians s^{-1}
A	amplitude of temperature oscillation	K
c	specific heat capacity	$J\ kg^{-1}\ K^{-1}$
C_v	volumetric heat capacity	$J\ m^{-3}\ K^{-1}$
C_m	specific moisture capacity	m^{-1}
D	thermal diffusivity	$m^2 s^{-1}$
H_p	pressure head	m
K	hydraulic conductivity	$m\ s^{-1}$
K_r	relative permeability	–
S_e	Effective saturation	–
T	temperature	°C or K
k	thermal conductivity	$W\ m^{-1}\ K^{-1}$
k_r	normalized thermal conductivity	–
l	Van Genuchten constitutive relation constant	–
m	Van Genuchten constitutive relation constant	–
Q_{source}	heat source	$W\ m^{-3}$
t	time	s
$\vec{v}$	fluid velocity	$m\ s^{-1}$
$\vec{x}$	spatial vector	m
z	vertical coordinate	m
$_w$	water	*Subscript*
$_a$	air	*Subscript*
$_e$	effective, total	*Subscript*
$_{dry}$	dry sediment	*Subscript*
$_{sat}$	saturated sediment	*Subscript*

Tab. 2.1: Mathematical symbol definitions. Throughout, subscripts are used to differentiate between different domains, materials, etc.

Schrefler, 2002, Stephansson et al., 2004). In the context of heat-tracing in unsaturated conditions, we consider only the physics of water flow and heat transport. The mathematical symbols used throughout this section are listed in Table 2.1 for ease of reference.

2.2.1 Water flow in unsaturated conditions

The fundamentals of water behaviour in the vadose zone have been well documented by many (e.g., Bear, 1979, Stephens, 1995, Domenico and Schwartz, 1998, Tindall et al., 1999). For certain aspects, analytical expressions can describe idealised behaviour; for others, such as empirical expressions have been developed. Here, we present equations of particular importance for heat-tracing in variably saturated conditions. *Richards'* equation (Richards, 1931), presented here in its mixed form (Celia et al., 1990), describes water transport in variably saturated conditions:

$$\frac{\partial \theta}{\partial t} - \nabla \cdot (K_e(H_p)\nabla H_p) - \frac{\partial K_e}{\partial z} = 0 \tag{2.1}$$

where θ is volumetric water content, t is time, K_e is effective hydraulic conductivity, H_p is hydraulic pressure head, and z is the vertical coordinate. Equivalently, the original 1-D formulation is:

$$\frac{\partial \theta}{\partial t} = \frac{\partial}{\partial z}\left[K_e(\theta)\left(\frac{\partial H_p}{\partial z} + 1\right)\right] \tag{2.2}$$

This equation is highly non-linear due to the dependence of hydraulic properties on saturation level and pressure. Various numerical and analytical methods for evaluating *Richards'* equation have been presented (e.g., Kirkland et al., 1992, Barry et al., 1993, Tocci et al., 1997, Paniconi et al., 2003, see also Section 2.5.3).

The soil water retention curve (SWRC) refers to the moisture content present in a given soil as a function of pF scale (Schofield, 1935), matric pressure, or depth above the water table (all equivalent). Several expressions for saturation level as a function of pressure head, $S_e(H_p)$, based on empirical measurements exist (e.g., Brooks and Corey, 1964, van Genuchten, 1980, Kosugi, 1996), although the most commonly used are the *van Genuchten* equations. The set of equations presented by van Genuchten (1980) – in what is likely the most-cited paper in vadose zone research – for the analytical definition of hydraulic properties at negative pressures $H_p < 0$ (i.e., unsaturated conditions) are (Figure 2.1):

$$\theta = \theta_r + S_e(\epsilon - \theta_r) \tag{2.3}$$

$$S_e = \frac{1}{(1 + |\alpha H_p|^{\frac{1}{1-m}})^m} \tag{2.4}$$

$$C_m = \frac{\alpha m}{1-m}(\epsilon - \theta_r)S_e{}^{\frac{1}{m}}(1 - S_e{}^{\frac{1}{m}})^m \tag{2.5}$$

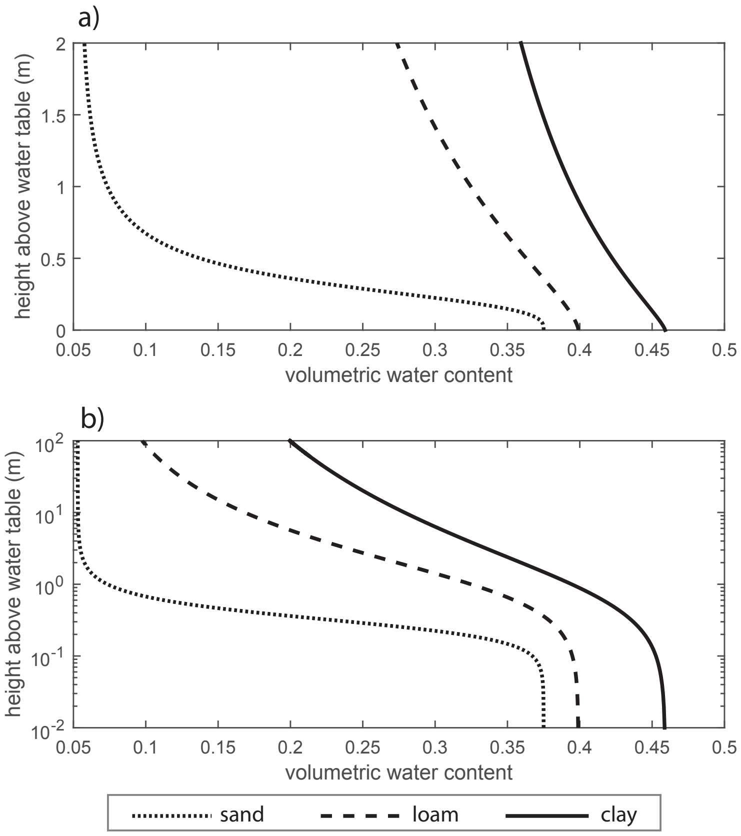

Fig. 2.1: Example of the soil water retention curve (Equations 2.3 and 2.4) of van Genuchten (1980) plotted to *a)* 2 m above the water table and to *b)* 100 m above the water table (logarithmic scale). Values for the van Genuchten parameters are averages from Schaap (2002): clay $\alpha = 1.496$ m^{-1}, $m = 0.202$, $\epsilon = 0.459$, $\theta_r = 0.098$; loam $\alpha = 1.112$ m^{-1}, $m = 0.321$, $\epsilon = 0.399$, $\theta_r = 0.061$; and sand $\alpha = 3.524$ m^{-1}, $m = 0.685$, $\epsilon = 0.375$, $\theta_r = 0.053$.

$$K_e = K_{sat} {S_e}^l \left[1 - (1 - {S_e}^{\frac{1}{m}})^m \right]^2 \tag{2.6}$$

Here, θ_r is the residual water volume fraction; ϵ, porosity; α, m, and l are *van Genuchten* constants; C_m, specific moisture capacity; and K_{sat}, saturated hydraulic conductivity. Where $H_p \geq 0$, it is assumed that $\theta = \epsilon$, $S_e = 1$, $C_m = 0$, and $K_r = 1$ and these expressions reduce to the fully saturated *Darcy* equation (Darcy, 1858).

The *van Genuchten* constitutive relation constants α, m, and l are material-dependent (Table 2.2), although the choice of the constraint $l = 0.5$ is often

Soil type	ϵ	θ_r	α (m^{-1})	m
Sand	0.375 ± 0.055	0.053 ± 0.029	$3.52^{+2.74}_{-1.54}$	$0.685^{+0.107}_{-0.162}$
Loam	0.399 ± 0.098	0.061 ± 0.073	$1.11^{+4.86}_{-0.90}$	$0.321^{+0.176}_{-0.237}$
Clay	0.459 ± 0.079	0.098 ± 0.107	$1.50^{+5.67}_{-1.18}$	$0.202^{+0.119}_{-0.140}$

Tab. 2.2: Average values of van Genuchten SWRC parameters for selected classes of soils in the ROSETTA database (Schaap et al., 2001, Schaap, 2002). Uncertainty ranges indicate one standard deviation.

made when basing analysis on data that does not include $K_e(S_e)$ measurements (Mualem, 1976, Schaap and van Genuchten, 2006). Many methods for estimating the values of these parameters exist, including pedotransfer functions based on the composition of the soil or by direct measurement of the SWRC by one of many methods (Vereecken et al., 2010). Measurements of the SWRC can be carried out with various methods: Tempe cell (e.g., Shouse et al., 1995, Leij et al., 1996), pressure cell (e.g., Wang and Benson, 2004, Nahlawi et al., 2007), or centrifuge (e.g., Khanzode et al., 2002, Šimunek and Nimmo, 2005, Han et al., 2010). Different sets of van Genuchten parameters may be required where hysteresis (i.e., a difference between the wetting and drying SWRC) is observed. The magnitude of hysteretic effects are dependent on the interfacial area between individual grains and thus hysteresis may need to be considered for certain classes of soils such as clay-rich sediments (Beliaev and Hassanizadeh, 2001).

2.2.2 *Heat transport in unsaturated porous media*

Heat transfer in the VZ occurs by two primary modes: advection and conduction. Advection refers to the transfer of thermal energy by mass exchange, namely, the movement of water in any fluid phase. Conduction or diffusion is the direct transfer of thermal energy on the nanoscopic scale by the collision of particles or phonons. Radiative heat transfer, while being a possible source of energy at the surface boundary, does not play a significant role in heat transfer in the subsurface. The propagation of thermal energy in porous media can be described by the advection-conduction-diffusion heat equation (Kaviany, 1995, Nield and Bejan, 2013), also known as the convection-diffusion or full heat transport equation:

$$C_{v,e}(t,\vec{x})\frac{\partial T(t,\vec{x})}{\partial t} + C_{v,w}(t,\vec{x})\vec{v}\cdot\nabla T(t,\vec{x}) = \nabla\cdot[k_e(t,\vec{x})\nabla T(t,\vec{x})] + Q_{\text{source}} \quad (2.7)$$

where $C_{v,e}$ is effective volumetric heat capacity; $C_{v,w}$, volumetric heat capacity of water; T, temperature; $\vec{x}$, spatial vector; $\vec{v}$, water velocity; k_e, effective thermal conductivity; and Q_{source}, rate of heat from a source. Simplified versions of this equation with the assumptions $\vec{v} = 0$ (zero advection) and $\nabla k_e = 0$ (uniform thermal conductivity) are often used in heat-tracing in the vadose zone (e.g., Béhaegel et al., 2007, Steele-Dunne et al., 2010, see Section 2.3.1), resulting in:

$$\frac{\partial T(t,\vec{x})}{\partial t} = \frac{k_e}{C_{v,e}}\nabla^2 T(t,\vec{x}) = D_e\nabla^2 T(t,\vec{x}) \quad (2.8)$$

Effective thermal diffusivity, D_e, is the ratio of thermal conductivity to volumetric heat capacity and is dependent on moisture content, θ or, equivalently, water saturation, S_e:

$$D_e(S_e) = \frac{k_e(S_e)}{C_{v,e}(S_e)} \quad (2.9)$$

An important aspect in VZ heat-tracing is the lack of a single-valued $S_e(D_e)$ function (Figure 2.2), which eliminates the possibility for simple one-to-one $D_e \to S_e$ mapping.

2.2.3 *Thermal properties of variably saturated porous media*

In heat-tracing applications, thermal properties must either be known or jointly evaluated (Duque et al., 2015). As outlined in Section 2.2.2, the principles of thermodynamics in the VZ depend greatly on saturation-dependent thermal properties. Effective volumetric heat capacity is a volume-weighted sum of the heat capacities of the components present, namely water, sediment, and air (Woodside and Messmer, 1961):

$$C_{v,e} = (1-\epsilon)C_{dry} + \epsilon S_{e,0}C_{v,w} + \epsilon(1-S_e)C_{v,a} \quad (2.10)$$

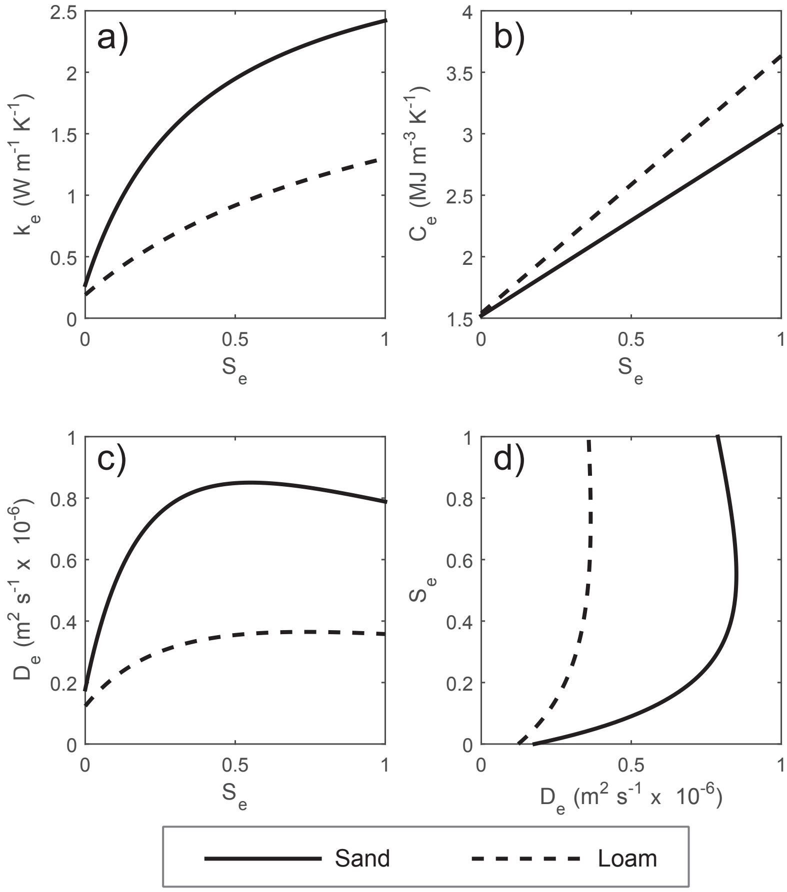

Fig. 2.2: Representative saturation dependence of a) thermal conductivity, b) volumetric heat capacity, and c) thermal diffusivity, as well as d) the multivalued inverse function $S_e(D_e)$. Thermal conductivity model and values from Côté and Konrad (2005) and heat capacity values from Ghuman and Lal (1985): sand $k_{dry} = 0.27$ W K^{-1} m^{-1}, $k_{sat} = 2.42$ W K^{-1} m^{-1}, $\epsilon = 0.37$, $C_{dry} = 1.52$ MJ m^{-3} K^{-1}; and loam $k_{dry} = 0.19$ W K^{-1} m^{-1}, $k_{sat} = 1.30$ W K^{-1} m^{-1}, $\epsilon = 0.50$, $C_{dry} = 1.54$ MJ m^{-3} K^{-1}.

where C_{dry} is the volumetric heat capacity of the dry sediment and $C_{v,a}$ is the volumetric heat capacity of air. Equivalently, in terms of densities and specific heat capacities, the equation is:

$$C_{v,e} = (1 - \epsilon)\rho_s c_s + \epsilon S_e \rho_w c_w + \epsilon(1 - S_{e,0})\rho_a c_a \tag{2.11}$$

where ρ_s, ρ_w, and ρ_a are the densities of the sediment, water, and air, respectively, and c_s, c_w, and c_a are the specific heat capacities of the aforementioned components. In practice, air is generally not considered due to its very small volumetric heat capacity (∼0.03% that of water at STP) compared with the other components and the precision to which C_{dry}, in particular, can be known. This results in:

$$C_{v,e} = (1 - \epsilon)C_{v,s} + \epsilon S_e C_{v,w} \tag{2.12}$$

While heat capacity has a linear dependence on effective saturation, thermal conductivity is notoriously non-linear and material-dependent. At low saturation level, water is adsorbed to the individual grains of the sediment and with increasing water content, bridges between the individual particles start to form until all voids are filled at full saturation (Dong et al., 2015c). Many models have been proposed for the macroscopic relationship between thermal conductivity and water saturation. Summaries of published measurements and models of the dependence of thermal conductivity on saturation level, $k_e(S_e)$, or, equivalently, volumetric water content, $k_e(\theta)$, have been presented in detail by Ochsner et al. (2001) and Dong et al. (2015c). A selection of models relevant to research that has been undertaken on VZ heat-tracing is presented here.

A general form for empirical models of thermal conductivity as a function of water content or effective saturation using the *Kersten* number (Kersten, 1949), k_r, also known as normalised thermal conductivity, is:

$$k_e = k_{dry} + (k_{sat} - k_{dry})k_r \tag{2.13}$$

where k_{sat} and k_{dry} are the thermal conductivities of the sediment when saturated and dry, respectively. Building on successes of early work by Kersten (1949) and Woodside and Messmer (1961), Johansen (1975) established a widely-used empirical model for unsaturated soils:

$$k_r = \beta_J \log(S_e) + 1 \tag{2.14}$$

where the equation is valid at $S_e > 0.05$ with $\beta_J = 0.7$ for coarse-grain soils and at $S_e > 0.1$ with $\beta_J = 1$ for fine-grain soils. Furthermore, Johansen (1975) proposed a geometric mean to estimate k_{sat} (see summary in Lu et al., 2007) and an empirical relation to estimate k_{dry}:

$$k_{dry} = \frac{0.135\rho_{dry} + 64.7\,\text{kg m}^{-3}}{2700\,\text{kg m}^{-3} - 0.947\rho_{dry}} \quad \text{W m}^{-1}\text{K}^{-1} \tag{2.15}$$

where ρ_{dry} is the bulk density of the dried material. As Equation 2.14 offers particularly poor agreement with measurements at low levels of saturation, the model of Chung and Horton (1987) was introduced to offer a simple empirical formulation valid for the entire saturation range:

$$k_e = b_{C1} + b_{C2}\theta + b_{C3}\theta^{\frac{1}{2}} \tag{2.16}$$

where b_{C1}, b_{C2}, and b_{C3} are regression parameters. Values of these parameters for clay, loam and sand soil textural classes were presented in the study.

Côté and Konrad (2005), noting that Farouki (1981) had found the Johansen (1975) model to give the best prediction of k_e in dry and saturated fine soils and sands, sought to improve upon the model using a similar framework and restricted k_r at the $S_e = 0$ and $S_e = 1$ bounds. Although they considered both frozen and unfrozen soils, only unfrozen soil thermal conductivity is of significant interest in the context of heat-tracing. The proposed relation is (Côté and Konrad, 2005):

$$k_r = \frac{\kappa_C S_e}{1 + (\kappa_C - 1)S_e} \tag{2.17}$$

where $\kappa_C = 3.55$ for medium and fine sands and $\kappa_C = 1.9$ for silty soils, clayey soils, silts and clays. A geometric mean to calculate k_{sat} based on the individual mineral components in the sediment was also set forth. Following Côté and Konrad (2005), Lu et al. (2007) developed a model with a simpler empirical formulation for the calculation of k_{sat} and successfully tested it against previously published data (Kersten, 1949, Johansen, 1975, Farouki, 1982) to determine parameters for soil classes. Their model for normalised thermal conductivity is:

$$k_r = \exp\left[\alpha_L(1 - S_e^{\alpha_L - 1.33})\right] \tag{2.18}$$

where $\alpha_L = 0.96$ for coarse-textured soils and $\alpha_L = 0.27$ for fine textured soils.

They also proposed a simple linear model for k_{dry} based only on porosity:

$$k_{dry} = -a_L \epsilon + b_L \tag{2.19}$$

where $a_L = 0.56$ and $b_L = 0.51$. They found good agreement with new $k_e(\theta)$ measurements of four soils. Barry-Macaulay et al. (2015) compared the Lu et al. (2007) model with the models of Côté and Konrad (2005) and Balland and Arp (2005), showing that, in general, model performance can be improved by fitting empirical parameters to sample measurements.

There is significant interest in the $k_e(S_e)$ relationship of sandy sediments, which have been observed to exhibit low hysteresis when subjected to wetting-drying cycles (Smits et al., 2010). Chen (2008) provided new thermal conductivity measurements of nearly pure quartz sand samples with different levels of compaction, noting the power function relationship between k_e and S_e. The study proposed a new empirical model for the dependence of thermal conductivity on porosity and water content in sands:

$$k_e = 7.5^{1-\epsilon} 0.61^{\epsilon} \left[0.9978 \cdot S_e + 0.0022 \right]^{0.87\epsilon} \tag{2.20}$$

Improved prediction of $k_e(S_e)$ in sands was observed when compared with the models of Johansen (1975) and Donazzi et al. (1979).

All models can be better constrained with direct measurements of the thermal properties when saturated and fully unsaturated. Measurement equipment is available to make direct measurements of C_e, k_e and D_e at any saturation level. The ability to measure k_{sat} and k_{dry}, in particular, undoubtedly improves unsaturated zone heat-tracing studies and renders the many proposed methods to estimate these values redundant. Probes exploiting the line heat source concept (Wechsler, 1992) such as the *KD2 Pro* from *Decagon Devices* or the *TP08* from *Hukseflux* offer rapid measurements with accuracy of a few percent. Many heat-tracing studies have employed these types of devices to help constrain sediment thermal parameters (e.g., Schmidt et al., 2007, Sayde et al., 2014, Halloran et al., 2016a, and Chapter 5).

2.3 Heat tracing methods

As heat-tracing in unsaturated subsurface conditions is still a young field of research, the development of models and methodologies is of paramount importance. Most saturated zone heat-tracing methods (e.g., Goto et al., 2005, Hatch et al., 2006, Keery et al., 2007, McCallum et al., 2012, Luce et al., 2013, Vandersteen et al., 2015) focus on determining subsurface water fluxes from temperature measurements. In the VZ the determination of saturation level, S_e, or, equivalently, water content, θ, is often the goal. Here, we examine recent advances in the development of VZ heat-tracing methods divided into two categories: passive (i.e., natural heat transport through ambient temperature variations) and active (i.e., induced heating). Many of these methods rely on the empirical thermal conductivity saturation models, $k_e(S_e)$, that are detailed in Section 2.2.3.

2.3.1 Passive heat tracing methods

Passive heat-tracing methods (Figure 2.3) offer the advantage of relative instrumentational simplicity, generally requiring only temperature-depth profiles or temperature time-series as well as reliable estimates of subsurface thermal properties. These methods rely on the effects that saturation-dependent thermal parameters have on the propagation of thermal signals from the ground surface (Figure 2.4). In particular, lower saturation can manifest itself via increased rates of amplitude decay and phase shift with depth in cyclic temperature signals. Pioneering work by Suzuki (1960) established the basis for passive heat-tracing by using a simplified form of Equation 2.7 to estimate percolation rates based on temperature measurements. Both Stallman (1965) and Bredehoeft and Papadopulos (1965) refined this approach to calculate vertical Darcy velocities from the damping of temperature amplitudes and the phase shift. While foundational, these early methods implicitly assumed uniformity of thermal conductivity and focused on constant flow rates, which renders their application restricted to heterogeneous saturated conditions.

Tabbagh et al. (1999) presented what is perhaps the first vadose zone passive heat-tracing study. The authors analyzed annual subsurface temperature records from weather stations to show how long-term and annual recharge rates through

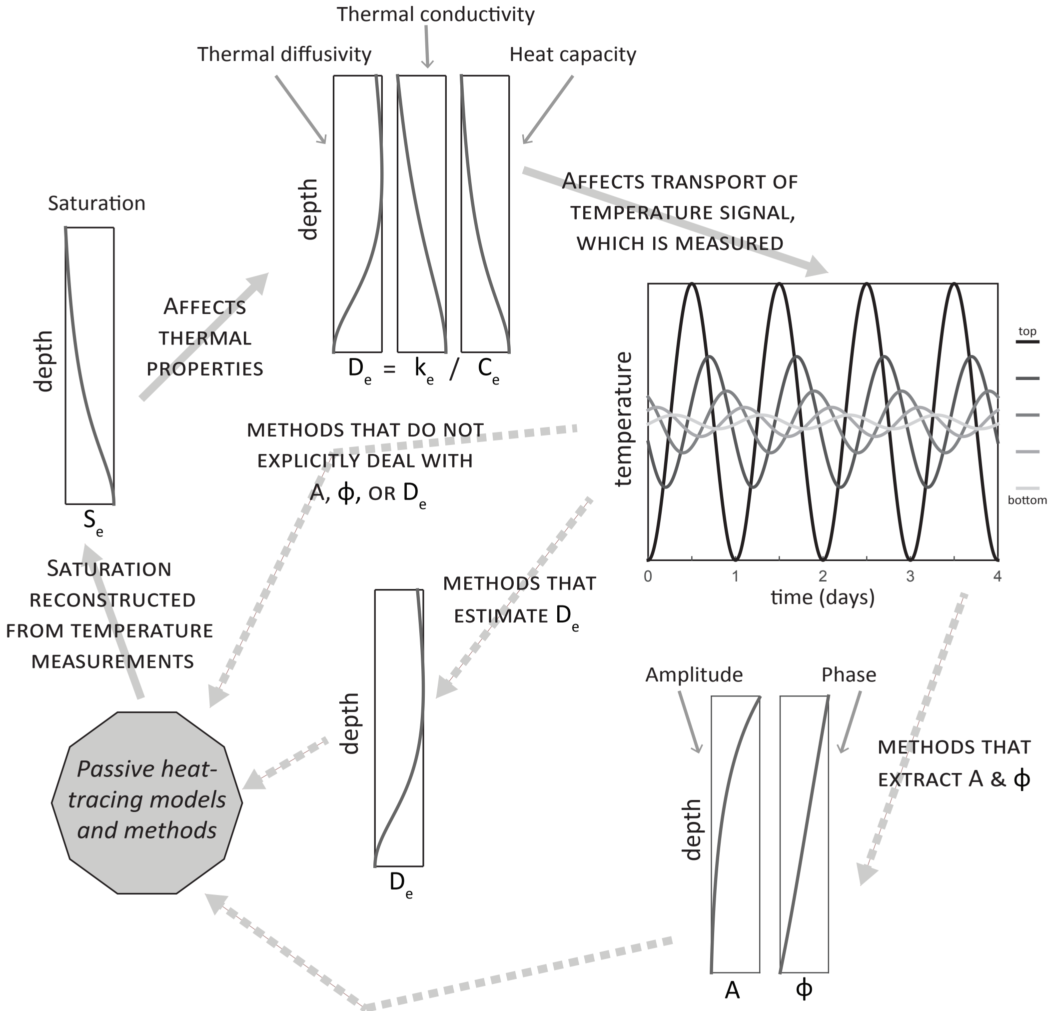

Fig. 2.3: Conceptual diagram of the principles of passive heat-tracing to determine saturation profiles in the vadose zone.

the VZ could be estimated based on the difference between amplitude-derived and phase-derived thermal diffusivity. Later, Constantz et al. (2003b) investigated annual and daily temperature profiles near three ephemeral streams in the southwestern arid zone of the United States and concluded that temperature was a robust qualitative tool for estimating percolation timing and duration in the vadose zone. In an ephemeral streamflow study, Blasch et al. (2006) used water saturation, temperature and hydraulic head measurements to constrain a variably saturated coupled thermal-water flow model. They found that infiltration rates at the onset of the flow event were 2–3 orders of magnitude

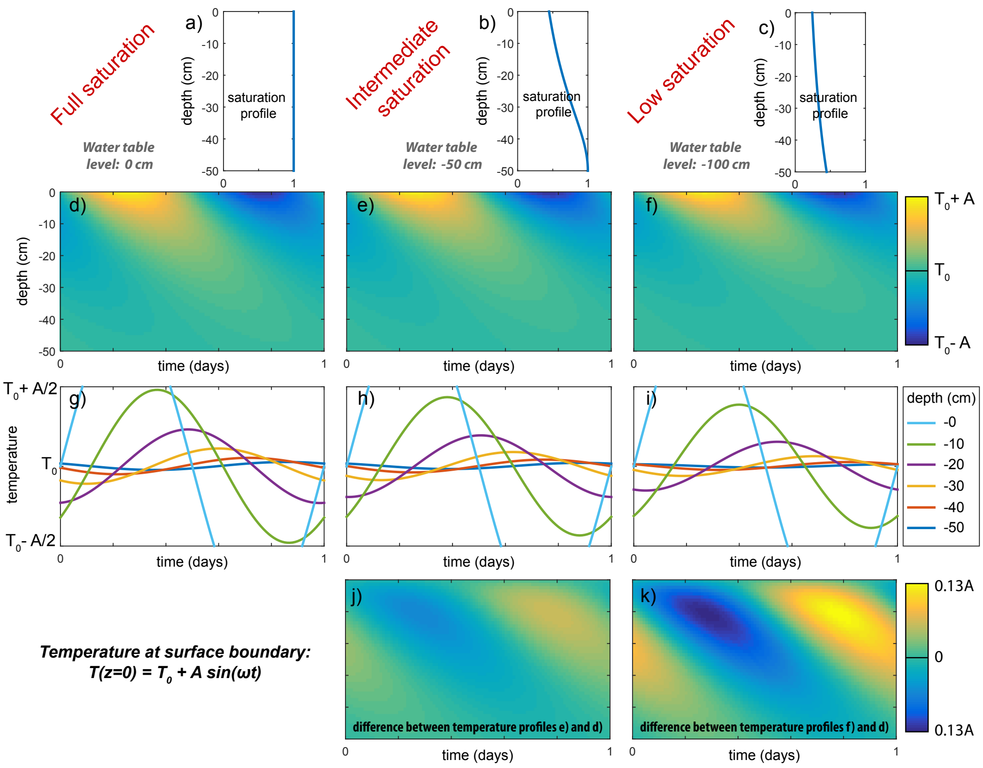

Fig. 2.4: Three different saturation profiles (*a*, *b*, & *c*) and their temperature profiles (*d*, *e*, & *f*) over one diurnal cycle when subject to the thermal boundary condition $T(z=0) = T_0 + A\sin(\omega t)$, where $\omega = 2\pi$ day^{-1}. *g*, *h*, & *i* show temperature time-series at selected depths. The difference between the temperature profiles of *e* & *d* is shown in *j* and that of *f* & *d* is shown in *k*. The values of thermal and hydraulic parameters used are identical to those in Chapter 4 (Halloran et al., 2016c) and hydraulic conditions are stable.

greater than steady-state rates under saturated conditions. This observation underscores how non-linear behaviour in the VZ must be taken into account when unsaturated conditions are present in studies of SW-GW interactions and other processes. A simple analytical equation to determine percolation rates in the vadose zone assuming diffusion-only was presented by Shan and Bodvarsson (2004). This analytical solution, which reduced to the Bredehoeft and Papadopulos (1965) solution in the single layer case, was investigated in a layered model giving good agreement with results from other numerical models. A sensitivity analysis showed a roughly linear effect of error in k_e estimates on the calculated velocities.

Béhaegel et al. (2007) presented a seminal study with the aim of estimating S_e from temperature measurements. The authors used a $\sim$14 month temperature time-series from the surface and from 60 cm depth in a loamy clay. Their study contained two parts: determination of the most suitable $k_e(S_e)$ empirical model and estimation of the vadose zone thickness and effective saturation level. They considered conduction only and found that, compared to the models of Woodside and Messmer (1961) and McCumber and Pielke (1981), the Johansen (1975) model resulted in the most physically acceptable results. A relatively simple two-layer saturated/unsaturated model, where thermal property values were fixed for each layer, was used with a *Laplace* inversion technique to estimate the depth of the top (unsaturated) layer and the depth-averaged effective saturation in the top 60 cm. The authors determined plausible vadose zone depths for all seasons and noted that estimation of saturation and VZ thickness would likely be much improved by the measurement of temperature time-series at several depths as well as accurate laboratory measurements of soil properties.

The introduction of fibre optic distributed temperature sensing (FO-DTS) to VZ heat-tracing by Steele-Dunne et al. (2010) added measurements at high spatial resolution. This feasibility study aimed to determine whether or not FO-DTS temperature data could be used to constrain VZ thermal properties and, subsequently, moisture content. Fibre-optic cables were buried at two depths ($\sim$8 and $\sim$10 cm) and, employing a diffusion-only approach (Equation 2.8) similar to Béhaegel et al. (2007) (although on daily, rather than monthly data), S_e estimates were calculated. For each section of the cable, the authors determined a single thermal diffusivity, D_e, value for the top 10 cm of the subsurface. They also investigated the impact of uncertainty of cable depth on thermal diffusivity. As their study dealt primarily with conditions where $S_e < 0.5$, direct $D_e \rightarrow S_e$ mapping functions using the models of Johansen (1975) and Campbell (1985) were possible. Both high and low S_e values were calculated when the solution was non-unique. They concluded that buried FO-DTS cables offered the potential for calculation of saturation, but that the constraints on cable vertical position and the $k_e(S_e)$ relationship were crucial for successful vadose zone heat tracing.

Krzeminska et al. (2012) deployed FO-DTS and discrete temperature probes in a clay-shale landslide, demonstrating the utility of FO-DTS in estimating spatio-temporal variations in thermal diffusivity and soil moisture. Like Béhaegel et al. (2007) and Steele-Dunne et al. (2010), they employed Equation 2.8 and did not explicitly consider advective heat transport. The methodology for estimating D_e, and subsequently S_e, was similar to that used by Steele-Dunne et al. (2010). Amplitude analysis and an inversion method showed promising qualitative and quantitative results for spatio-temporal changes in thermal diffusivity. The authors noted that at $S_e < 0.1$ and $S_e > 0.5$ the low sensitivity of thermal diffusivity to saturation (e.g., Figure 2.2) rendered S_e estimation difficult, although clearer relationships were observed when the analysis divided the data into three distinct spatial zones with different properties assumed for each.

In a novel approach, temperature time-series with 1 mK precision from a high-precision platinum thermistor array installation were used to evaluate soil moisture profiles (Bechkit, 2011, Bechkit et al., 2014). Six thermistors were buried at depths between 12 and 34 cm. Building on earlier work by Tabbagh et al. (1999), the authors based their 1-D vertical finite element calculations on the full advection-conduction-dispersion heat transport equation (Equation 2.7) but used the simple linear model by (Cosenza et al., 2003) for $k_e(S_e)$. This approach is unlikely to be reliable over the full range of possible saturation for many classes of sediments. Relative variations in calculated soil moisture content were compared to those from TDR sensor data, showing correlation values between 0.67 and 0.75.

Two studies (Dong et al., 2015a,b) developed novel methods for the calculation of soil moisture from temperature measurements using HYDRUS-1D, a one-dimensional coupled heat and soil moisture model (see Section 2.5.3). The Dong et al. (2015b) study used numerical models to test a data assimilation approach using the ensemble *Kalman* Filter (e.g., Evensen, 2003), a *Monte Carlo* implementation of a type of recursive filter. Their results indicated the approach might be useful in estimating soil moisture profiles using FO-DTS. In Dong et al. (2015a), particle filter and particle batch smoother approaches (Moradkhani et al., 2005), two related *Monte Carlo* filtering methodologies, were introduced. Tests on point temperature time-series at two shallow depths (4 and 8 cm) showed that the particle batch smoother method offered more consistent results than did the particle filter. The ability to estimate uncertainty was also noted as an advantage. Falocchi et al. (2015) provided a parametrisation methodology, applicable to the VZ, for the estimation of temperature time-series and heat fluxes. The developed Fourier series method can reproduce shallow subsurface temperature records based only on surface measurements, but requires estimates of thermal properties to evaluate fluxes and moisture content. Halloran et al. (2016d) (Chapter 3) demonstrated the caveats of applying various established saturated-zone heat tracing methods when unsaturated conditions are present. The authors developed a matrix approach that calculates and visualises amplitude damping, phase shift, and associated derived quantities for all possible temperature time-series pairs recorded by discrete sensors or FO-DTS. The method provides a robust way to compare passive heat-tracing methods and to identify subsurface heterogeneity and can be applied to the VZ.

Halloran et al. (2016c) (Chapter 4) took a first-principles physics approach to estimating S_e from temperature and integrated the $k_e(S_e)$ model of Côté and Konrad (2005) into their study. The authors derived a semi-analytical expression for effective saturation as a function of depth-dependent amplitude and phase of cyclic temperature signals. The developed methodology was applied to numerically synthesised test cases representing a variety of VZ states and water fluxes. The method predicted water saturation profiles to within 2% for a no-flow case and to within the 1-day range of saturation values for percolation rates up to 10 cm/day. The authors noted that performance could be improved by the introduction of an independent depth-dependent velocity estimate.

Finally, Hu et al. (2016) developed sine wave and *Fourier* series fitting methods to estimate thermal properties and temperature records in the subsurface. Although not explicitly developed for the VZ, the demonstrated ability to estimate variably saturated thermal diffusivity could offer utility in estimating saturation levels.

2.3.2 Active heat tracing methods

While passive methods offer the simplicity of utilising ambient temperature variations primarily due to the diurnal heating cycle, improvements in temporal resolution and accuracy can be made by adding an active heating element. This may be but at the cost of greater experimental complexity and can compromise measurement of ambient subsurface temperatures which may of interest. The foundation for many of the studies discussed in this section is the heat pulse probe (Campbell et al., 1991), whose theoretical basis was established by de Vries and Peck (1958) and Carslaw and Jaeger (1959). Heat pulse probes, including a wide range of commercially available devices, have been used to measure thermal conductivity, heat capacity and thermal diffusivity, and, upon soil-specific calibration, soil moisture (e.g., Noborio et al., 1996, Basinger et al., 1997, Bristow, 1998, Ren et al., 2000, Heitman et al., 2002, Mori et al., 2003, 2005, Liu, 2011). These devices use parallel heating and measuring probes or a single probe to heat and record temperature response in order to measure thermal properties. Active heating soil moisture studies have generally focused on an integrated source/sensor configuration which is akin to the single probe variety of these devices. Several studies (Weiss, 2003, Perzlmaier et al., 2004, Aufleger et al., 2005, Perzlmaier et al., 2006) showed the feasibility of using active heating to estimate soil moisture content. Perzlmaier et al. (2004) and Perzlmaier et al. (2006) showed that it was possible to make a qualitative distinction between fully saturated, fully unsaturated and partially saturated sediments. Weiss (2003), using an asymptotic analysis of the thermal response, demonstrated that FO-DTS could be used to detect moisture intrusion to a soil landfill cap, although small changes ($\sim$2%) at $\gtrsim$6% moisture content could not be reliably detected due to poor signal-to-noise ratio in the investigated set-up.

Sayde et al. (2010) performed a laboratory study on the feasibility of measuring soil moisture with active heating fibre optics (AHFO). Measurements from a coiled fibre and electrical resistance heater configuration installed in a medium-grain sand column showed that using the time-integral of change in temperature could predict the volumetric soil moisture content to $\pm$0.001 at $\theta = 0.05$ and $\pm$0.046 at full saturation ($\theta = \epsilon = 0.41$), with roughly linear dependence of the absolute error on saturation level. Ciocca et al. (2012) presented results from a similar laboratory test using loam and 2-minute heat pulses. The developed technique included a time correction (de Vries, 1952, Shiozawa and Campbell, 1990, Bristow et al., 1994) to enable use of the transient (pre-asymptotic decay) temperature response to heating. The approach avoided the need for large data sets of soil-specific empirical thermal property moisture-dependence by introducing a version of the $k_e(S_e)$ model by Lu et al. (2007) with modified empirical parameters adapted to the studied sediment. The authors demonstrated water content estimation within 0.01–0.035 of the true value and noted that using the transient temperature response decreased the testing times and improved accuracy at low saturation.

Striegl and Loheide II (2012) performed a field demonstration of AHFO in a 130 m transect in a silt-dominated sediment with 3 calibration points, obtaining volumetric water content estimates with an error of 0.016 for drier conditions ($\theta \leq 0.31$) and errors of 0.05 for wetter conditions. The authors noted that further research into the optimisation of cable installation and configuration, heating schemes, and interpretation techniques would likely improve performance. The AHFO approach was refined and applied in a field trial to map soil moisture along a 240 m transect (Sayde et al., 2014). The method was calibrated to the lab-measured temperature response of the sandy loam in a pivot-irrigated agricultural field. While reliable soil moisture estimates were obtained at shallow depths for a larger range of values than those of Weiss (2003), the deepest depth studied (90 cm) presented difficulties due to heterogeneity.

As is also the case with passive soil moisture methods, many active heating soil moisture studies have concluded that there is greater uncertainty when measuring higher levels of saturation. Depending on the approach, this may be related to the form of the $k_e(S_e)$ curve. The minimum slope (and therefore lowest sensitivity) of the relation occurs at high saturation level. The $D_e(S_e)$ curve (Figure 2.2) may have a maxima in the interval $0 < S_e < 1$ and thus does not offer a unique inverse function (see Section 2.2.3, Chapter 4, and Halloran et al., 2016c). The results of existing laboratory and field studies demonstrate the usefulness of AHFO in measuring soil moisture at spatial scales of interest for field studies (0.25 - 1000 m) where other methods may be inapplicable or impractical.

2.4 Thermal regimes in the unsaturated subsurface

The study of thermal regimes in various hydrogeological contexts is of interest to a broader audience, including researchers working with heat-as-a-tracer in the vadose zone. Heat and water transport dynamics affect, and are affected by, a variety of types of other processes related to geochemistry, morphology, and meteorology, among others. Analysis of thermal regimes aids understanding of the dynamics of thermal energy transport. Furthermore, the underlying thermal-hydro physics are relevant and of interest for VZ heat-tracing applications.

2.4.1 Near-surface vadose zone

Shallow vadose zones, in particular those in coastal environments, can be highly transient due to meteorologic, tidal, morphological and other effects. While there exist several studies investigating stream and streambed thermal regimes (e.g., Cardenas and Wilson, 2007, Leach and Moore, 2011, Caissie et al., 2014), only a few to date have explicitly considered variably saturated conditions. Nevertheless, these studies may be useful to vadose zone researchers in the context of long-term climate change where certain regions may become more arid and, correspondinly, have a VZ that becomes deeper and drier (Allan and Soden, 2008). Cardenas and Wilson (2007) investigated the effects of dune-covered sediments on SW-GW exchange and subsurface heat flow. The authors noted that large vertical fluxes to and from deep groundwater decrease the zone of hyporheic water exchange and the render the SW-GW heat fluxes almost entirely vertical. In another study in which the VZ was not explicitly examined, measurements of the groundwater temperature in German cities revealed the spatial extent of urban heat islands (Menberg et al., 2013). Investigations such as these represent opportunities for the characterisation of the effects of variable saturation on shallow thermal regimes.

The effects of trapped gas on streambed thermal regimes were studied by Cuthbert et al. (2010). Microbial denitrification can produce non-negligible quantities of gas in streambeds (up to 14% by volume in the study), which significantly alters the effective water-filled porosity and the streambed temperature dynamics. It renders unsaturated what would normally be considered the saturated zone. The authors observed that the significant quantity of gas weakened the decay of diel temperature signals, allowing them to penetrate deeper, and also increased recharge rates during periods of low stream flow.

Coastal studies and arid saline areas represent cases where soil moisture measurements with common TDR and TDT probes may not be possible, due to high electrical conductivity caused by the high level of dissolved salts. Thus, for these scenarios temperature-based methods may be of particular interest (Section 2.3). For coastal environments a large body of work exists on morphological (e.g., Masselink et al., 2006, Harley et al., 2011, Splinter et al., 2014) and salinity-related (e.g., Turner and Acworth, 2004, Michael et al., 2005, Robinson et al., 2006) phenomena that may have implications for coastal thermal regimes via coupling with VZ hydraulic and thermal processes.

In the coastal zone, heat transport in unsaturated conditions can play an important role in the overall thermal regime. Befus et al. (2013) reported a net heat export from the subsurface in the outer foreshore and import to the subsurface in the near foreshore in a tropical sandy intertidal zone, although the authors considered unsaturated conditions to be negligible in at the investigated site. While beach settings may experience sediment transport and swash, which will affect or even eliminate the VZ, in estuaries these processes may be negligible. Estuarine streams have been shown to be an intriguing setting for studying the dynamics of a highly transient VZ (Land and Paull, 2001, Halloran et al., 2015b, 2016a, and Chapter 5). By integrating a fully coupled thermo-hydraulic finite element model into their analysis, Halloran et al. (2016a) (Chapter 5) included estimates of transient saturation levels in the analysis of heat exchange in the variably saturated subsurface. They also compared the magnitude of tidal and diurnal temperature forcing, finding a more rapid decay in the tidal temperature effects for the investigated sandy tidal streambed.

Distributed near-surface soil moisture and temperature networks may provide opportunities for the evaluation of shallow thermal regimes at basin scale. Such networks (e.g., Su et al., 2011, Bircher et al., 2012, Al Bitar et al., 2012) have been set up with the motivation, in part, to validate satellite-based soil moisture measurement tools (e.g., Kerr et al., 2001). While research on groundwater recharge (e.g., Andreasen et al., 2013) has been carried out using these networks, the scope for large scale shallow thermal regime studies has not yet been realised.

2.4.2 The deep vadose zone

The body of research on heat transport in the deep vadose zone is similarly limited. Reiter (2001), drawing on earlier work (Reiter et al., 1989), tested the idea that temperature logs from the deep vadose zone could be used to estimate VZ water fluxes. By including hydraulic head information from piezometers to constrain vertical and horizontal fluxes, he obtained reasonable estimate of unsaturated water fluxes for most of the deep ($\sim$100 m) temperature profiles investigated in the study.

Dowman et al. (2003) observed good agreement between temperatures recorded in an air-filled borehole and those from nearby buried thermistors during an infiltration experiment in an arid zone with a deep water table. Through numerical forward modelling, they determined that subsurface temperatures were most influenced by the temperature and flux of the infiltrating water and the specific heat capacity of the dry soil. As the borehole temperature measurements required 4 hours of equilibration time the described method would likely be problematic for short-duration flow events. Reiter (2004) used temperature probes with rapid time-constants in air to measure spatial temperature gradients in the deep vadose zone, improving upon the vertical and temporal resolution of previous logs of deep vadose zone temperature (e.g., Dowman et al., 2003, Sass et al., 1988). The work demonstrated how vertical temperature profiles can be used to evaluate thermal regimes, namely depth- and time-dependent temperature gradients, in the deep vadose zone. While the equilibration time of temperature measurements was small, the single-sensor technique required measurements to be taken during the lowering of the probe which may make it impractical to measure the temporal evolution of VZ temperature profiles. Finally, in a global context, borehole records have been used to quantify heat exchange between the lithosphere and atmosphere (e.g., Beltrami et al., 2002) and to reconstruct past climate (e.g., Pollack and Smerdon, 2004). However, the heat-transport effects of unsaturated sediments which have thermal conductivity – in particular, those in arid zones where the effect may be most pronounced – has not yet been analysed and thus may be an opportunity for future deep vadose zone thermal studies.

2.5 Practical considerations

2.5.1 Measurement equipment

2.5.1.1 Point-in-space temperature measurement

The temperature measurement equipment applicable for unsaturated zone heat-tracing is much the same as for saturated SW-GW interaction studies. A variety of discrete or spatial temperature probes with various specifications are

Probe	Diameter (mm)	Length (mm)	Resolution (mK)	Accuracy (mK)	Storage (datapoints)
Star-Oddi DST milli-T	13	39.4	32	100	87k
Solinst Levelogger	22	159	3	50	120k
Onset HOBO Pro v2	30	114	20	210	42k
Maxim iButton DS1922L*	16	8	62.5	500	4k
In-situ TROLL series	18	216	10	100	130k
Campbell Sci. 107-LC	8	104	10	200	none onboard

Tab. 2.3: Size, resolution, accuracy, and memory size specifications for selected discrete temperature probes used in heat-tracing. Resolution is generally more important than absolute accuracy in the context of heat-tracing. *Resolution and storage values are for high-precision mode (iButton).

available off-the-shelf (Table 2.3). Any device that can record temperature as a time-series in the subsurface can conceivably be used for heat-tracing, although in practice the choice of probe is made based on parameters such as cost, size, resolution, robustness of construction, ease of deployment, and thermal response time. Probes such as *Sensornet HOBO* loggers and *Solinst Leveloggers* have been widely used in the saturated zone (e.g., Rau et al., 2010, Doucette and Peterson, 2014, Kellner and Hubbart, 2015) but their size limits the potential vertical resolution in a probe array. This is an important concern for VZ heat tracing as fine spatial resolution data will better constrain soil moisture estimates. Small *iButton* probes are used in probe arrays such as the *SensorRod* (Naranjo and Turcotte, 2015) and have been used to study heat transport dynamics in the variably saturated zone (e.g., Chapter 5, Halloran et al., 2016a).

Arrays of platinum resistance thermistors can offer temperature resolution to ± 1 mK in a relatively small package (e.g., Bianchin et al., 2010, Rau et al., 2012b, Bechkit et al., 2014), although implementations may require extensive calibration and customisation and cost may be a concern when many sensors are required. These can be highly stable, but require a constant current source so that the voltage can be measured, digitised and converted to temperature.

In general, the ideal sensor for heat tracing is small, robust, and inexpensive; has a rapid equilibration time constant; offers high precision and accuracy (ideally to the millikelvin level to maximise the applicable depth); and has ample integrated storage. As no single temperature sensor has all of these attributes, a compromise of these criteria will need to be made when choosing a discrete temperature sensor for heat-tracing.

2.5.1.2 Distributed temperature sensing

Fibre-optic distributed temperature sensing (FO-DTS) has proven to be a very powerful tool in thermal hydrophysical studies. By exploiting the differential temperature dependence of back-scattered Stokes and anti-Stokes (energy-shifted) photons in a laser-illuminated fibre, temperature can be inferred (Dakin et al., 1985). While the tool has seen much use in fields such as petroleum and civil engineering since the 1990's (Rao and Huang, 2008), interest in the hydrology community has steadily grown since its introduction to the fields of hydrology and hydrogeology by Selker et al. (2006a).

Linear spatial resolutions are typically 1 m with sampling resolution of 0.5 m, such as offered by the *Sensornet Oryx* acquisition unit which has been used in many studies (e.g., Curtis and Kyle, 2011, Sebok et al., 2013, Halloran et al., 2016d, and Chapter 3). Recent advances have improved resolution to 0.29 m, with measurements every 0.125 m by the *Silixa Ultima* (Sayde et al., 2014). While thick, robust, multi-core cables may be useful for groundwater seepage identification applications (e.g., Lowry et al., 2007, Sebok et al., 2013, Andersen et al., 2015), for heat-tracing, standard OM3 fibres with 900 μm outer diameter and 50 μm core diameter have become popular due to their price, availability, small bend radius and low linear thermal mass (e.g., Vogt et al., 2010, Roshan et al., 2014, Zeeman et al., 2015, Halloran et al., 2016a, and Chapter 5).

To measure profiles with finer spatial resolution, as is required in VZ heat-tracing, one can effectively increase the spatial resolution by coiling a fibre around a cylinder such as a PVC pipe. This technique has provided a vertical resolution of $\sim$1 cm in applications to both the saturated (Vogt et al., 2010, Suárez et al., 2011, Briggs et al., 2012b, Halloran et al., 2016d, and Chapter 3) and unsaturated zone (Steele-Dunne et al., 2010, Halloran et al., 2016a, and Chapter 5). Research on distributed temperature sensors is rapidly developing and new materials and methods (e.g., Chin et al., 2012, Vo et al., 2014, Soto et al., 2016) may result in apparatuses offering subcentimeter resolution without the need for fibre coiling in the future. Such a development would be a boon for heat-tracing.

The temperature resolution of FO-DTS installations is dependent on measurement time, cable length, cable and splice quality, calibration, and measurement set-up. Typical RMS noise of approximately $\pm$0.05 °C in a calibration bath has been reported when using 10 minute recording intervals (e.g., Suárez et al., 2011, Blume et al., 2013, Halloran et al., 2016d, and Chapter 3). Details regarding FO-DTS calibrations and temperature resolution have been investigated in depth by many (e.g., Hausner et al., 2011, van de Giesen et al., 2012). Error in photon counts, the ultimate source of temperature data in FO-DTS, will vary as $t^{-\frac{1}{2}}$ and thus applications must consider the trade-off between temporal and temperature resolution.

While FO-DTS provides extensive coverage and/or fine resolution (e.g., when deployed in a coiled configuration) that give it an advantage over arrays of discrete temperature sensors, the technology does have some drawbacks. For any FO-DTS deployment, a relatively expensive acquisition unit and power source are required which can cause logistical issues (e.g., power supply, vandalism) for long term deployment. Calibration generally requires multiple loops of fibre-optic cable to be immersed in continuously agitated baths with independent temperature loggers (Hausner et al., 2011, van de Giesen et al., 2012). Furthermore, fibre-optic cables can be easily damaged and care must be taken to avoid compromising an installation. Finally, when a coiled configuration is used, a removable guide tube will generally need to be driven into the subsurface and carefully extracted after the coil is installed. This necessitates fusion splicing in a field setting(e.g., Vogt et al., 2010, Halloran et al., 2016d, and Chapter 3), which may result in step losses in the cable due to suboptimal ambient conditions.

2.5.2 Applicability of VZ heat-tracing

While several methods for the measurement of soil moisture exist (see the review by Robinson et al., 2008, and Section 2.1 here), heat-tracing fills a spatio-temporal applicability gap at shorter durations and smaller spatial scales (Figure 2.5). The methods outlined in Section 2.3 offer characterisation of soil moisture on scales ranging from on the order of centimetre resolution vertically (e.g., Bechkit et al., 2014, Dong et al., 2015b, Halloran et al., 2016c, and Chapter 4) to coverage of several kilometres horizontally (e.g., Striegl and Loheide II, 2012, Sayde et al., 2014). For applications over large horizontal scales, as is also the case in saturated zone heat tracing, the use of FO-DTS (Section 2.5.1.2) can expand the applicable range. Additionally, in a coiled configuration the technology can aid applications at smaller scales where fine (<10 cm) resolution is needed.

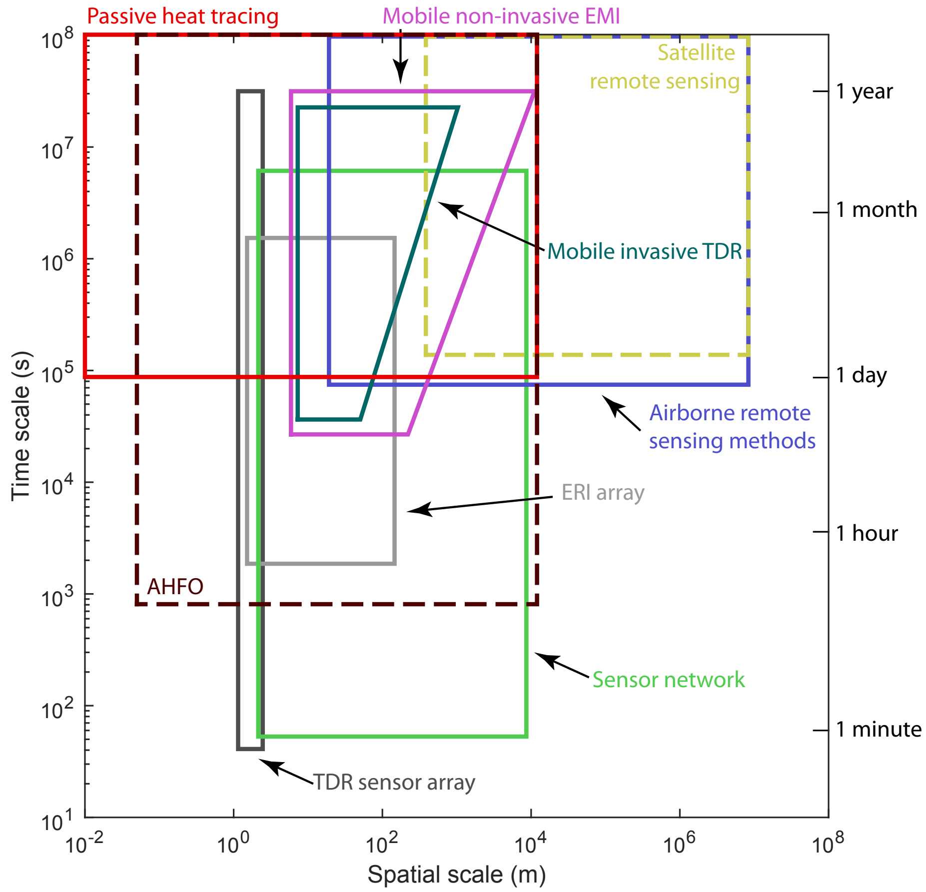

Fig. 2.5: Indicative spatial and temporal applicability of various soil moisture measurement methods adapted from Robinson et al. (2008). Here, passive heat-tracing and active heating fibre-optics (AHFO) and included.

For all heat-tracing methods, characterisation and measurement of the thermal properties of the subsurface are crucial for obtaining reliable soil moisture estimates. As is the case in most hydrogeology investigations, heterogeneity that is not accounted for will be detrimental to results and thus it is important to understand the variability of the thermal and hydraulic properties of the subsurface in an investigated domain. Therefore, independent measurements of soil moisture should be taken to validate results from heat-tracing applications.

While calibration or soil property measurements are generally required for VZ heat-tracing, using heat-as-a-tracer to measure soil moisture offers advantages over other methods applicable at comparable scales. Soil moisture measurements using TDR and TDT probes (Robinson et al., 2003, Vereecken et al., 2008) can be compromised by high pore water electrical conductivity, which limits their application in coastal zones in particular. Furthermore, temperature-based methods can provide finer vertical resolution and, when FO-DTS is incorporated, much wider coverage, than these electromagnetic methods. The installation of TDR and TDT probes may also require significant disturbance of the subsurface, potentially altering thermal and hydraulic properties. This can also be the case for installation of FO-DTS cables, although the use of cylindrical probe arrays (e.g., Rau et al., 2010, Naranjo and Turcotte, 2015, Constantz et al., 2016) or coiled FO-DTS (e.g., Steele-Dunne et al., 2010, Vogt et al., 2010, Halloran et al., 2016d, and Chapter 3) minimizes subsurface disturbance. When compared to neutron probes (Bell, 1987, Chanasyk and Naeth, 1996), temperature measurements offer the advantages of autonomy and lack of radioactive material. Heat-tracing is able to determine soil moisture from a readily measurable quantity that is often, in and of itself, of interest. Accordingly, for VZ studies where temperature measurements are required, heat-tracing can provide measurements of soil moisture with little extra data required. No single technique offers a complete solution for soil moisture measurement. Nonetheless, VZ heat-tracing provides a rapidly expanding set of tools that is suitable for applications in a wide variety of settings.

2.5.3 Software packages for coupled thermo-hydraulic VZ studies

Evaluation of the coupled thermo-hydraulic physics of the variably saturated zone (Section 2.2) can be performed by a variety of modelling software packages currently available. There exist software packages such as HYDRUS (Šimunek and van Genuchten, 2008) and VS2DI (Healy, 2008) which are specialised in the hydro-physics of the vadose zone, although only a minority of packages offer fully coupled thermo-hydraulic modelling. An excellent review of vadose zone modelling software is available in Šimunek and Bradford (2008).

For most temperature scales investigated in ambient conditions – with the notable exception of frozen conditions (e.g., Kurylyk and Watanabe, 2013, Kurylyk et al., 2014) – coupling between thermal and hydraulic physics enters primarily through the water velocity $v(\vec{x}, t)$ term. The finite difference (FD), finite element (FE), and finite volume (FV) methods lend themselves well to the modelling of coupled thermo-hydraulic (or even thermo-hydro-mechanic or thermo-hydraulic solute transport) physics in variably saturated porous media. Although Simpson and Clement (2003) noted the advantages of FE over FD in better incorporating hydraulic conductivity variations in unsaturated zone flow modelling, to our knowledge no studies exist that compare these methods in the context of thermo-hydraulic vadose zone modelling.

Software packages that are explicitly set up for coupled heat-flow and variably-saturated water flow are now available and been applied to a variety of problems. Hecht-Méndez et al. (2010) presented an overview of software available for heat transport in shallow geothermal systems with GW flow and some of these packages, among others, are applicable to the vadose zone. *COMSOL Multiphysics* (e.g., Li et al., 2009, Pryor, 2011) is a powerful proprietary FE software package that offers *Richards' equation* and *Heat transport in porous media* modules that can be coupled and customised as needed for 1-D to 3-D transient or steady-state applications. Several groundwater heat-transport studies using *COMSOL* have been published (e.g., Wörman et al., 2012, Maier et al., 2015, Rau et al., 2015), although very few have included variable saturation processes. One study which developed a semi-analytical model for determining saturation from passive temperature measurements demonstrated a robust implementation of a transient saturation boundary and custom Côté and Konrad (2005) $k_e(S_e)$ relations in *COMSOL* (Chapter 5, Halloran et al., 2016a). The manual implementation of thermal conductivity and heat capacity relations is necessary as, by default, saturation-independence is assumed. Users of all modelling packages should ensure that the desired saturation-dependent thermal property equations are implemented; this often requires modification of the standard settings.

HydroGeoSphere (Therrien et al., 2010, Brunner and Simmons, 2012) is a proprietary water resources modelling package that offers treatment of the VZ and heat transport. Brookfield et al. (2009) employed the package to study heat transport between the unsaturated and saturated zone and Raymond et al. (2011) used it in a study of interaction between a heat pump and the ground, assuming negligible advective heat transport in the VZ. Furthermore, some of the various implementations of the popular *FEFLOW* (Trefry and Muffels, 2007) software package are applicable to VZ heat-flow modelling. Shija and MacQuarrie (2014) used the software to model heat transport at a concrete-clay interface with VZ conditions. Wagner et al. (2014) included heat exchange between the saturated and unsaturated zones in *FEFLOW* in a heat-tracing study.

HYDRUS (Saito et al., 2006, Šimunek and van Genuchten, 2008), developed specifically for flow processes in variably saturated porous media, is available in freeware 1-D and commercial 2-D/3-D versions. The software has been widely used in vadose zone research, including heat-transport applications. For example, Dong et al. (2015a) used *HYDRUS 1-D* as a forward model integrated into a temperature-based soil moisture inversion method. The package has also been used to study heat transport dynamics at an unsaturated soil surface boundary (Assouline et al., 2013) and to evaluate VZ thermal regimes (Dahiya et al., 2007, Kodešová et al., 2014). Other commercial water resources and geotechnical software such as *Geostudio Universal* (with *TEMP/W* and *VADOSE/W* modules) can also solve coupled thermo-hydraulic VZ studies, although no research exists using these modules together.

The *US Geological Survey* (*USGS*) has been active in producing freely available software that can be applied to a variety of coupled thermo-hydraulic problems in the VZ. *SUTRA* and *SUTRA-MS* (Hughes and Sanford, 2004) are FE packages capable of modelling solute and heat flow in saturated and unsaturated conditions. For example, a modified version of *SUTRA* has been used to model biodegradation in unsaturated conditions with heat transport (El-Kadi, 2001). *HST3D* (Kipp Jr, 1987) is a similar but older package that may also be relevant for VZ thermal investigations. *VS2DH* and *VS2DI* (Hsieh et al., 2000, Healy, 2008) are relevant 2-D FD packages available from the *USGS*. These packages have been employed to evaluate the temperature-dependence of infiltration and the sensitivity of flow patterns to thermal and hydraulic property variations (Ronan et al., 1998), as well as the sensitivity of thermal records to parameters during ephemeral stream infiltration.

When selecting a numerical package for coupled thermo-hydraulic modelling in variably saturated conditions, care should be taken to ensure proper coupling of the physical processes. An ideal package allows for customisation of thermal parameter relations (i.e., $k_e(S_e)$ and $C_e(S_e)$) and VZ hydraulic parameters (i.e., SWRC parameters).

2.6 Summary and future directions

As illustrated in this review, temperature offers a means for indirect measurement of various quantities in the variably saturated subsurface, most notably soil moisture content. Vadose zone heat tracing expands the spatio-temporal range where soil moisture can be measured (Figure 2.5). Research in this domain relies heavily on a solid understanding of the saturation dependence of thermal properties in natural porous materials. Accurate characterisation of these dependencies, specifically $k_e(S_e)$, is crucial for the accurate application of VZ heat-tracing. Heat-tracing has now become commonplace in SW-GW interaction studies (Constantz, 2008, Rau et al., 2014) and an increasing body of research has focused on broadening the applicability of methodologies to now include the VZ. Nonetheless, there remain multiple opportunities for future research and several notable knowledge gaps exist.

No single model yet exists for thermal conductivity in variably saturated sediment that is applicable to all soil types. While acceptable agreement between models and measurements has been reported, we foresee the potential for further work on generalised empirical models for a larger class of sediments, including those with higher amounts of organic content, which would improve applications in agricultural and other contexts.

While many measurements of dry, wet, and partially saturated soil thermal conductivity have been reported (e.g., Barry-Macaulay et al., 2015, Dong et al., 2015c), there exist very few sets of measurements of both thermal and hydraulic properties of the same sample (e.g., the sand samples in Chapter 5, Halloran et al., 2016a). Characterisation of thermal and hydraulic properties of a large class of sediments would greatly aid heat-tracing and thermal modelling in the variably saturated subsurface. A database containing the following measurements would help to bridge this knowledge gap: dry, wet, and intermediate thermal conductivities; porosity; density; heat capacity; and van Genuchten SWRC parameters. Furthermore, a statistical analysis of the dependence of the various parameters on one another, notably the coupling between hydraulic and thermal parameters, would be a significant advance in understanding of thermo-hydraulics in the VZ. Such studies would tighten constraints on relevant parameters by establishing empirical relationships between them. This would, in turn, greatly improve VZ heat-tracing by reducing the amount of data required for the implementation of developed methods and by allowing for parameter estimates to be made based on other data.

As outlined, the majority of thermal regime studies to date have focused on the saturated zone. As saturated conditions are generally only found underneath or near bodies of water or in the deeper subsurface, an understanding of the relative strengths and propagation depths of natural thermal signals and the associated effects of moisture content and transport in the VZ is of broad interest. As groundwater levels are affected by excessive groundwater extraction (especially in the semi-arid and arid zones) as well as climate change, the characterisation of VZ thermal regimes in a variety of settings, ideally coupled with geochemical or ecological measurements, would constitute an important advancement of knowledge.

To date, method development has formed the crux of efforts to expand the body of VZ heat-tracing research and there is still room for improvement in both passive and active methodologies. Future efforts in this direction should seek to: a) improve accuracy in water saturation estimates, b) reduce the amount of material data required to accurately predict saturation profiles, c) improve the temporal and spatial resolution of saturation estimates, and d) expand and evaluate the applicability of heat tracing to various sediment classes. Additionally, testing and comparison of recently developed heat-tracing methods under a variety of conditions, such as low saturation, high saturation and active percolation at various rates, is an obvious next step. For inspiration and ideas on method testing, researchers need not look further than the large body of work on saturated zone heat-tracing (Anderson, 2005, Constantz, 2008, Rau et al., 2014). Novel implementation methods using FO-DTS, for example, may widen the scope of applicability and help constrain limitations on VZ heat-tracing methods.

Heat-tracing in the variably saturated subsurface is still in its relative infancy. Here, we have summarised the current state of research into relevant models, methods, tools, and field studies and have presented suggestions for further research directions. Temperature, omnipresent and relatively straightforward to measure on various temporal and spatial scales, offers great promise for future applications and investigations in the vadose zone.

Acknowledgements

Landon Halloran acknowledges support from the *UNSW School of Civil and Environmental Engineering*, the *Gary Johnston fund*, and the *Fonds de recherche du Québec – Nature et technologies* (FRQNT) (173538).

3. MATRIX METHOD FOR ANALYSIS OF VERTICAL TEMPERATURE PROFILES AND HEAT-TRACING APPLICATIONS

This chapter has been published as a journal article:
L.J.S. Halloran, H. Roshan, G.C. Rau, M.S. Andersen, and I. Acworth (2016). "Improved spatial delineation of streambed properties and water fluxes using distributed temperature sensing," *Hydrological Processes*. doi:10.1002/hyp.10806

Abstract

A new method was developed for analysing and delineating streambed water fluxes, flow conditions, and hydraulic properties using coiled fibre-optic distributed temperature sensing (FO-DTS) or closely-spaced discrete temperature sensors. This method allows for a thorough treatment of the spatial information embedded in temperature data by creating a matrix visualisation of all possible sensor pairs. Application of the method to a 5-day field dataset reveals the complexity of shallow streambed thermal regimes. To understand how velocity estimates are affected by violations of assumptions of 1-D, saturated, homogeneous flow and to aid in the interpretation of field observations, the method was also applied to temperature data generated by numerical models of common field conditions: horizontal layering, presence of lateral flow and variable streambed saturation. The results show that each condition creates a distinct signature visible in the triangular matrices. The matrices are used to perform a comparison of the behaviour of 1-D analytical heat-tracing models. The results show that the amplitude ratio-based method of velocity calculation leads to the most reliable estimates. The minimum sensor spacing required to obtain reliable velocity estimates with discrete sensors is also investigated using field

data. The developed method will aid future heat-tracing studies by providing a technique for visualizing and comparing results from FO-DTS installations and testing the robustness of analytical heat-tracing models.

3.1 Introduction

Surface water-groundwater (SW-GW) exchange is an important control on biogeochemical processes in streams and streambeds (Findlay, 1995). Water fluxes in streambeds are notoriously variable both temporally and spatially (e.g., Boulton, 1993, Ward et al., 2010, Briggs et al., 2012b). This raises demanding requirements on methodologies when determining the impacts of hydrologic change on hyporheic exchange. An understanding of the hydrological processes that occur at the stream-streambed interface is also vital for evaluating rates of recharge to and discharge from aquifers to inform environmental management decisions.

The expanding use of heat tracing methods in investigating SW-GW interaction has been well documented by Anderson (2005), Constantz (2008) and Rau et al. (2014). The passive, omnipresent nature of thermal energy fluctuations and the relative ease and high precision of temperature measurements make it a very useful tracer for hydrological investigations (Johnson et al., 2005, Kalbus et al., 2006, Constantz, 2008). Hatch et al. (2006) and Keery et al. (2007) provided an overview of the method that quantifies vertical streambed fluxes from the downward propagation of diurnal thermal signals, while McCallum et al. (2012) and Luce et al. (2013) provided further development of this method, unifying the amplitude ratio-dependent and phase-shift-dependent equations. The performance of these analytical solutions has not yet been compared directly using temperature data with centimetre-scale resolution.

Following a formal introduction of the measurement technique to the hydrology community by Selker et al. (2006a), fibre-optic distributed temperature sensing (FO-DTS) has seen a growing amount of interest (e.g., Henderson et al., 2009, Tyler et al., 2009, Sayde et al., 2010, Curtis and Kyle, 2011, Briggs et al., 2012a). The technique, first demonstrated by Dakin et al. (1985), exploits the different degree to which back-scattered Stokes and anti-Stokes photons exhibit dependence on temperature, thus allowing the measurement of temperature at spacings of $\lesssim$ 1 m along fibre glass many kilometres in length (Selker et al., 2006b). FO-DTS has been employed in the identification of geothermal sources in ice caves (Curtis and Kyle, 2011), the characterization of hydrostratigraphy (Bahr et al., 2011), the analysis of soil thermal properties in a landslide (Krzeminska et al., 2012), and the identification of zones of seasonal discharge in a lake (Sebok et al., 2013) due to its applicability at larger scales.

In other applications, in particular those related to vertical spatial variability of saturation in the vadose zone or of flow rate and material properties in streambeds, spatial resolution finer than the 1 m offered by most modern FO-DTS systems is required. By coiling the cable around a cylinder, a much finer resolution along a single axis can be obtained with FO-DTS. The use of coiled-configuration FO-DTS systems to study SW-GW interaction is still in early stages of development but has provided detailed insight into near-surface hydraulic processes in deployments using active heat sources (e.g., Sayde et al., 2010, Ciocca et al., 2012, Liu et al., 2013) and ambient temperature variations. Those employing coiled FO-DTS without active heating (Vogt et al., 2010, 2012, Briggs et al., 2012b, Halloran et al., 2015a, and Chapters 3 & 5) have demonstrated the potential for data from this high vertical resolution configuration to inform 2-D and 3-D models. Vogt et al. (2010) explored the effect of sensor separation on heat-tracing calculations by fixing the top time-series location to the SW-boundary and altering the depth of the lower time-series in the pair during velocity calculation. This demonstrated the ability of heat-tracing with coiled FO-DTS to locate discontinuities and to accurately estimate seepage rates in the hyporheic zone. In Vogt et al. (2012), the authors showed how a transect of coiled FO-DTS installations could be used to explore lateral flow components and preferential flow via spatial maps of time shifts. Briggs et al. (2012b) used an adaptive window size for increasing depths to analyse their multiple coil installation and produce month-long plots of vertical flux. The work in our study takes a similar approach to Vogt et al. (2010) but allows the depths of the top and bottom temperature time-series used in the calculations to vary. This illustrates the effects of relative and absolute sensor depths and allows for simultaneous calculation of velocities for all spacings.

Datasets collected using FO-DTS technology provide very detailed records of the temporal and spatial variability of temperature. Beyond straightforward visual investigation of plots of temperature as a function of space and time, various analysis techniques have been applied to FO-DTS data sets. Wavelet analysis, which encompasses dynamic harmonic regression (DHR) and other similar techniques, has been applied to DTS data by several (Henderson et al., 2009, Vogt et al., 2010, 2012, Becker et al., 2013, Briggs et al., 2012b, Onderka et al., 2013). Wavelet methods can be considered a mathematical extension of the discrete time Fourier transform (DTFT) and are useful when a variety of frequencies are of interest. Other analysis methods involving relative temperature anomalies have been used to determine regions of inflow and outflow in fractured media and streams (e.g., Read et al., 2013, Matheswaran et al., 2014). These methods, along with the diel signal-isolation method presented in this study, work towards a realisation of the full potential that FO-DTS data presents for SW-GW interaction investigations.

Much progress in understanding SW-GW processes through the use of point-in-space time-series measurements of temperature has been made over the past decade (refer to the reviews of Constantz (2008) and Rau et al. (2014)). However, the limitations of point measurements often lead to large uncertainties, as well as possible misinterpretation of data. This is particularly true in heterogeneous streambed environments where spatially variable flow prevails (e.g., Cardenas, 2010, Schornberg et al., 2010, Ferguson and Bense, 2011, Roshan et al., 2012, Cuthbert and Mackay, 2013). A better understanding of the effects of spatial sensor density (i.e., sensor depth and separation) on estimates of vertical flow rates is needed in order to improve the interpretation of field data.

In this paper we present a novel technique for centimetre-scale delineation of streambed thermal regimes, hydraulic properties, and water fluxes using distributed temperature sensing (DTS). Using measured and modelled temperature data, we illustrate how this technique can be used to identify the presence and location of layers of contrasting hydraulic and thermal properties, as well as how the methods of Hatch et al. (2006), Keery et al. (2007), McCallum et al. (2012) and Luce et al. (2013) perform when the underlying assumptions behind heat-tracing are violated. The method utilises the full breadth of spatial information contained in coiled FO-DTS measurements that has previously been underutilized. This significantly aids in identifying regions with distinct hydrodynamic activity or zones of deviating streambed physical properties.

3.2 Methodology

3.2.1 Triangular matrices method

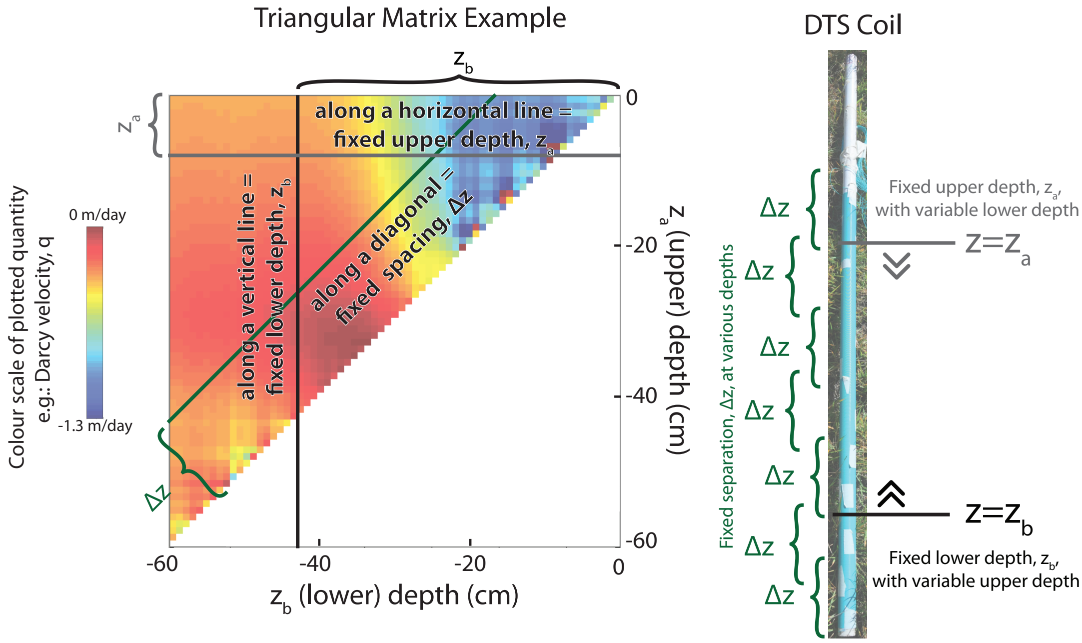

Fig. 3.1: How to interpret triangular matrices. The values along the horizontal grey line correspond to a fixed upper depth, $z = z_a$. By moving right-to-left along this line, the values in the matrix correspond to those calculated with a z_b at increasing depth (i.e., a bigger separation between the temperature "sensors" with a fixed upper location). Similarly, values along the vertical black line are from a fixed lower depth, $z = z_b$, and the values moving from bottom to top correspond to increasing separation between the positions of the temperature "sensors." The green diagonal line corresponds to all values where $z_a = z_b + \Delta z$. Along this line the values in the matrix correspond to those with a fixed separation between the upper and lower "sensor" locations.

Heat tracing uses the amplitude and phase information of cyclic temperature fluctuations. When temperature is recorded at two or more depths, the phase shift and the amplitude ratio of the dominant diurnal components can be calculated. As the phase shift and amplitude ratio are altered by the vertical water fluxes when compared to no-flow (conduction only) conditions (Stallman, 1965, Hatch et al., 2006, Keery et al., 2007), vertical flux can be quantified. Here, we develop a new approach to quantify and visualise the amplitude ratio, phase shift, and ultimately the water flux using the fine spatial resolution offered by coiled FO-DTS data and other fine-scale temperature measurement methods. Two vertical points of measurement (z_a and z_b), required for flux quantification using temperature phase and amplitude, can be shifted independently along the depth axis. To avoid redundancy only combinations where $z_b \leq z_a$ are evaluated. The result is a triangular matrix of the type illustrated in Figure 3.1 which contains data from the unique combinations of all possible sensor locations. The new approach enables visualisation and analysis of the information contained in temperature time-series recorded at high spatial resolution, such as those obtained from coiled FO-DTS.

We test this new method with a temperature dataset from a field deployment of coiled FO-DTS and also with temperature data generated from models of different field conditions. The new method allows more detailed delineation of the spatial changes in streambed thermal regime, water fluxes, and hydraulic properties compared to what is possible with discrete point temperature measurements. The increased spatial information facilitates the possibilities for sequential comparison on a pair-by-pair basis (i.e., using all possible pairs of time-series recorded at different depths), an approach whose full potential has so far not been exploited. Triangular matrices provide an easy means for visualising and analysing velocities derived from temperature pairs by fixing the lower or upper depths of these effective sensors, as well as by fixing the separation between the two sensors (Figure 3.1). These aid in the identification of heterogeneous conditions, determination of average velocities across sections of interest, and evaluation of the effects of sensor spacing.

3.2.2 Measured and modelled temperature time-series

3.2.2.1 High-resolution FO-DTS streambed deployment

A coiled FO-DTS dataset was recorded at 10 minute intervals for approximately 5 days at a field site on Maules Creek, NSW, Australia while groundwater abstraction (pumping) was carried out at a nearby borehole (Figure 3.2). Surface water flow in this section of Maules Creek is generally groundwater-fed outside times of flood with the upper reaches usually dry (i.e., no runoff from the upper catchment). At the Elfin Crossing study site the surface water groundwater

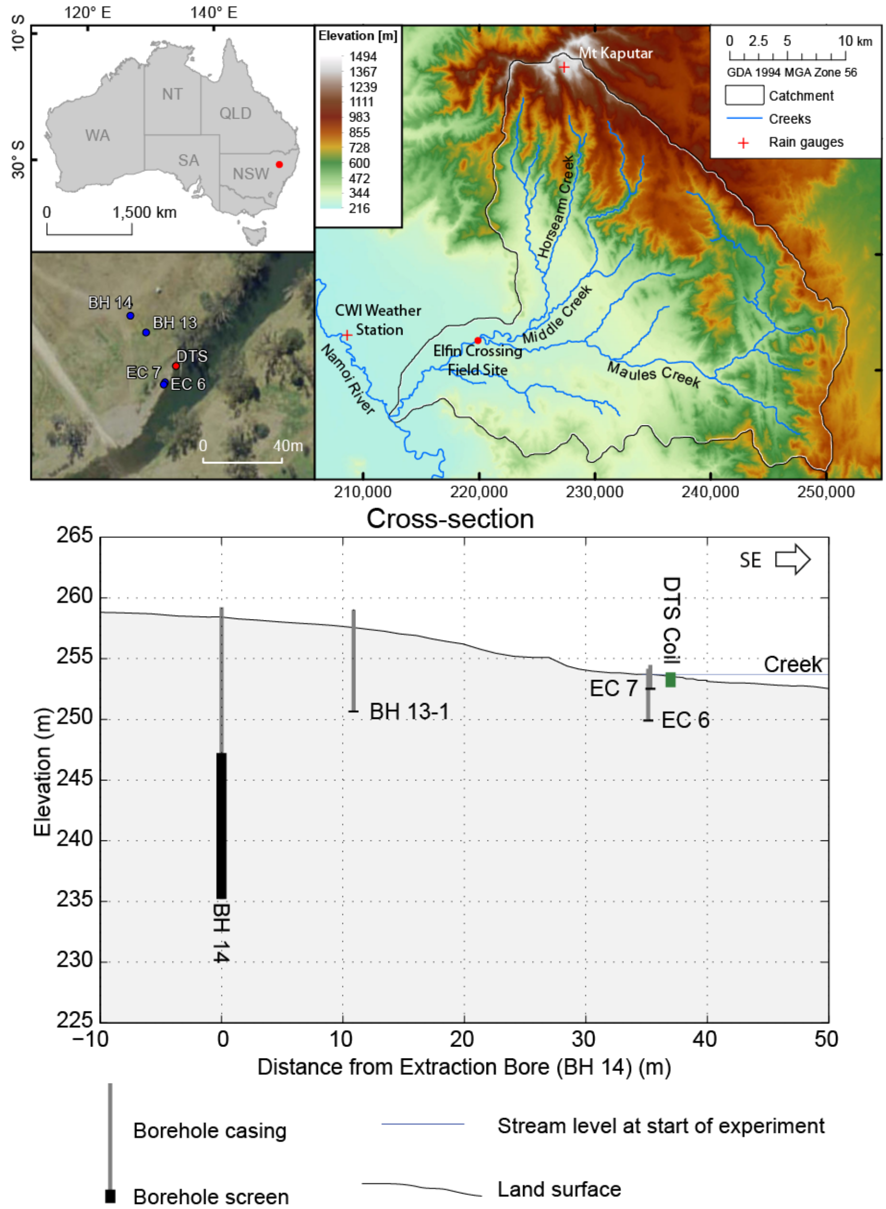

Fig. 3.2: The Elfin Crossing research site within the Maules Creek sub-catchment and a cross-section of the site. Elevations are relative to GDA94, zone 56.

interactions vary with the conditions, but are generally losing (Andersen and Acworth, 2009, Rau et al., 2010).

The 1 m resolution of the Oryx FO-DTS unit, the sealed PVC pipe diameter of 32 mm, and fibre diameter of 900 μm resulted in a 8.80 ± 0.05 mm vertical resolution when the fibre was wound around the pipe. The installation was

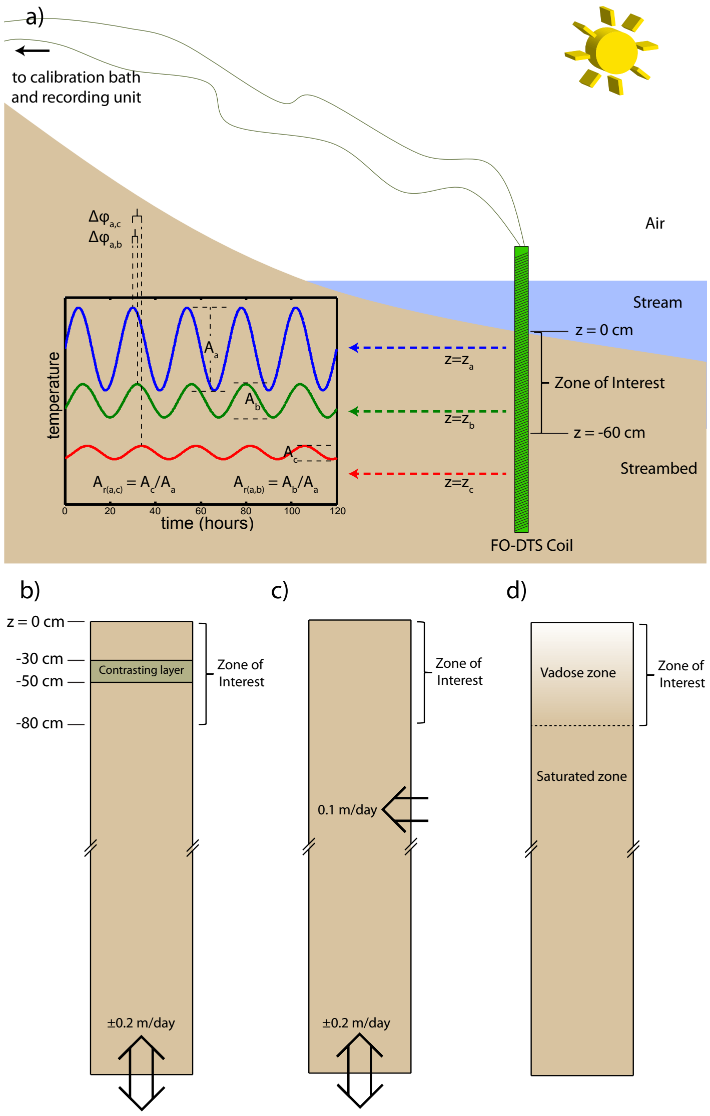

Fig. 3.3: a) Installation of FO-DTS coil in the streambed. Here, an indicative, not-to-scale cross-section of the FO-DTS coil installation is shown. In this idealised representation, the amplitude of the diel temperature signal is decreasing with depth, while the phase shift is increasing. $z = 0$ is defined at the stream-streambed interface and z is decreasing in the downward direction. The schematic for numerical modelling is shown in b) with a layer of contrasting hydraulic conductivity, c) a horizontal flow component and d) variably saturated conditions.

carried out by manually boring a guide hole in the streambed, inserting the FO-DTS coil, and removing the metal guide pipe so that the sediment was in direct contact with the fibre-optic cable. When installed vertically in the streambed, portions of the coil were exposed to air, surface water, and the subsurface (Figure 3.3), although only subsurface measurements are used in this work and transfer of heat from solar radiation in the air- and surface water- exposed portions is assumed negligible. Calibration was carried out by immersing extra lengths of cable, ∼14 m and ∼95 m long, at both ends of the double-ended cable in a continuously agitated calibration bath containing two independent Onset Hobo Pro v2 temperature loggers.

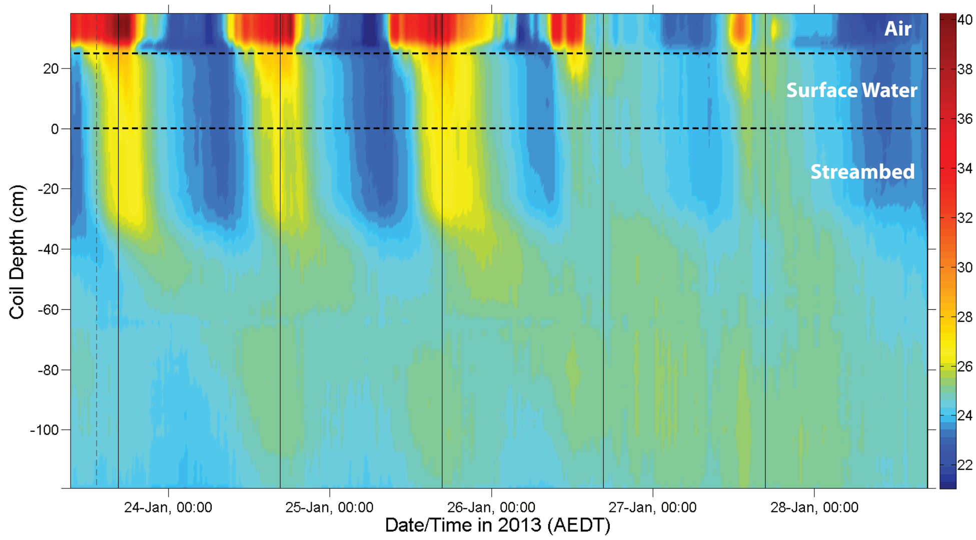

Fig. 3.4: Coiled FO-DTS temperature data from Maules Creek. The upper dotted horizontal line at 24.7 cm indicates the surface water–air interface at the beginning of the measurement period. The lower dotted horizontal line at 0.0 cm indicates the streambed–surface water interface. The vertical black lines indicate the investigated 24-hour periods and the vertical grey dashed line indicates the time when abstraction commenced. Temperature units are degrees Celsius. Data from depths, -60 cm $\leq z \leq 0$ cm, is analysed in this study.

The calibrated 127-hour coiled FO-DTS dataset has 765 time steps (Figure 3.4). No erosion around the installed coil was observed and the surface water level was stable for the majority of the acquisition with the exception of a rapid rise in the stream water level from 0.25 m to 1.69 m due to flooding over the course of the final 2 hours of measurement, which resulted in fibre-optic cable breakage. RMS noise in the calibration bath portion of the cable was found to be $\lesssim$0.05 °C; however, noise in the coiled portion of the cable is likely to be higher as the raw Stokes/anti-Stokes signal strength is weaker further from the FO-DTS acquisition unit. Losses in the raw Stokes signal were found to be $\sim$0.19%/m for the coiled section, slightly higher than the $\sim$0.12%/m loss in a section of buried cable running from the FO-DTS coil to the mobile lab housing the acquisition unit.

The individual data files recorded during the experiment were combined and the data corresponding to the connected cable lengths were extracted. The two extracted sections of cable that were placed in the bath (shorter sections than the total length in the bath in order to avoid edge effects) spanned 8 m between l_{1a} and l_{1b} and 90 m between l_{2a} and l_{2b}. These sections, whose mid-points are separated by $L_{sep} = \frac{l_{2a}+l_{2b}-(l_{1a}+l_{1b})}{2}$, provide for a two-point calibration. Averages of these sections of the FO-DTS data, as well as the independently measured temperature of the bath, T_{logger}, were used in the calibration procedure. For each time step, the following calibration was applied to the raw data (T_{raw}):

$$T_{calib}(l) = T_{raw}(l) - \left(\eta \frac{x - x_0}{L_{sep}} + \xi\right), \tag{3.1}$$

where

$$\xi = \overline{T}_{raw}(l_{1a} \leq l \leq l_{1b}) - T_{logger}, \tag{3.2}$$

$$\eta = \overline{T}_{raw}(l_{2a} \leq l \leq l_{2b}) - \overline{T}_{raw}(l_{1a} \leq l \leq l_{1b}), \tag{3.3}$$

x refers to length along the FO cable and x_0 is the appropriate offset for the beginning of the coiled data with respect to the sections of cable in the calibration bath. Following the recommendations of Hausner et al. (2012), the raw forward and reverse Stokes and anti-Stokes data were inspected for step losses caused by cable damage. Some natural step losses were observed along the cable at the expected locations where there is a clear temperature contrast such as the boundary between air- and water-exposed portions (Hausner et al., 2012).

Temperature data acquired by FO-DTS was divided into 5 segments of 24 hours in duration with an offset of 24 hours between the segments (i.e., no overlap between the selected segments). As the sampling frequency was 10 minutes, this resulted in subsets of 144 samples each for each 24 hour period. One advantage of subdividing the data in this way is the ability to select the diel signal in a single frequency bin in the Fourier domain.

3.2.2.2 Numerical modelling of assumption-violating conditions

Five 2-D models were constructed in COMSOL Multiphysics 5.0 to generate synthetic streambed temperature data to test the behaviour of the velocity equations for a range of conditions that violate some of the underlying assumptions. The model domain was a rectangle 1 m wide and 10 m deep with the top 80 cm, where the thermal signal is strongest, being the focus of the study. Two models that contain a contrasting layer (heterogeneity) (Figure 3.3b), two models that have a lateral flow component (Figure 3.3c), and one model that has an unsaturated portion (Figure 3.3d) were created. These show how the widely-used methods of Hatch et al. (2006), where amplitude ratio and phase shift are used independently, and that of McCallum et al. (2012), where amplitude ratio and phase shift are both used in one equation, perform under various conditions.

	Field data	Modelled data	Modelled data (contrasting layer)
porosity, ϵ	0.33	0.404	0.323
thermal conductivity, k_s (W/m·K)	1.8	2.833	3.604
mass heat capacity, C_p (J/kg·K)	1183	910	910
ρ (kg/m^3)	1776	1550	1938
	α_{vG} (m^{-1})	6	
van Genuchten SWRC	m	0.4	
(vadose zone)	l	0.5	
	θ_r	0.1	

Tab. 3.1: Thermal properties and soil water retention curve (SWRC) properties used for calculation of velocities and for creating the finite element models. For the field data, the properties are from a previous study at the same location (Rau et al., 2010) and for the modelled data, the properties are typical of sands (Chen, 2008).

The model was constructed with thermal parameters characteristic of a sand (Table 3.1) and hydraulic conductivity of $K = 10$ m/day. For the two models containing a heterogeneous layer, the layer between $z = -50$ and -30 cm was defined with a different porosity and thermal properties (Table 3.1) and hydraulic conductivity of $K = 1$ m/day. For the unsaturated model, the standard soil water retention curve (SWRC) of van Genuchten (1980) was used with realistic parameters for a sand (Table 3.1):

$$\theta = \theta_r + \frac{\epsilon - \theta_r}{(1 + |\alpha_{vG} H_p|^{\frac{1}{1-m}})^m} \tag{3.4}$$

where ϵ is the porosity, θ is the water content, $H_p < 0$ is the suction pressure, θ_r is the residual water content, and α_{vG} and m are van Genuchten parameters.

For all models, a 24-hr period sinusoidal temperature signal of mean 20 °C and amplitude 10 °C was applied. The model sides were insulated and the bottom at -10 m fixed at 20 °C. Hydraulic boundary conditions for the layered system were set to be a prescribed flux of ±0.2 m/day at the bottom boundary, atmospheric pressure at the top boundary, and no flow at the side boundaries. For the lateral flow models, the bottom and top boundary conditions were the same as those of the layered system and the side boundaries were set to have a uniform lateral flow rate of 0.1 m/day and the boundaries thermally insulated. In the unsaturated model, the system was in hydraulic equilibrium (without flow) and the saturation boundary was set to a depth of -0.8 m, resulting in a saturation level at $z = 0$ m of 0.35 as described by the van Genuchten SWRC.

All models were executed for 10 days and 100 samples per day were recorded at 1 cm increments along the centre line of the domain. While the initial conditions of the five modelled domains were set to 20°C, the cyclic thermal behaviour didn't change after $2-3$ days. As we only require one 24-hour segment of each time-series, the final simulation day was selected for analysis. All of the models were executed with fine mesh settings and mesh points explicitly set at 1 cm increments vertically along the centre line of the domain.

3.2.3 *Quantifying vertical streambed fluxes*

3.2.3.1 *Extracting phase shifts and amplitude ratios*

The diel signal is usually the dominant spectral component in temperature records obtained from streambeds (Wörman et al., 2012). In our case it amounted to $\gtrsim 10\times$ the power of the second-highest component ($f = 2$ day^{-1}) in the measured surface water temperature data. We therefore focus on this component and develop a new algorithm for the calculation of the phase shift and amplitude ratio between all time-series pairs. It deploys the discrete Fourier transform, $\mathcal{F}$, of the temperature signal, $T(t)$, defined here as:

$$\mathcal{F}(T(z,t_j)) = \hat{T}(z,f_k) = \gamma \sum_{j=1}^{N} T(z,t_j) e^{-2\pi i (j-1)(k-1)/N}, \tag{3.5}$$

where γ is a normalisation constant; t_j, the jth time value; and f_k, the kth frequency value. When $N = 144$ and $\Delta t = t_{j+1} - t_j$, the frequency components are $f_k = 0, 1, 2 \ldots 144$ day^{-1}. This permits a straightforward extraction of the diel component by isolating $\hat{T}(z, f_2)$.

The relative phase difference, $\Delta\phi_{a,b}$, between two depths, $z_b < z_a$, was extracted from the diel frequency (f_d) component, $f_d = f_2 = 1$ day^{-1}, of the discrete Fourier transforms so that

$$\Delta\phi_{a,b} = \phi_a - \phi_b \tag{3.6}$$

where

$$\phi_a = \arctan\left(\frac{\Im\{\hat{T}(z_a, f_d)\}}{\Re\{\hat{T}(z_a, f_d)\}}\right) \tag{3.7}$$

$\arctan$ represents four-quadrant inverse tangent; $\Im$, the imaginary component; and $\Re$, the real component. This phase shift, $\Delta\phi$, is generally increasing in magnitude with depth.

In some publications on the use of heat as a groundwater tracer (e.g., Hatch et al., 2006, McCallum et al., 2012), the term "phase-shift" has been incorrectly employed to describe a time-lag. Here, "phase-shift" ($\Delta\phi$) refers to the relative phase difference between a pair of temperature time-series at different depths and can readily be converted to a time-lag by $\Delta t = (24 \times 60^2 \text{ s}/2\pi)\Delta\phi$, for phase data in radians.

Similarly, the amplitude ratio, $A_{r\,(a,b)}$, generally <1, can be calculated from a simple ratio of the magnitudes of the diel components of the time-series:

$$A_{r\,(a,b)} = \frac{\overline{\hat{T}}(z_a, f_d)}{\overline{\hat{T}}(z_b, f_d)} \tag{3.8}$$

for two given depths, $z_b < z_a$ (i.e., z_b below z_a), where $\hat{T}$ denotes the forward Fourier transform of $T(t)$. Note that when using the Fourier transform the frequency of interest also defines the time resolution of parameters derived from temperature data, such as the water flux or thermal diffusivity.

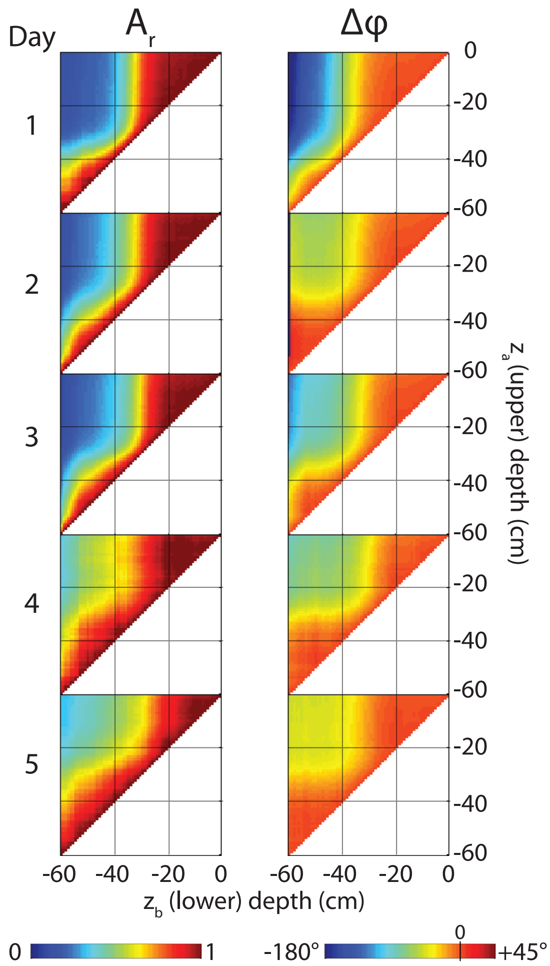

Fig. 3.5: Matrices showing the amplitude ratio (Equation 3.8) and phase shift (Equation 3.6) calculated between an upper depth (vertical axis) and a lower depth (horizontal axis) for the coiled FO-DTS field data. Scales at the bottom left and right apply to A_r and $\Delta\phi$, respectively. The matrix is triangular due to the restriction $z_a > z_b$, which avoids reduncancy. To determine A_r or $\Delta\phi$ between two given depths, find the upper depth on the vertical axis and the lower depth on the horizontal axis. For example, those calculated with an upper depth of $z_a = 0$ can be found along the very top of each matrix, with the depth z_b increasing in magnitude from right to left along this line.

Phase shifts, $\Delta\phi$, and amplitude ratios, A_r, were calculated using the diel component of the discrete Fourier transformed time-series subset $\hat{T}$. This was repeated for all depth pairs of modelled data and field data (the buried section of the coil), although our analysis focuses on the upper portion where the signal is strongest ($-60\text{cm} \leq z \leq 0$ cm). Figure 3.5 shows the resulting triangular matrices for the field FO-DTS data. The usefulness of these two components, evaluated at all depth pairs, in detecting interfaces and regions of particular interest is discussed later.

In these figures, the depth of the upper time-series, z_a, is displayed on the y-axis and the depth of the lower time-series, z_b on the x-axis. In evaluating and displaying the data this way, we make use of the entire data set in day-duration increments and can display A_r and $\Delta\phi$ as calculated from every possible pair of measurements in the streambed. This visual representation of the evolution of the thermal signal is useful for identifying abnormalities and zones of change in the system. It is also useful for comparing the performance of the one-dimensional analytical methods of calculating the advective thermal velocity.

3.2.3.2 Vertical flux and diffusivity estimates

The advective heat tracing method set forward by Hatch et al. (2006) has been used in many heat tracing investigations using discrete temperature sensors. Here, we deploy our new methodology that visualises the spectral analysis of temperature-depth data. Advective thermal velocities, v_t, can be determined by feeding the A_r and $\Delta\phi$ triangular matrices into the equations:

$$v_t(A_r) = \frac{2D_{eff}}{\Delta z} \ln A_r + \sqrt{\frac{\alpha + v_t}{2}} \tag{3.9}$$

and

$$v_t(\Delta\phi) = \pm\sqrt{\alpha - 2\left(\frac{2\Delta\phi D_{eff}}{\Delta z}\right)^2} \tag{3.10}$$

where, $\alpha = \sqrt{v_t^4 + (8\pi D_{eff}/P)^2}$ (Hatch et al., 2006), Δz is the vertical separation between the two temperature measurements, D_{eff} is the effective thermal diffusivity, and P is the period of the thermal oscillation. The phase-based Equation 3.10 requires knowledge of the direction of flow, which we assume based on the sign of the velocity estimates resulting from Equation 3.9. To facilitate direct comparison with the subsurface flow velocities derived from hydraulic heads, the advective thermal velocity is converted to the Darcy velocity,

q, by:

$$q = \frac{\rho_b c_b}{\rho_w c_w} v_t = \left(n + (1-n)\frac{\rho_s c_s}{\rho_w c_w} \right) v_t \tag{3.11}$$

where ρ_s, ρ_w, and ρ_b are the sediment, water and bulk densities, respectively; c_s, c_w, and c_b are the sediment, water and bulk specific heat capacities, respectively; and n is the porosity. As Equations 3.9 and 3.10 are implicit, here we present explicit analytical equations for advective thermal velocity that, to our knowledge, have not been previously published:

$$\begin{aligned} v_t(A_r) = \frac{5\,a}{6} + &\left(\sqrt{\left(\frac{b - 4\,a^4}{16\,a} + \frac{55\,a^3}{216} \right)^2 - \frac{a^6}{46656}} - \frac{b - 4\,a^4}{16\,a} - \frac{55\,a^3}{216} \right)^{\frac{1}{3}} \\ &+ \frac{a^2}{36 \left(\sqrt{\left(\frac{b-4\,a^4}{16\,a} + \frac{55\,a^3}{216} \right)^2 - \frac{a^6}{46656}} - \frac{b-4\,a^4}{16\,a} - \frac{55\,a^3}{216} \right)^{\frac{1}{3}}} \end{aligned} \tag{3.12}$$

$$v_t(\Delta\phi) = -(c(-4c^2 + b))^{1/2}/(2c), \tag{3.13}$$

where $a = \frac{2D_{eff}\log(A_r)}{\Delta z}$, $b = \left(\frac{8\pi D_{eff}}{P}\right)^2$, and $c = \left(\frac{2\Delta\phi D_{eff}}{\Delta z}\right)^2$. Equations 3.9 and 3.10 are valid for $v_t \subset \Re$ and $A_r < 1$. In these equations, a positive velocity is in the upwards direction (i.e., GW discharge).

As the thermal dispersivity term is assumed to be negligible for the velocities in this study (Rau et al., 2012a), the effective thermal diffusivity coefficient is defined here as:

$$D_{eff} = \frac{k_f^n k_s^{1-n}}{\rho_b c_b} \tag{3.14}$$

where k_f is the water thermal conductivity and k_s is the matrix thermal conductivity. Table 3.1 contains the physical property values that were used in calculating D_{eff} for the velocity methods of Hatch et al. (2006).

The amplitude ratio and phase shift that characterise the vertical column thermal profiles can also be used to calculate the vertical advective thermal velocity, v_t, and effective thermal diffusivity, D_{eff} using the equations derived by McCallum et al. (2012):

$$v_t(A_r, \Delta\phi) = \frac{2\pi\Delta z\left((\ln A_r)^2 - (\Delta\phi)^2\right)}{P\Delta\phi\left((\ln A_r)^2 + (\Delta\phi)^2\right)} \tag{3.15}$$

and

$$D_{eff} = \frac{-2\pi(\Delta z)^2 \ln A_r}{P\Delta\phi\left((\ln A_r)^2 + (\Delta\phi)^2\right)} \tag{3.16}$$

For the method of Hatch et al. (2006), the porosity, heat capacity, and density of the porous medium were estimated for the field data based on a previous study (Rau et al., 2010) and were known explicitly for the modelled data. The approach of McCallum et al. (2012) requires no such material data. Calculating v_t by Equation 3.15 using the time-series data from the streambed portion of the coil installation is accomplished by taking the triangular matrices $A_r(z_a, z_b)$ and $\Delta\phi(z_a, z_b)$ as inputs to the equations and setting $\Delta z = z_a - z_b$ and $P = 1$ day. This analysis produces the triangular matrix $v_t(z_a, z_b)$ which shows the advective thermal velocity as calculated for all $z_a > z_b$ in the streambed.

To compare the performance of the three outlined velocity equations (3.9, 3.10 and 3.15), both field and modelled datasets are used. This will allow insight into how the methods behave for uncontrolled field conditions that may be encountered when investigating the near-subsurface, as well as under conditions where assumptions are violated.

3.2.3.3 Effects of varying Δz

As previously indicated, an advantage of the triangular matrices method is that the full spatial information is made available for visualisation through sequential analysis. The terms where $\Delta z = z_a - z_b$ is a fixed value correspond to those along a given diagonal in Figure 3.1. For example, given that the vertical resolution of the coiled FO-DTS field data is 0.880 cm, the terms where $\Delta z = 8.80$ cm (i.e., 10× the resolution step) are $M_{a+10,a}$ for a given matrix, M, where a is any valid index.

By selecting these data subsets at various fixed Δz values, we can investigate the effect that sensor separation has on experimentally resolving and characterising the spatial hydrodynamics of the hyporheic zone. This is useful for optimising the spacing of discrete temperature sensor array deployments, such as used in Rau et al. (2010) and Bianchin et al. (2010).

3.3 Results

3.3.1 Results from FO-DTS field deployment

Figure 3.4 summarises the temperature data as a function of depth and time recorded during 5 days of deployment at Maules Creek. During the first three days of measurement, predominantly clear weather conditions were observed. At about 14:00 on January 26th, light rain was recorded as a large storm system neared the Maules Creek catchment. The air-exposed FO-DTS measurements display a sudden drop in temperature around this time. As is obvious from the measurements, the daily temperature fluctuations and thermal effects of the change in local weather conditions are most pronounced in the data from the top 13.4 cm of the coil which, with the exception of the last two hours of measurement when the water rose rapidly, was exposed to the air. In the surface water, which represents the upper thermal boundary condition for the investigated zone, the temperature varied diurnally with a minimum of 22.2 °C and a maximum of 28.9 °C over the course of the FO-DTS measurements. As precipitation commenced and the air temperature decreased towards the end of the measuring period the magnitude of the diel variation and the average temperature of the surface water both decreased.

The amplitude of the diel temperature signal in the streambed generally decreases with depth (Figure 3.5); the isolated diel signal amplitude ranges from ~1.7 °C at $z > -5$ cm and ~0.21°C at $z \approx -60$ cm in the first 24-hour segment to ~0.47 °C at $z > -5$ cm and ~0.13 °C at $z \approx -60$ cm in the fourth 24-hour segment. Below $z \approx -30$ cm, the temperature signal strength decreases at a higher rate and the phase lag becomes greater than in the top 30 cm (Figure 3.5). Below $z = -60$ cm the diel signal strength becomes so weak that it is impossible to extract reliable phase data and velocity estimates become spurious. As diel signal strength is sufficiently higher than the measurement noise above $z = -60$cm, these depths allow for the clearest comparison of Equations 3.9, 3.10, and 3.15 in the triangular matrix technique.

The local hydrological conditions at the stream-aquifer interface at which the coiled FO-DTS was installed (Supplementary Figure 3.A) reached a new steady state at around the beginning of the second 24-hour FO-DTS measurement segment (Figure 3.4). Plausible ranges of the vertical and horizontal Darcy velocities (Figure 3.A) in the subsurface near the FO-DTS coil installation were estimated using hydraulic head data from bores EC 6, EC 7 and BH13-1 (Figure 3.2) in conjunction with slug test measurements of hydraulic conductivity, K, (upper estimate $K = 2.47\times10^{-3}$m/s; lower estimate $K = 1.77\times10^{-4}$m/s). These estimates provide an order-of-magnitude comparison for the velocities derived from the FO-DTS data. However, it should be noted that the true vertical Darcy velocities are likely to be on the lower end of the range as regions of lower hydraulic conductivity, K, not intercepted by the slug test will limit flow rates. Due to the proximity of BH 13-1 to the abstraction bore (BH-14), the hydraulic gradient between it and EC 6 will be high and decreasing with distance from BH 14 towards the stream, implying that the true horizontal Darcy velocity in the proximity of the FO-DTS coil is probably closer to the lower end of the estimated range.

3.3.2 *Triangular matrices with vertical Darcy velocity from field deployment*

Figure 3.6 shows the triangular matrices with Darcy velocities calculated using the $v_t(A_r)$, $v_t(\Delta\phi)$ and $v_t(A_r, \Delta\phi)$ for each temperature time-series data pair in the field FO-DTS data. Essentially, these vertical thermal velocity matrices are produced by using the matrices of Figure 3.5 as inputs in Equations 3.9, 3.10, and 3.15. The vertical Darcy velocities in the top section, 0 to ~ -25 cm, vary between methods: approximately -0.8 to -1.3 m/day by the $v_t(A_r)$ method, -4 to -12 m/day by the $v_t(\Delta\phi)$ method, and -2 to -10 m/day by the combined $v_t(A_r, \Delta\phi)$ approach. For clarity, it is worth noting that these ranges and the velocity scales displayed in Figure 3.5 differ as velocities outside these bounds are observed for z_a or $z_b \lesssim -25$ cm. From approximately -25 to -30 cm the velocities decrease in magnitude and from approximately -30 to -45 cm they attain values between -0.1 to -0.8 m/day for the $v_t(A_r)$ method, 0 to -1 m/day for the $v_t(\Delta\phi)$ method, and 0 to -1.5 m/day for the combined $v_t(A_r, \Delta\phi)$ method. Below about -45 cm the methods that employ phase show little discernible trend. Thus generally for all three methods in the top $\sim$25 cm of the streambed, we observe a larger magnitude of discharge than the region immediately below. The

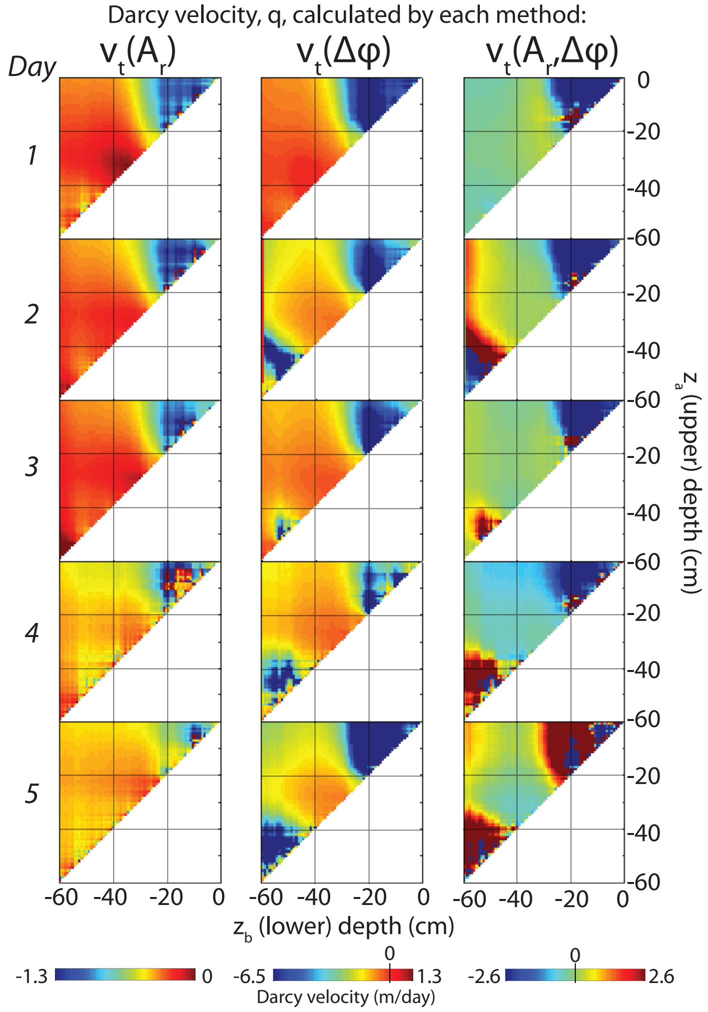

Fig. 3.6: Matrices showing the Darcy velocity, q, for the field FO-DTS data calculated by three methods: $v_t(A_r)$ (Equation 3.9), $v_t(\Delta\phi)$ (Equation 3.10), and $v_t(A_r, \Delta\phi)$ (Equation 3.15). Negative velocities denote a downwards direction of flux. Darcy velocities have been converted from advective thermal velocities by Equation 3.11. Note the different colour scales for each method.

results for the three methods generally differ throughout the domain during the measurement period. The $v_t(A_r)$ and $v_t(\Delta\phi)$ methods offer more consistent and less noisy results, particularly during days 1-3, when the signal-to-noise ratio was greater. Figure 3.7 shows the effect of fixed Δz separation corresponding to selected off-diagonal elements in the triangular matrices of Figure 3.6. This subset of the triangular matrix data illustrates the compromise between vertical resolution and noise.

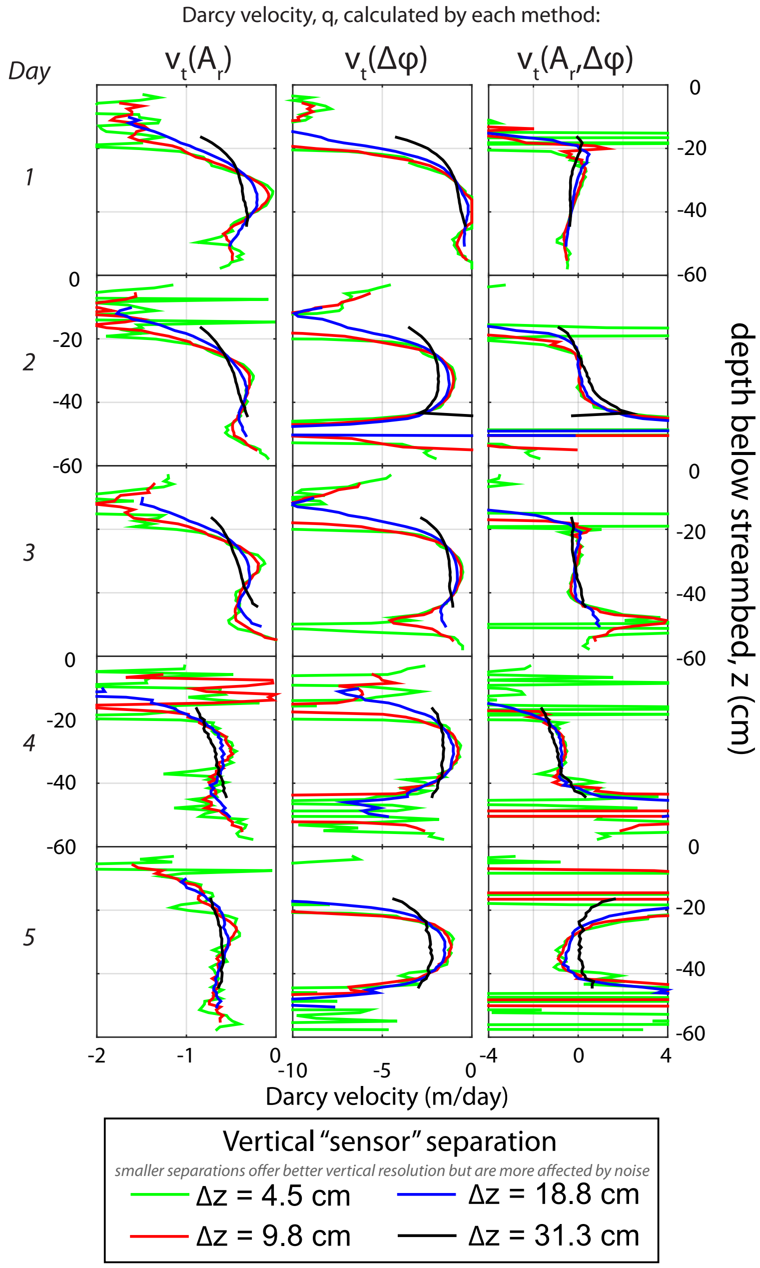

Fig. 3.7: Velocity profiles for the coiled FO-DTS field data calcuated at different Δz values with three methods: $v_t(A_r)$ (Equation 3.9), $v_t(\Delta\phi)$ (Equation 3.10), and $v_t(A_r, \Delta\phi)$ (Equation 3.15). These values correspond to the velocities along the k^{th} diagonal, where k corresponds to the fixed separation Δz between the upper and lower measurement, in Figure 3.6.

3.3.3 Triangular matrices with vertical Darcy velocity from modelled conditions

Figure 3.8 displays the results of the three velocity equations applied to the five modelled configurations described in Section 3.2.2.2 (difference maps have also been included in Supplementary Figure 3.B). Here, we can see the effects of heterogeneity and of a lateral flow component on the velocity calculations. We can also see how spurious results can be obtained when these techniques are blindly applied to an unsaturated zone.

For the models with the contrasting layer between -30 and -50 cm (Figure 3.8a–b), when z_a or z_b is located at the boundary of the contrasting zone the error was <10% for the $v_t(A_r)$ method at small Δz and decreasing with increasing Δz. Interestingly, the heterogeneous layer appears to affect velocity estimates in the amplitude ratio method to a lesser degree in downwelling conditions than in upwelling conditions, which may be due to the different nature of signal dampening in the two flow regimes. For the $v_t(\Delta\phi)$ method, a similar behaviour is seen, with an error of ~20% at small Δz and smaller errors with larger Δz. The $v_t(A_r, \Delta\phi)$ method overestimated the velocities by $\sim$ 12% where z_a and z_b are both located in the zone above or below the contrasting layer (i.e., no violation of assumptions). The contrasting layer had the effect of introducing relative errors of up to ~10%.

In the models with a lateral flow component (Figure 3.8c–d), the induced errors were $<$ 10% for all methods. While in the $v_t(A_r)$ and $v_t(A_r, \Delta\phi)$ methods the magnitude of the velocity estimates decreased with deeper z_a and z_b, in the $v_t(\Delta\phi)$ method the magnitude increased. In the vadose zone model (Figure 3.8e), we see that these methods are clearly not applicable to unsaturated conditions. This is due to the effect that the soil moisture-dependent thermal diffusivity, D_{eff}, has on the rates of heat transfer. For all of the conditions, with exception of the variable saturation for which none of the methods can be said to give reasonable results, the combined $v_t(A_r, \Delta\phi)$ method appears to generally overestimate the magnitude of the velocity although it is less affected by heterogeneous conditions.

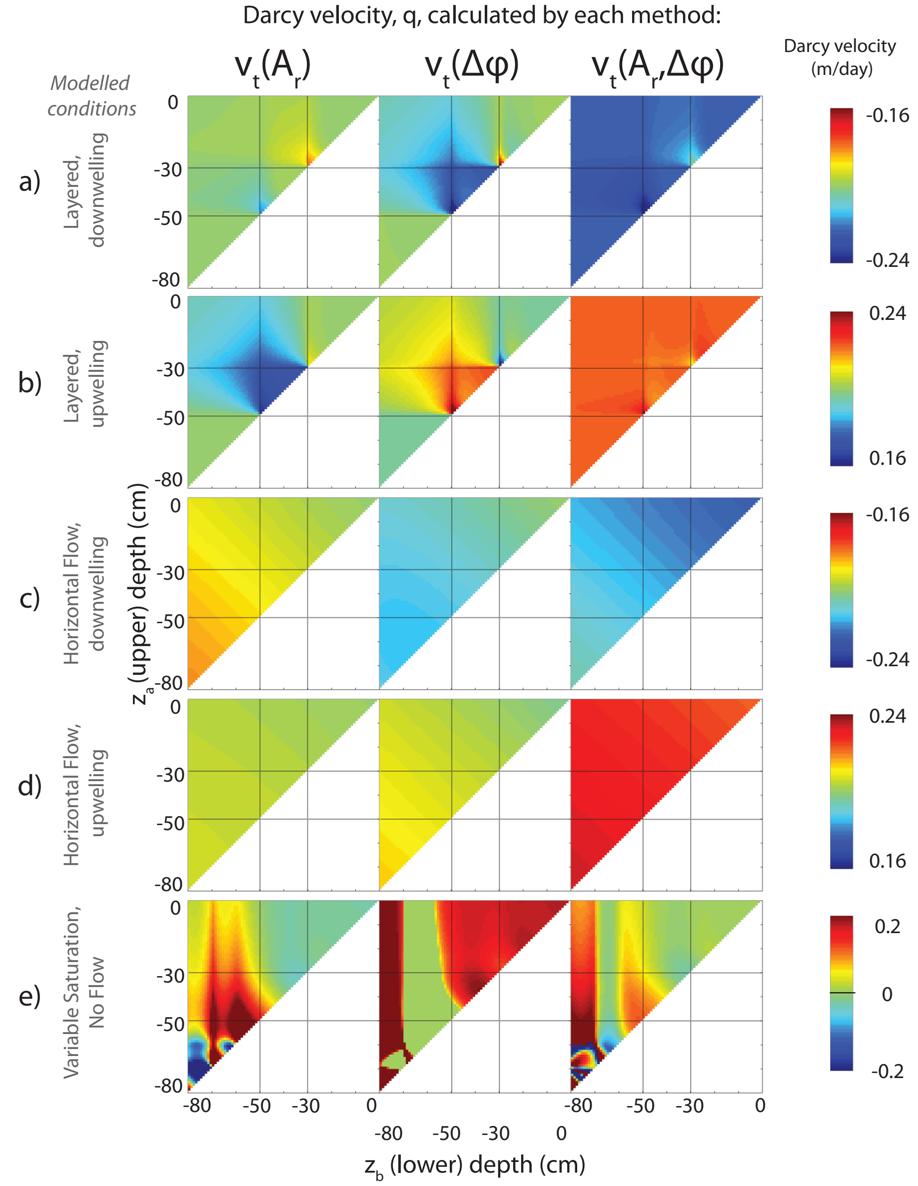

Fig. 3.8: Matrices showing the calculated velocities from all time-series pairs from the output of finite element models: a) $q_z = -0.2$ m/day with heterogeneous layer, b) $q_z = 0.2$ m/day with heterogeneous layer, c) $q_z = -0.2$ m/day with 0.1 m/day horizontal flow, d) $q_z = 0.2$ m/day with 0.1 m/day horizontal flow, and e) vadose zone with no flow. See Section 3.2.2.2.

3.4 Discussion

3.4.1 Triangular matrices increase the spatial information

Field estimations of groundwater recharge and discharge rates using vertical arrays of temperature time-series measurements have been demonstrated in many field deployments (e.g., Constantz et al., 2003a, Rau et al., 2010, Anibas et al., 2016). By coiling a fibre-optic cable around a cylinder in a method first demonstrated by Vogt et al. (2010), temperature measurements can approach a vertical continuum and a more detailed analysis of the variability of the shallow thermal regime and its usefulness for flux estimates in streambeds (i.e., the hyporheic zone) can be undertaken. Previous results, however, focused on a subset of sensor pairs and may have left some of the full spatial information embedded in the data unexploited.

Here, it is convenient to refer to a time-series measurement at a given depth as that of a virtual discrete temperature "sensor" at that depth. Triangular matrices are a useful way to expand on the spatial resolution and present the resulting large amount of data for direct comparison in four ways (Figure 3.1):

- fixed upper sensor location,
- fixed lower sensor location,
- fixed separation distance between the sensors, and
- the results from multiple velocity calculation techniques.

When visualised as colour or gradient plots, triangular matrices can facilitate a thorough assessment of the streambed thermal regimes and water fluxes.

The presented method of calculating amplitude ratios, phase shifts and advective thermal velocities in matrix form is a useful extension of the heat tracing analysis that has been performed by Vogt et al. (2010). For the FO-DTS data collected in this study, as the smallest virtual sensor spacing is 0.88 cm, this delimits the smallest possible value of Δz and gives 2211 unique pairings for the investigated depths $0 \geq z \geq -60$ cm. The triangular matrices provide a novel treatment of the data, allowing for the determined values of A_r and $\Delta\phi$ from all unique depth pairs to be used in matrix implementations of Equations 3.9, 3.10, and 3.15, thus exploring the potential of spatial information contained in coiled FO-DTS deployments, although it is important to note that not all sensor pairs will reveal meaningful results. Small separations, as illustrated in Figure 3.7, are notably prone to the effects of noise. At small Δz (near the diagonal in the matrix plots) errors may dominate resulting in decreased method sensitivity. At Δz of $\lesssim$4 cm, we sometimes observe $A_r > 1$ which is caused by an inadequate temperature signal-to-noise ratio. The matrix method, along with an analysis of the diagonals that represent fixed separations (Figure 3.7), can inform FO-DTS and discrete temperature sensor users of the trade-off between vertical resolution and the effects of noise for a given type of conditions and installation. Data below a certain depth will be dampened and its utility affected by low signal-to noise. This depth was deemed to be ~ -60 cm in our downwelling field example, but may be as shallow as ~ -20 cm (Briggs et al., 2012b) in certain conditions such as GW discharge.

3.4.2 Effects of common subsurface conditions on the velocity triangular matrices

In a purely vertical hydraulic flow field with a constant rate of recharge from the stream and homogeneous sediment conditions, the phase shift relative to the stream-streambed boundary is expected to be negative and increasing in magnitude at a constant rate with depth; however, this is seldom the case in field measurements such as our FO-DTS data (Figure 3.5) where positive phase shifts are seen at some small Δz. The apparent phase shift in Figure 3.5 is increasingly negative with increasing Δz at all time steps. The phase shift appears to be more sensitive than the amplitude ratio to lower signal strength in the deeper zone of the investigated depths. The implications of this are seen in the advective thermal velocity calculations involving $\Delta\phi$ where, at the deepest measurements and hence lowest signal-to-noise values (bottom left corners of matrices in second and third columns in Figure 3.6), the estimates vary more strongly with small changes to z_a or z_b.

Velocity results from the FO-DTS streambed deployment presented in Figure 3.6 exhibit interesting patterns that can reveal streambed processes or the presence of layering by comparison with results derived from numerically modelling common field conditions (Figure 3.8). However, in practice, application of this qualitative method may be complicated by the presence of multiple layers and depth-dependent horizontal flow. The datasets produced from the numerically modelled conditions allow for a controlled testing of the triangular matrices method. For example, in a system with a layer of contrasting thermal properties (Figure 3.8a–b), the above mentioned phase effect is more pronounced for the phase-derived velocity (second column in Figure 3.8). Where both z_a and z_b are either above or below the contrasting layer, the $v_t(A_r)$ and $v_t(\Delta\phi)$ equations correctly estimate the velocity. For all saturated model configurations (Figure 3.8a–d) the magnitude of the velocity is overestimated by the $v_t(A_r, \Delta\phi)$ equation. However, the layer with contrasting thermal and hydraulic properties appears to only affect results at the layer boundaries and has little effect on the velocity estimates elsewhere with this method. The error introduced by the layer is similar for both the upward and downward flux cases in the methods using $\Delta\phi$; however, the $v_t(A_r)$ method produces more consistent estimates in the downwelling case than the upwelling case, with significant errors only occurring for small Δz where both z_a and z_b are in or near the layer boundary. The effect of a lateral flow component shows as a small variation of inverted velocities with sensor depth (Figure 3.8c–d). The $v_t(A_r)$ and $v_t(\Delta\phi)$ methods result in $< 5\%$ error when compared to the true vertical velocity; the $v_t(A_r, \Delta\phi)$ gives errors up to $\sim$10%. While identification of horizontal flow may be possible, we believe the identification of layers and their depth ranges is one of the strongest capacities of the proposed method.

The heat tracing velocity equations studied here were developed for saturated conditions under the assumptions of 1-D flow and constant effective thermal diffusivity throughout the domain. Figure 3.8e clearly shows that variable saturation violates these conditions. However, these techniques could be blindly applied to field data if it was not known that an unsaturated zone had developed or that gas had accumulated in the streambed (Cuthbert et al., 2010). Even for the simple case of a stagnant unsaturated zone in a no-flow state (Figure 3.8e), the methods estimate a variety of erroneous non-zero flow rates. Our modelling shows that it is important to verify that streambed conditions are fully saturated.

3.4.3 Triangular matrices reveal vertical zones with different flow conditions

Field data (Figure 3.6) facilitates comparison of the different methods using amplitude and phase data separately (Hatch et al., 2006, Keery et al., 2007) or combining them (McCallum et al., 2012, Luce et al., 2013). Disagreement between velocity calculations from amplitude ratios and phase shifts has also been observed by Rau et al. (2010) at the same field site. Roshan et al. (2012) and Cuthbert and Mackay (2013) have shown that horizontal flow can cause disagreement, but only under conditions that cause thermal anisotropy (e.g., non-uniform flow). Further, Rau et al. (2012b) has shown in the laboratory that even homogeneous materials can induce non-uniform flow fields and non-uniform gradients through groundwater pumping that cause thermal anisotropy. Given that field observations show a heterogeneous streambed at this site, it is reasonable to conclude that thermal anisotropy due to non-uniform flow is present in the upper 20-30 cm of the streambed.

The $v_t(\Delta\phi)$ method performs poorer than the $v_t(A_r)$ method when applied to our FO-DTS data in determining flow rates for velocities close to zero (Figure 3.6). This is due to the singularity in $\frac{\partial\phi}{\partial v_t}$ as noted by Hatch et al. (2006) and Lautz (2010), although Roshan et al. (2012) supports the use of $v_t(\Delta\phi)$ in upwelling conditions. At larger Δz separations, only the $v_t(A_r)$ method results in estimates that vary smoothly with a spatial and temporal range of velocities that could be expected at this site. For comparison, vertical Darcy flux estimates from borehole data range between ~ -0.2 m/day and ~ -2.5 m/day with the lowest and highest hydraulic conductivity values (Figure 3.A). However, the true value is likely to be on the lower end of this range of estimates. This implies that the values obtained from the $v_t(\Delta\phi)$ and $v_t(A_r, \Delta\phi)$ equations are unlikely to be reliable. Only the $v_t(A_r)$ approach shows a discernible trend of increasing velocity over time (first column in Figures 3.6 and 3.7), as would be expected due to nearby groundwater abstraction. While small, this trend is also seen in the hydraulic head-derived q_{ver} data (Figure 3.A). By allowing D_{eff} to vary without constraint, the $v_t(A_r, \Delta\phi)$ method of McCallum et al. (2012) appears prone to producing large spatial and temporal variations in advective thermal velocities, and subsequently Darcy velocities, that may be unphysical. This lack of reliability in the phase-based velocity calculations in non-uniform conditions was also discussed by Lautz (2010), Roshan et al. (2012) and Cuthbert and Mackay (2013). Finally, when considering non-stationary temperature signals such those resulting from rapidly-changing flow regimes, it is important to remember that no analytical heat-tracing method will be able to offer complete accuracy in flow rate quantification (Rau et al., 2015).

By analysing the general form of the matrices in Figure 3.8 and applying this knowledge to the field data matrices (Figure 3.6), we can make the conjecture that both lateral flow and depth-dependent thermal properties may be present in the field data. A sharply contrasting layer may be present above ~ -20 cm and possibly another below -45 cm, although we would expect such a change to be evident by all three methods. The behaviour of the velocity estimates in the zone $-45 < z < -20$ cm (for both z_a and z_b) also indicates that lateral flow may be present, as is supported by the head measurements (Figure 3.A). Furthermore, the large magnitude of change in the apparent vertical Darcy velocity seen at the depth of around -20 cm from about -1.3 to -0.3 m/day by the $v_t(A_r)$ method (Figure 3.7) is impossible to explain if the flow at the location of the FO-DTS coil installation is truly 1-D and vertical. A relatively higher porosity and larger average grain size in this zone could cause the top layer to be more permeable, thus providing a thermal property contrast as well as a higher rate of lateral flow. Since the flow field was manipulated by nearby groundwater abstraction during FO-DTS deployment, this is highly likely. As a consequence of the groundwater abstraction, vertical gradients and horizontal gradients were observed in the aquifer near the creek (Figure 3.A), which indicate that flow near the FO-DTS device is not vertical along the coil. When lateral flow is present, hydraulic head evaluated at two depths may not represent two points on a flowpath continuum and therefore the calculation of Darcy flux is prone to error. In general, heat tracing may be advantageous in oblique flow fields due to heat signals being being propagated through all media and therefore across multiple flowpaths. It is likely that a combination of all of these factors contributes to the large change in the apparent vertical Darcy velocity seen at around -20 cm. The triangular matrices method, combined with the ability to measure continuous depth profiles using coiled FO-DTS cables, illustrates that variations in the flow field and streambed properties can be delineated from temperature data with high spatial resolution. Such observations, not easily made based on data from a small number of discrete temperature sensors, indicate that simplistic interpretations based on 1-D flow models may be invalid.

3.4.4 Effects of sensor spacing on velocity estimates

Figure 3.7 shows the vertical streambed flux calculated using different sensor spacings. Four values of Δz have been chosen from the matrix data (Figure 3.6) to explore the effect of small, large and intermediate "sensor" separation on velocity estimates using the field FO-DTS data in each of the three calculation methods. The data is plotted with the depth value corresponding to the mid-point between the depths of z_a and z_b; thus, the effect of the vertical separation between two temperature sensors on flux estimates can be directly compared. Here, it is obvious that velocities inverted from smaller values of Δz (4.5 cm) are prone to erroneous velocity variations caused by combination of the noisy nature of the FO-DTS data and the small changes in A_r and $\Delta\phi$ of neighbouring depths. For example, pairs of temperature time-series where the upper of the two has a weaker diel signal (i.e., $A_r > 1$) can violate the thermal advective velocity methods. Hence, there is a lower limit for sensor spacing at which velocity values become meaningless. On the other hand, large Δz values may under-resolve spatial variability in the zone of interest. This can lead to a smoothing effect where regions of contrasting streambed flow, as previously discussed, cannot be accurately identified because of excessive averaging over depth. The differing values of $v_t(z)$ calculated with varying Δz (Figure 3.7) can provide guidance for determining an optimal vertical separation of discrete temperature sensors in hyporheic zone experiments, such as those discussed by Constantz (2008). A researcher can optimize the quality of data obtained from a study with multiple discrete temperature probe arrays by adjusting the sensor spacing and depth according to information obtained by performing analysis as per the methods outlined here with data from a trial FO-DTS coil installation.

A separation of $\Delta z \gtrsim 10$ cm may be required to make accurate estimates of the vertical advective thermal velocity (and subsequently, vertical Darcy velocity), although this will depend on the grain size distribution in the sediment and the magnitude of the velocities. At the other extreme, a separation greater than 30 cm may under-resolve complex flow behaviour that may be present (Figure 3.7). Furthermore, vertical positioning of discrete measurement points, as used by many field studies (e.g., Rau et al. (2010), Jensen and Engesgaard (2011)), is often based on criteria involving practical instrument and installation considerations instead of previous knowledge about streambed zones. This demonstrates that FO-DTS or closely spaced discrete sensors in combination with triangular matrices evaluation offers a valuable way to investigate streambeds using heat as a tracer. For discrete installations of N temperature sensors, a matrix with $N(N-1)/2$ independent points can be calculated, so the triangular matrix method will offer an increasingly useful visualisation tool with a greater number of sensors. By evaluating and visualising all possible combinations of depth and spacing that can be achieved with a pair of temperature measurements, zones of distinct thermal regimes can be identified. Flux calculations can then be adapted to zones where conditions are appropriate for vertical flux estimations in order to optimise the results. The matrix method aids the assessment of the vertical streambed hydrodynamics using heat as a tracer. Further work in both the field and using laboratory experiments with controlled streambed hydraulic and flow conditions would aid in characterizing the limitations and abilities of triangular matrices in determining streambed thermal regimes and water fluxes.

3.5 Conclusions

A methodology for visualizing and using coiled FO-DTS datasets to delineate streambed thermal regimes, hydraulic properties, and water fluxes was developed. Three common methods for estimating SW-GW exchange fluxes with vertical temperature time-series measurements were compared and analysed using this methodology. As these models are based on pairs of measurements, the developed method results in triangular matrices that facilitate a comparison of behaviour of the methods as a function of sensor depths and spacing. The method was applied to both field and modelled data. The modelled data allowed for the visualisation of the behaviour of the three methods under variable saturation, sediment heterogeneity, and deviation from vertical flow. A detailed temperature profile with vertical resolution of $\sim$0.9 cm, recorded with a coiled FO-DTS setup allowed for five separate 24-hour periods to be analysed and conclusions about the presence of layers and non-vertical flow to be made. The advective thermal velocity equation that uses only the amplitude ratio as an input was the only method that resulted in fluxes consistent with those calculated from borehole hydraulic head data. The triangular matrix method is a novel visualisation technique and offers a complete treatment of high spatial resolution temperature data with various subsets of the data representing fixed separations or fixed upper or lower temperature measurement depths. By analysing fixed vertical separation subsets of these matrices, limits can be placed upon the separation of discrete temperature sensors for future installations for long-term monitoring. While the theoretical approach of phase-shift-based methods for the calculation of advective thermal velocities is sound, the large degree of variability of these results in time, depth, and Δz, shows that obtaining accurate velocity values via these methods proves challenging with field measurements.

Acknowledgements

Funding for this research was provided by the *National Centre for Groundwater Research and Training (NCGRT)*, an Australian Government initiative, supported by the *Australian Research Council* and the *National Water Commission*. Research infrastructure at Maules Creek is supported by *NCRIS Groundwater Infrastructure* (formerly *GEIF*), an Australian federal government scheme. The primary author also acknowledges the support by the *Fonds de recherche du Québec – Nature et technologies (FRQNT)* and the *Gary Johnston Fund*. We thank former and current UNSW staff and students; Mark Cuthbert, Andrew McCallum, Ander Guinea, Sam McCulloch, Hamish Studholme, Jonathan Frecker, and Helen Rutlidge; as well as Ben Gilfedder, Harald Hofmann, Nick Unland, Alexander Atkinson, and Matthew Yu of Monash University; for their assistance during the pumping experiment. We also thank Editor David Boutt and the anonymous reviewers for greatly improving the manuscript with their feedback.

3.A Supplementary Figures

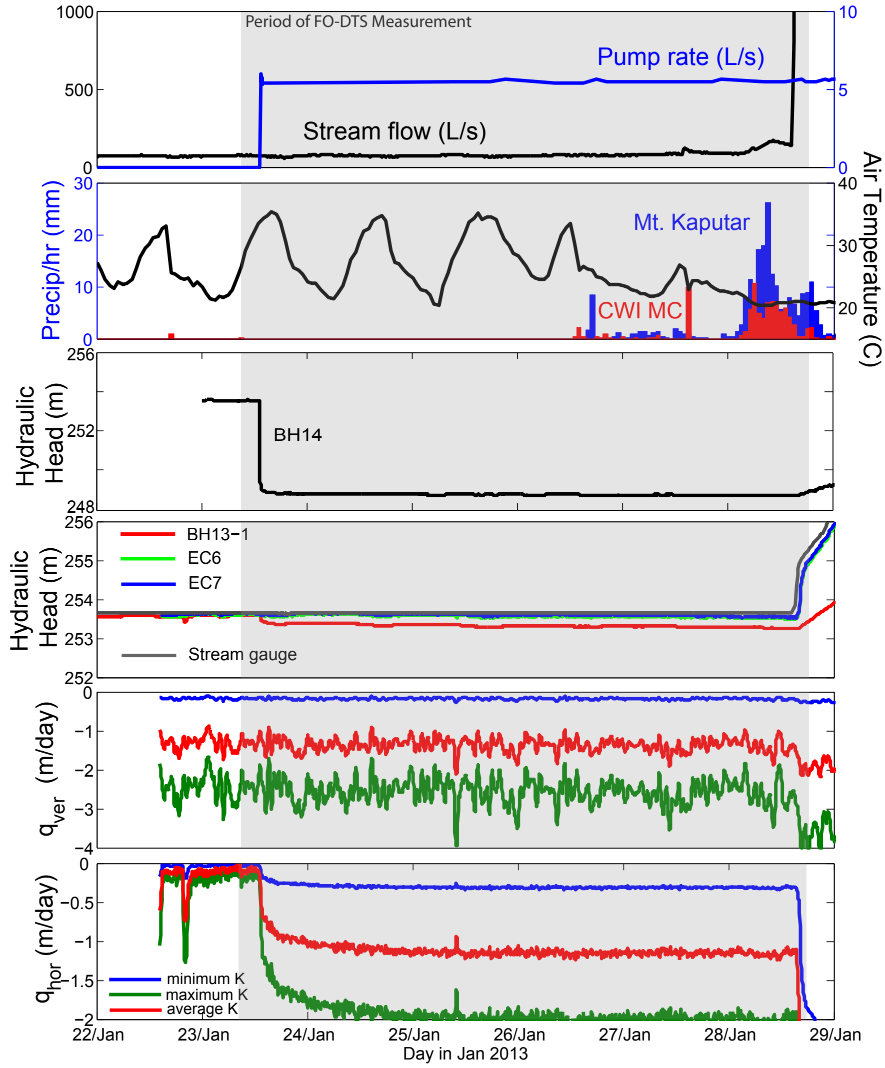

Fig. 3.A: Meteorologic and hydraulic data. For the precipitation data, Mt. Kaputar is in the upper catchment, while CWI MC is in the valley. Hydraulic head elevations are relative to the Geocentric Datum of Australia (GDA94). The vertical Darcy flux (q_{ver}) and horizontal Darcy flux (q_{hor}) estimates are from EC6 & EC7 and BH13-1 & EC6, respectively. Darcy velocities with the highest (2.47×10^{-3}m/s), lowest (1.77×10^{-4}m/s), and average (1.31×10^{-3}m/s) hydraulic conductivities are shown.

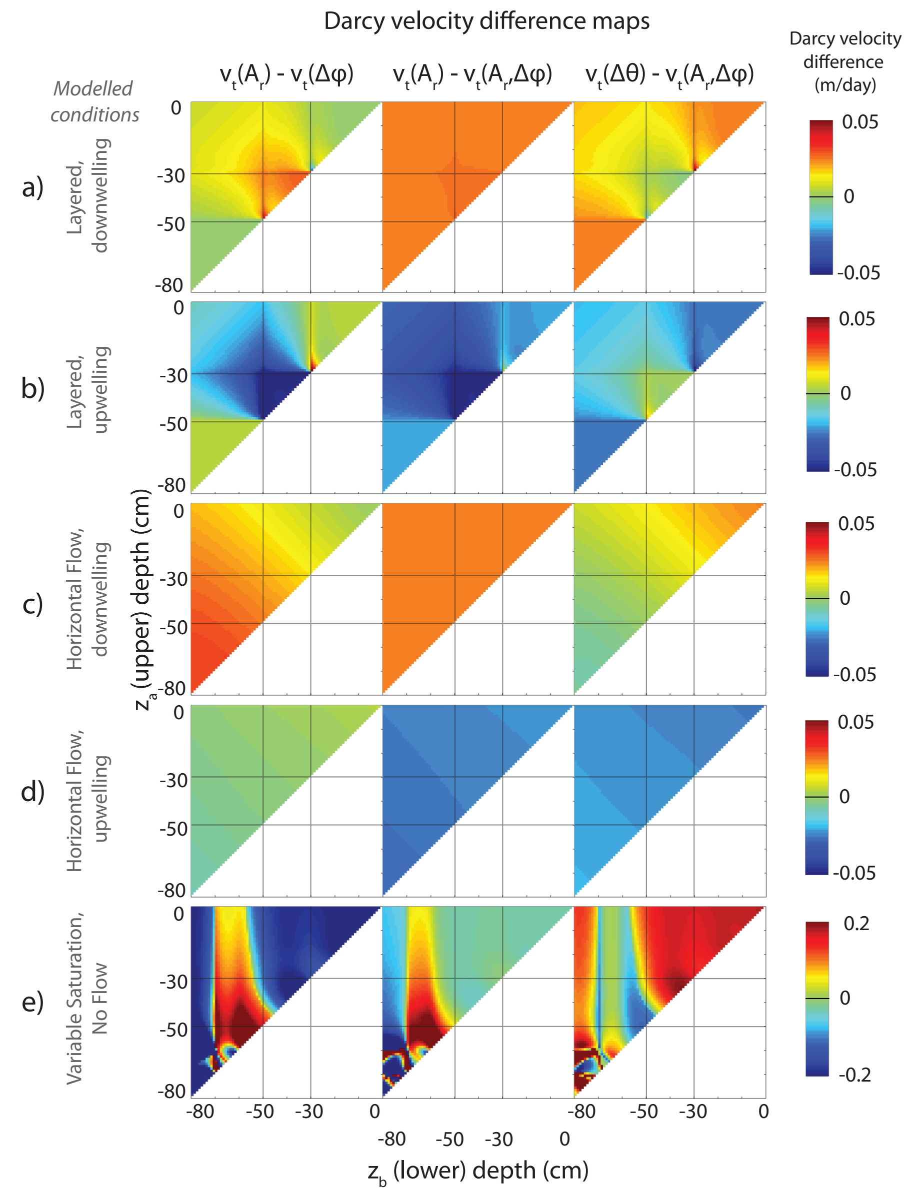

Fig. 3.B: Velocity difference maps for the modelled conditions. The diffence between the matrices in Figure 3.8 is shown.

4. SEMI-ANALYTICAL MODEL FOR VADOSE ZONE HEAT-TRACING

This chapter has been published as a journal article:
L.J.S. Halloran, H. Roshan, G.C. Rau, and M.S. Andersen (2016). "Calculating water saturation from passive temperature measurements in near-surface sediments: Development of a semi-analytical model," *Advances in Water Resources*, **89**, pp. 67-79. doi:10.1016/j.advwatres.2016.01.007

Abstract

A novel semi-analytical model for the calculation of water saturation levels in the near subsurface using passive temperature measurements is derived. The amplitude and phase of dominant natural diel temperature variations are exploited, although the solution is general so that a cyclical temperature signal of any period could be used. The model is based on the first-principles advection-conduction-dispersion equation, which is fully general for porous media. It requires a single independent soil moisture estimate, but directly considers the spatially variable saturation dependency of thermal conductivity which has been avoided in previous studies. An established empirical model for the thermal conductivity of variably saturated porous media is incorporated and two solutions for saturation are derived. Using data from numerical models, a spatially sequential implementation of one of these solutions is shown to predict the vertical saturation profile to within 2% for a hydraulically stable case and to within the saturation range observed over a single day for percolation rates up to 10 cm/day. The developed model and methodology can aid in the analysis of archived temperature data from the vadose zone and will serve as a powerful tool in future heat-tracing experiments in variably saturated conditions.

4.1 Introduction

Accurate transient measurements of soil moisture levels are of vital importance to investigations in the areas of agronomy (e.g., Brandt, 1992, Bolten et al., 2010), geochemistry (e.g., Rousseau et al., 2004, Robinson et al., 2009), and near-surface hydrogeology (e.g., Vereecken et al., 2010, Stewart et al., 2013). Many indirect methods of soil moisture measurement have been developed and are applicable at a large range of spatial and temporal scales (Robinson et al., 2008). Methods such as neutron probes (Bell, 1987), ground penetrating radar (Daniels et al., 1988), cosmic rays (Zreda et al., 2008), and time-domain transmissometry/reflectometry (Noborio, 2001) all offer benefits and disadvantages and no single method is applicable for all types of studies. At the sub-meter scale, time-domain reflectometer (TDR) and time-domain transmissometer (TDT) probes offer accurate measurements of water content in a variety of conditions and their use is widespread (e.g., Sleep et al., 2000, Rousseau et al., 2004). However, the cost of the multiple sensors needed to measure moisture content to a high degree of spatial resolution with these probes can be prohibitive. Furthermore, the probes also fail in environments with high pore water electrical conductivity, limiting their use in studies of coastal, estuarine or saline arid zones. Many TDT/TDR probes do not offer a spatial resolution on the scale of <10 cm due to the volume-averaging principle of the measurement. Temperature measurements, which are routinely performed during vadose zone studies, can provide another indirect method to measure soil moisture on the sub-meter scale with the potential for centimetre-scale vertical resolution.

The use of heat-as-a-tracer in surface water and groundwater studies has seen a large amount of interest over the past decade (see the reviews of Anderson, 2005, Constantz, 2008, Rau et al., 2014). Temperature offers the advantage of being relatively straightforward and inexpensive to measure automatically. High spatial resolution or large-scale measurements can be made through the use of fibre-optic distributed temperature sensing (FO-DTS) (Selker et al., 2006a), which can be deployed in a coiled configuration for fine (~1 cm) vertical resolution measurements (e.g., Briggs et al., 2012b, Vogt et al., 2012, Halloran et al., 2016d, and Chapters 3 & 5). Through analysis of the hydrothermodynamics of a system, time-series measurements of temperature can be used as a proxy for estimating other physical quantities, such as thermal diffusivity or vertical water exchange rates (Goto et al., 2005, Hatch et al., 2006, McCallum et al., 2012, Luce et al., 2013).

Thus far, the majority of work on heat-tracing in subsurface research has been limited to saturated conditions, although some investigations showing the potential for the expansion of the techniques to the unsaturated zone have been published. Béhaegel et al. (2007) extracted water content and saturation boundary depth from surface and 60 cm depth temperature time-series by two modelling approaches, finding acceptable results using monthly data and employing the Johansen (1975) model for effective thermal conductivity as a function of effective saturation, $k_e(S_e)$. Steele-Dunne et al. (2010) demonstrated the feasibility of using passive FO-DTS measurements to estimate soil moisture levels and, in turn, compared the performance of $k_e(S_e)$ models from Johansen (1975) and Campbell (1985). The simplified diffusion-only heat-transfer model used in the Steele-Dunne et al. (2010) study assumes that k_e is spatially uniform. Ciocca et al. (2012) provided a method for estimating S_e using active heating and coiled fibre-optic distributed temperature sensing cables. Bechkit et al. (2014) presented a study comparing TDR data and finite difference calculations based on time-series from platinum thermistors which confirmed the utility of heat tracing in estimating soil moisture. Research in the field of unsaturated zone heat-tracing is accelerating as evidenced by recent works (Dong et al., 2015b,a) that investigate the use of the Hydrus-1D model and data assimilation including a particle batch smoother to estimate soil moisture from temperature measurements.

A key aspect in estimating effective saturation (S_e), the degree of water saturation between 0 and 1, with temperature data is the dependence of thermal conductivity and heat capacity on temperature. While the dependence of volumetric heat capacity ($C_{v,e}$) can be calculated as a simple volumetric average of the materials present (i.e., the sediment, water and air), the relationship between temperature and thermal conductivity (k_e) is non-linear and material-dependent and must be investigated empirically. Much research exists in this field (e.g., Kersten, 1949, de Vries, 1963, Johansen, 1975, McCumber and Pielke, 1981, Campbell, 1985, Verhoef et al., 1996, Côté and Konrad, 2005, Lu et al., 2007) and multiple models have been proposed for various material classes. The $k_e(S_e)$ model proposed by Johansen (1975) saw widespread uptake since its formulation, but it did not accurately describe the relationship at low saturation levels. More recently, Côté and Konrad (2005) provided a generalized empirical model that can be inverted to obtain an explicit expression for effective saturation as a function of thermal conductivity.

Temperature in combination with the full heat transport equation offers an indirect and passive approach for measuring soil moisture content. The aim of this paper is to develop a new method for the quantification of soil moisture content in near-surface sediments by building on the fundamental physics that govern heat transport in the variably saturated subsurface (Figure 4.1). Previous efforts in determining soil moisture from natural temperature variations have primarily avoided an analytical approach and have not treated the thermal conductivity term as a quantity that varies spatially due to moisture content, leading to an incomplete consideration of the physics governing the coupling of soil moisture and temperature. We develop and propose a closed-form solution for soil moisture as a function of the amplitude and phase of cyclic temperature variations in the subsurface, akin to SW-GW exchange velocity solutions proposed by others (Hatch et al., 2006, McCallum et al., 2012, Luce et al., 2013). A first-principles approach is taken and, by incorporating the empirical model for thermal conductivity of Côté and Konrad (2005), we derive two explicit soil moisture solutions that depend on the spatial and temporal behaviour of the amplitude and phase of naturally occurring cyclical temperature signals. We then illustrate that our new method accurately predicts saturation profiles for certain implementations using numerically modelled temperature data. The developed method is a robust tool for estimating water saturation levels using natural temperature variations and avoids the assumption of constant thermal conductivity that prior studies have made. The semi-analytical model and outlined method of sequential implementation will aid future field studies in the near-surface vadose zone.

4.2 Method development

Throughout, parameters are defined as they are introduced. For quick reference, definitions of parameters and mathematical notation symbols can be found in Appendix 4.A.

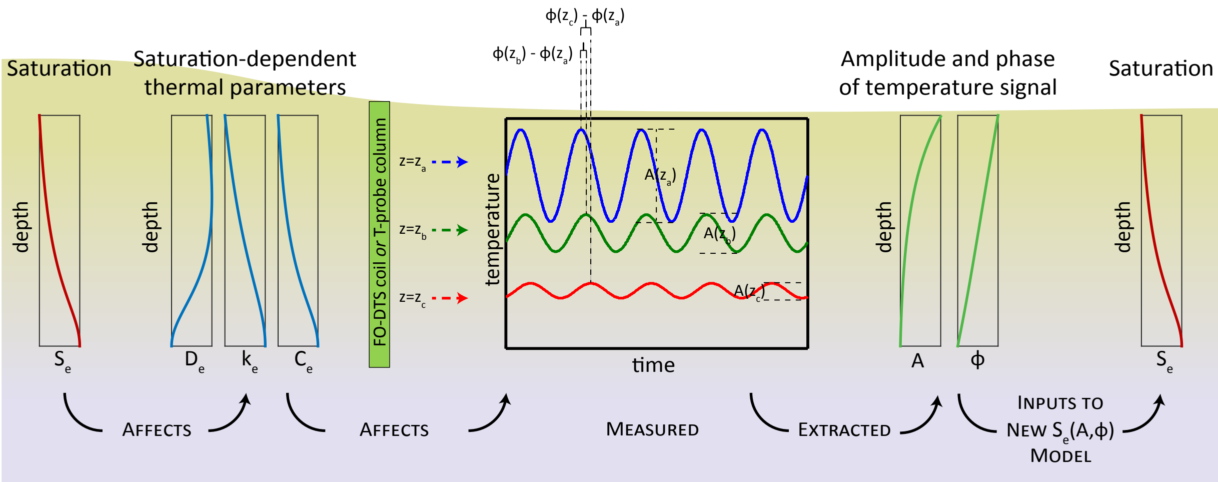

Fig. 4.1: Conceptual illustration showing the parameters dependent on saturation level, S_e, that govern thermodynamics in the vadose zone: effective saturation level, S_e; thermal diffusivity, D_e; thermal conductivity, k_e; and volumetric heat capacity, C_e. These parameters affect the behaviour of the temperature signal induced by the diurnal heating cycle at the surface. The amplitude, A, and phase, ϕ, of this signal are used to reconstruct S_e by the method developed in this study.

4.2.1 *Advection-conduction-dispersion equation with sinusoidal temperature*

The advection-conduction-dispersion heat equation describes the behaviour of thermal energy propagation in a porous medium (Nield and Bejan, 2013):

$$C_{v,e}(t,\vec{x})\frac{\partial T(t,\vec{x})}{\partial t} + C_{v,f}(t,\vec{x})\vec{v}\cdot\nabla T(t,\vec{x}) = \nabla\cdot\left[k_e(t,\vec{x})\nabla T(t,\vec{x})\right] \tag{4.1}$$

where T is temperature; $C_{v,e}$, the total effective volumetric heat capacity; $C_{v,f}$, the fluid (water) volumetric heat capacity; $\vec{v}$, the fluid velocity; and k_e, the effective thermal conductivity. In porous media, this equation is valid when there is no active heat source. We note that a simplified version of this equation, involving the assumptions $\vec{v} = 0$ and $\nabla k_e = 0$, is used in the approaches of Béhaegel et al. (2007) and Steele-Dunne et al. (2010):

$$\frac{\partial T(t,\vec{x})}{\partial t} = \frac{k_e}{C_{v,e}}\nabla^2 T(t,\vec{x}) = D_e\nabla^2 T(t,\vec{x}) \tag{4.2}$$

where D_e is the effective thermal diffusivity. For a typical range of values for sands (Chen, 2008), the inverse of function of $D_e(S_e)$ is non-unique (Figure 4.2).

This eliminates the possibility of a one-to-one D_e-to-S_e mapping function, even if we accept the unfounded assumption of $\nabla k_e = 0$.

Here, we base our derivation on first-principles (Equation 4.1) and assume that the temperature, T, at any given point in space, $\vec{x}$, varies sinusoidally in time with a fixed period, $P = \frac{2\pi}{\omega_0}$, where ω_0 is the angular frequency, and a spatially and temporally variable amplitude, A, and phase, ϕ:

$$T(t, \vec{x}) = A(t, \vec{x}) e^{i(\omega_0 t + \phi(t, \vec{x}))} \tag{4.3}$$

Because a continuous signal can be reconstructed from its Fourier decomposition, this assumption does not affect the generality of the derivation, although in practice other non-sinusoidal signal components may have an effect on results (Rau et al., 2015). By combining Equations 4.1 and 4.3 and isolating the real and imaginary parts (see Appendix 4.B for details of the derivation), we arrive at two independent expressions for thermal conductivity. The real part results in:

$$k_e = \frac{C_{v,e} A' + C_{v,f} \vec{v} \cdot \nabla A - \nabla k_e \cdot \nabla A}{\nabla^2 A - A(\nabla \phi)^2} \tag{4.4}$$

And the imaginary part gives:

$$k_e = \frac{C_{v,e} A(\omega_0 + \phi') + C_{v,f} A \vec{v} \cdot \nabla \phi - A \nabla k_e \cdot \nabla \phi}{2 \nabla A \cdot \nabla \phi + A \nabla^2 \phi} \tag{4.5}$$

4.2.2 *Empirical model of thermal conductivity*

The dependence of thermal conductivity on saturation does not follow a linear relationship and several empirical models of this relationship have been proposed. We recognize the models of Johansen (1975) and Lu et al. (2007), but base our derivations on that of Côté and Konrad (2005). While all three models perform well in sandy sediment, the model of Côté and Konrad (2005) allows for a closed-form $S_e(A, \phi)$ solution to be determined without mathematical approximation and also agrees with k_e measurements of others (e.g., Smits et al., 2010). Under certain assumptions that simplify Equation 4.1, these models may lead to solutions for S_e, but the formulation of the Côté and Konrad (2005) model allows for us to remain general at this point. In these models the normalized thermal conductivity k_r, proposed by Johansen (1975) (also known as the *Kersten* number) is useful:

$$k_e = k_{dry} + (k_{sat} - k_{dry})k_r \tag{4.6}$$

where k_{dry} and k_{sat} are the thermal conductivities of the dry and fully saturated sediment, respectively. Both Ochsner et al. (2001) and Hopmans et al. (2002) have presented foundational research on the empirical determination of k_e at varying levels of saturation.

Côté and Konrad (2005) recognized the limitations in the empirical formula of Johansen (1975) at low saturation and proposed a new model:

$$k_r = \frac{\kappa_c S_e}{1 + (\kappa_c - 1)S_e} \tag{4.7}$$

where κ_c is a material class parameter equal to 3.55 for unfrozen medium and fine sands and to 1.9 for unfrozen silty soils, clayey soils, silts, and clays (Côté and Konrad, 2005). Combining Equations 4.6 and 4.7, we obtain:

$$k_e = k_{dry} + (k_{sat} - k_{dry})\frac{\kappa_c S_e}{1 + (\kappa_c - 1)S_e} \tag{4.8}$$

We see in Equations 4.4 and 4.5 that the spatial derivative of the effective thermal conductivity is required:

$$\nabla k_e = \kappa_c(k_{sat} - k_{dry})\left[\frac{1}{(1 + (\kappa_c - 1)S_e)^2}\right]\nabla S_e \tag{4.9}$$

We also require the expression for effective volumetric heat capacity:

$$C_{v,e} = \epsilon S_{e,0} C_{v,f} + (1 - \epsilon)C_{dry} \tag{4.10}$$

where $S_{e,0}$ is a reference effective saturation level (see Equation 4.18), ϵ is the porosity, and C_{dry} is the volumetric heat capacity of the dry sand or other soil. This expression behaves linearly with effective saturation and ignores the volumetric heat capacity of air, negligible compared to that of soils or water.

4.2.3 Development of the saturation model

To determine the dependence of the effective saturation on cyclic temperature amplitude and phase, we combine Equation 4.4 with Equations 4.8 and 4.9:

$$\frac{1}{J}\left[H - \frac{MF}{(1+BS_e)^2}\nabla S_e\right] = G + \frac{FS_e}{1+BS_e} \tag{4.11}$$

where $B = \kappa_c - 1$, $F = \kappa_c(k_{sat} - k_{dry})$, $G = k_{dry}$, $H = C_{v,e}A' + C_{f,e}\vec{v}\cdot\nabla A$, $J = \nabla^2 A - A(\nabla\phi)^2$, and $M = \nabla A$. Similarly, with Equation 4.5 we obtain:

$$\frac{1}{P}\left[L - \frac{WF}{(1+BS_e)^2}\nabla S_e\right] = G + \frac{FS_e}{1+BS_e} \tag{4.12}$$

where $L = C_{v,e}A(\omega_0+\phi') + C_{v,f}A\vec{v}\cdot\nabla\phi$, $P = 2\nabla A\cdot\nabla\phi + A\nabla^2\phi$, and $W = A\nabla\phi$. We note the duality of these equations when the substitutions $H \leftrightarrow L$, $J \leftrightarrow P$, and $M \leftrightarrow W$ are made. Rearranging Equations 4.11 and 4.12, we obtain the partial differential equations:

$$(H-JG) + (2B(H-JG) - JF)\,S_e + \left(B^2(H-JG) - JFB\right)S_e^2 = MF\nabla S_e \tag{4.13}$$

and

$$(L-PG) + (2B(L-PG) - PF)\,S_e + \left(B^2(L-PG) - PFB\right)S_e^2 = WF\nabla S_e \tag{4.14}$$

To proceed further, we will reduce the analysis to a 1-D vertical case and parameterise the equations with the following:

$$\alpha_{1R} = H - JG \tag{4.15a}$$

$$\alpha_{2R} = 2B(H-JG) - JF \tag{4.15b}$$

$$\alpha_{3R} = B^2(H-JG) - JFB \tag{4.15c}$$

$$\alpha_{4R} = MF \tag{4.15d}$$

$$\alpha_{1I} = L - PG \tag{4.16a}$$

$$\alpha_{2I} = 2B(L - PG) - PF \tag{4.16b}$$

$$\alpha_{3I} = B^2(L - PG) - PFB \tag{4.16c}$$

$$\alpha_{4I} = WF \tag{4.16d}$$

The subscripts R and I indicate the substitutions in the Equations 4.13 and 4.14 which stem from the real and imaginary parts of Equation 4.32 (Appendix 4.B). Due to the identical form of Equations 4.13 and 4.14, we will discard the R and I subscripts to solve the differential equations. Rearranging, we obtain a general form of Equations 4.13 and 4.14:

$$\alpha_1 + \alpha_2 s + \alpha_3 s^2 = \alpha_4 \frac{ds}{dz} \tag{4.17}$$

where s is a variable taking the place of saturation level. To solve for s, we rearrange and integrate between two depths, z_0 and $z_0 + \Delta z$, and the corresponding saturation levels at theses depths, $S_{e,0}$ and S_e:

$$\int_{z_0}^{z_0+\Delta z} \frac{dz}{\alpha_4} = \int_{S_{e,0}}^{S_e} (\alpha_1 + \alpha_2 s + \alpha_3 s^2)^{-1} ds \tag{4.18}$$

This treatment implicitly assumes that the α terms are spatially constant for a given Δz separation. The implications of the assumptions are explored in Section 4.3. Evaluating Equation 4.18 and introducing the substitution $\beta_1 = \sqrt{\alpha_2^2 - 4\alpha_1\alpha_3}$, we obtain (see Appendix 4.C for proof of validity):

$$\frac{\Delta z}{\alpha_4} = \frac{1}{\beta_1} \ln\left(\frac{\beta_1 - 2\alpha_3 s - \alpha_2}{\beta_1 + 2\alpha_3 s + \alpha_2}\right)\Bigg|_{s=S_{e,0}}^{S_e} \tag{4.19}$$

This results in:

$$\frac{\beta_1 \Delta z}{\alpha_4} = \ln\left(\frac{\beta_1 - 2\alpha_3 S_e - \alpha_2}{\beta_1 + 2\alpha_3 S_e + \alpha_2}\right) - \ln\left(\frac{\beta_1 - 2\alpha_3 S_{e,0} - \alpha_2}{\beta_1 + 2\alpha_3 S_{e,0} + \alpha_2}\right) \tag{4.20}$$

By rearranging and introducing the substitution $\beta_2 = \frac{\beta_1 - 2\alpha_3 S_{e,0} - \alpha_2}{\beta_1 + 2\alpha_3 S_{e,0} + \alpha_2}\exp(\frac{\beta_1 \Delta z}{\alpha_4})$, we arrive at a general expression for effective saturation:

$$S_e = \frac{-\beta_2(\beta_1 + \alpha_2) + \beta_1 - \alpha_2}{2\alpha_3(\beta_2 + 1)} \tag{4.21}$$

Reintroducing the R and I subscripts, the following equations are obtained:

$$S_e = \frac{-\beta_{2R}(\beta_{1R} + \alpha_{2R}) + \beta_{1R} - \alpha_{2R}}{2\alpha_{3R}(\beta_{2R} + 1)} \tag{4.22}$$

$$S_e = \frac{-\beta_{2I}(\beta_{1I} + \alpha_{2I}) + \beta_{1I} - \alpha_{2I}}{2\alpha_{3I}(\beta_{2I} + 1)} \tag{4.23}$$

To apply these equations, in addition to the multi-depth temperature time-series data, measurements or estimates of sediment thermal properties k_{dry}, k_{sat}, ϵ and C_{dry} are required, as well as an independent single-point estimate of saturation, $S_{e,0}$, and an estimate of v for transient conditions (as outlined below). The long, explicit form of Equation 4.22 is available in Supplementary Material[1].

4.2.4 Estimation of velocity

The terms H and L in Equations 4.22 and 4.23 contain the parameter v. Thus, for periods when there is vertical flow, an estimate of velocity should be made. As the equations already require saturation to be known independently at one point, we propose a simple mass-balance estimate based on the soil water retention curve (SWRC) of van Genuchten (1980) calculated at two points in time using measurements of soil moisture at the surface interface, giving a first-order estimate of velocity. First, the van Genuchten SWRC is calculated (van Genuchten, 1980):

$$S_e^*(z) = \frac{1}{\epsilon}\left(\theta_r + \frac{(\epsilon - \theta_r)}{(1 + (\alpha_{vG} z)^{1/(1-m)})^m}\right) \tag{4.24}$$

where the parameters α_{vG}, m, and θ_r can be estimated from hierarchical models (e.g., Schaap et al., 2001), soil textural tables (e.g., Ghanbarian-Alavijeh et al., 2010), or some form of direct SWRC measurement (e.g., Nimmo, 1990, Šimunek and Nimmo, 2005). The independent value of S_e at the surface boundary is used

[1] `http://dx.doi.org/10.1016/j.advwatres.2016.01.007`

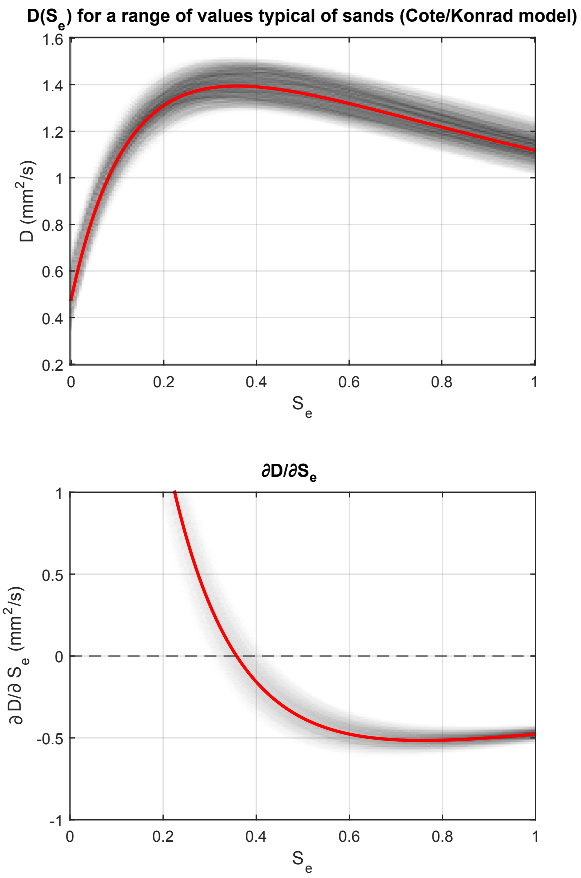

Fig. 4.2: Thermal diffusivity as a function of effective saturation and its first derivative, following the Côté and Konrad (2005) empirical model of thermal conductivity. The red line shows the model for average values of k_{dry}, k_{sat}, and ϵ. The intensity of the grey area corresponds to frequency that $D(Se)$ has a given value. These values (Table 4.1) are based on thermal parameters and uncertainties in Chen (2008).

to estimate the saturation curve $S_e^*(z, t = t)$ for the depth range of interest, $z_{min} < z < 0$ cm. A curve is also determined using the independent S_e measurement at a time Δt prior to the time of interest, $S_e^*(z, t = t - \Delta t)$. The difference of the two SWRC curves (the same curve, but shifted assuming different $S_e(z = 0 \text{ cm})$ values) is used to calculate a mass balance and estimate the average velocity:

$$v = \frac{\epsilon}{\Delta t} \int_{z_{min}}^{0} [S_e^*(z, t) - S_e^*(z, t - \Delta t)] \tag{4.25}$$

parameter	value
porosity ϵ	0.4043
unsaturated thermal conductivity k_{dry}	0.4013 W m^{-1} K^{-1}
saturated thermal conductivity k_{sat}	2.8325 W m^{-1} K^{-1}
water volumetric heat capacity, $C_{v,f}$	4.187 MJ K^{-1} m^{-3}
unsaturated volumetric heat capacity C_{dry}	1.942 MJ K^{-1} m^{-3}
van Genuchten parameter α_{vG}	4 m^{-1}
van Genuchten parameter m	0.5
van Genuchten parameter l	0.5

Tab. 4.1: Values of parameters (Chen, 2008) used to visualise the parameter space in Figures 4.3 and 4.4 and to generate synthetic data using a finite element model to test various implementations of the developed model (Figure 4.5).

This method gives a first-order estimate and will likely be unreliable during periods of rapid temporal change in flux ($\gtrsim$ 0.5 m d^{-2}) when non-stationarity also plays a role (Rau et al., 2015). Here it should also be noted that all passive heat-tracing methods relying on the dominant diel temperature signal are prone to error when transient conditions are experienced (Rau et al., 2015). In the vadose zone, these issues are exacerbated because the true velocity distribution in a variably saturated soil profile with a transient water table boundary is non-linear due to the dependence of hydraulic conductivity on saturation (Schaap and van Genuchten, 2006, Vereecken et al., 2010). There may be other possibilities for obtaining an estimate of v using independent S_e measurements from two points or by using hydraulic head measurements at some point in the soil profile. The proposed method of estimating v suffices for our testing of the semi-analytical model for $S_e(A, \phi)$ developed here (Equations 4.22 and 4.23) as it requires no additional information other than the soil type.

4.3 Method testing

4.3.1 Saturation equation parameter space

In order to understand the developed S_e model, it is useful to examine the parameter space using realistic physical values. To investigate the response of Equations 4.22 and 4.23, we use typical values for compacted sands from Chen (2008) (Table 4.1). The effective volumetric heat capacity is defined in Equation 4.10 and a dominant diurnal temperature signal is assumed ($\omega_0 = 2\pi$ day^{-1}). κ_c is set to 3.55 as prescribed by Côté and Konrad (2005) for unfrozen medium and fine sands.

In the visualisation of the $\nabla\phi$ and ∇A parameter space, we assume negligible fluid velocity, a constant rate of phase shift with depth (i.e., $\nabla^2\phi = 0$), and a temperature amplitude that decays exponentially with depth (z increases positively upwards):

$$A(z) = A_0 e^{z/\tau} \tag{4.26}$$

where τ is a decay constant we have set to 0.5 m. Therefore, the dependency $\nabla^2 A = \frac{\nabla A}{\tau}$ was used in investigating the parameter space. The displacement between the location of known reference saturation $S_{e,0}$ and the location of interest, Δz, is set to -0.1 m (Figure 4.3) and $+0.1$ m (Figure 4.4). This choice allows for a wide range of S_e values to be visualised and is on the order of typical sensor separations encountered in field temperature array installations. In the parameter space figures (Figures 4.3 and 4.4), unphysical values where $\Im(S_e) \neq 0$, $S_e > 1$, or $S_e < 0$ are not shown.

Figure 4.3 shows the parameter space of Equations 4.22 and 4.23 under the conditions $S_{e,0} = 0$ and $\Delta z = -0.1$. In this scenario, where the location of the known reference saturation $S_{e,0}$ is at a higher position than the location of interest, one expects the amplitude and phase gradient to be negative (equivalent to an amplitude ratio < 1 and a phase shift < 0). Thus, while it is useful to visualise the equations' responses over a large amplitude gradient and phase gradient parameter space, it is the third quadrant that contains physically meaningful values. Similarly, in Figure 4.4, $S_{e,0} = 1$ and $\Delta z = 0.1$, implying moving upwards from z_0, thus the physically meaningful values occur in the first quadrant where ∇A and $\nabla\phi$ are both positive. Figures 4.3 and 4.4 represent a small subset of the $S_e(A', \nabla A, \nabla^2 A, \phi', \nabla\phi, \nabla^2\phi, \vec{v})$ parameter space, but one that will be encountered in steady state systems where fully saturated or fully unsaturated conditions are seen.

4.3.2 Numerical test of the new saturation model

Here, multiple finite element models are used to test Equations 4.22 and 4.23. Implementation methods are first evaluated for a hydraulically

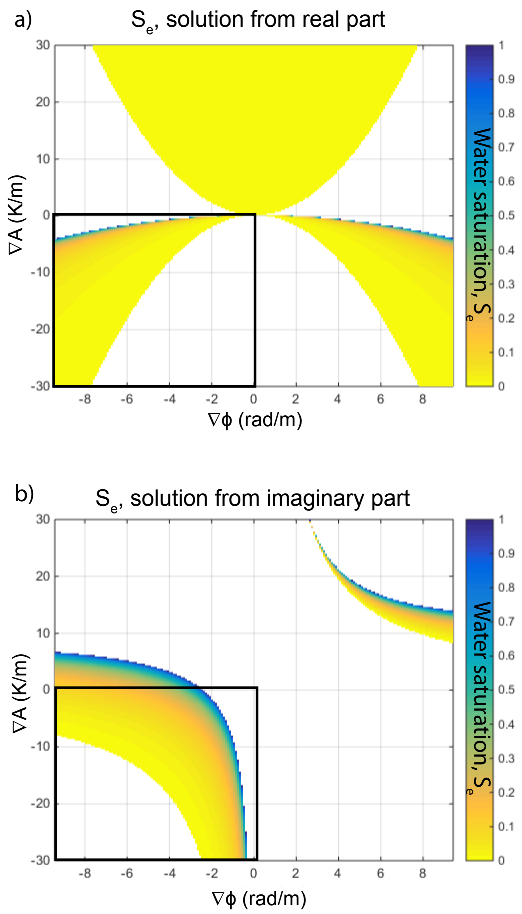

Fig. 4.3: The ∇A, $\nabla\phi$ parameter space of a) Equation 4.22 and b) Equation 4.23, where $\Delta x = -0.1m$ and $S_{e,0} = 0$. The third quadrant ($\nabla A < 0$, $\nabla\phi < 0$) contains the physically meaningful values.

stable case to determine the optimal type of implementation. Subsequently, the implementation that displays the best agreement with the true saturation profile for the stable case is tested with various hydraulically transient examples.

4.3.2.1 *Generating temperature data*

To evaluate the performance of the model, 2-D finite element (FE) models with zero velocity and with transient hydraulic conditions were constructed in COMSOL Multiphysics v5.0 (COMSOL, 2014), fully coupling both heat transport

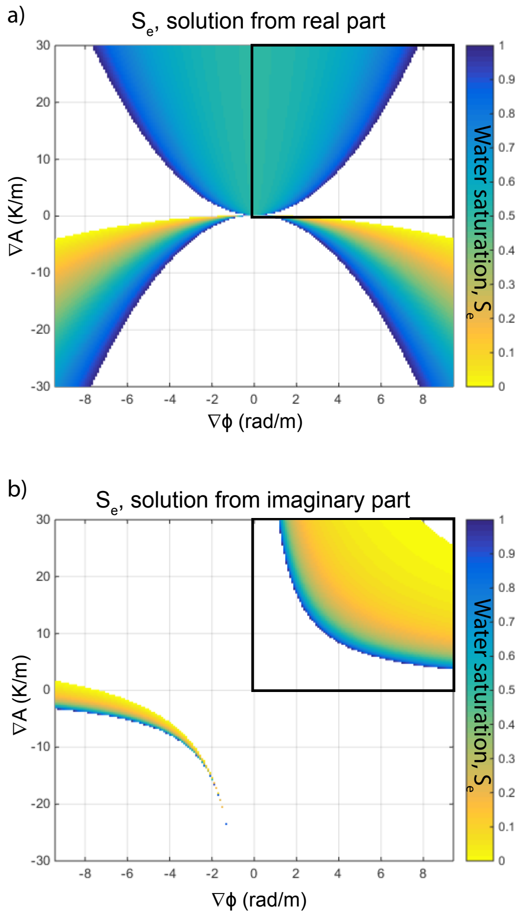

Fig. 4.4: The ∇A, $\nabla \phi$ parameter space of a) Equation 4.22 and b) Equation 4.23, where $\Delta x = 0.1m$ and $S_{e,0} = 1$. The first quadrant ($\nabla A > 0$, $\nabla \phi > 0$) contains the physically meaningful values.

in porous media and *Richard's* Equation. The FE modelling package takes into account the saturation dependence of thermal and hydraulic parameters both temporally and spatially. For the hydraulically stable model, the hydraulic head was set to -0.5 m, the modelled domain was extended to depth of 5 m below the water table and to a height of 0.5 m above the water table resulting in a vadose zone 0.5 m deep. The material parameter definitions were selected based on typical values for sands as in Section 4.3.1 (Table 4.1). The *van Genuchten* model (van Genuchten, 1980) was used for the soil moisture retention curve with realistic parameters for sandy sediment (Table 4.1).

The top boundary of the domain was subjected to a sinusoidal variation of temperature with a period of 1 day. As the diurnal mean temperature is constant and the amplitude of the temperature oscillations is <0.02% of that at the surface at 5 m depth, all other boundaries were insulated. The FE model was evaluated for a duration of 10 days with a time-step of 0.01 days and the saturation level and temperature exported at 1 cm intervals in the unsaturated portion of the column. The temperature amplitudes and phases were then evaluated at these locations by way of the discrete Fourier transform with a window length of 1 day, ending at the last time step.

The transient flux models were constructed in a similar manner, although the initial and bottom boundary hydraulic conditions differed. The transient condition was implemented as a time-dependent pressure head at the bottom boundary which resulted in selected percolation rates of −0.2, −0.1, −0.05, 0, 0.05, 0.1, and 0.2 m/day for the seven examples investigated here. For the positive rates, representing a rising water table, the initial saturation boundary was set to < -1.4m. For the negative rates, the model was set to be initially fully saturated. All numerical models were executed with at least 8 days of lead time to minimize potential artefacts from the constant temperature initial conditions. The methodology developed in Section 4.2 was evaluated at times where the saturation boundary was at −0.8 and −1.0 m below the surface to test different saturation conditions.

4.3.2.2 Implementing the new model

Firstly, we test four implementation methods of Equations 4.22 and 4.23 to evaluate the predictive abilities in stable conditions. In this case, as the FE model is in a steady-state hydraulically, A' and ϕ' are assumed to be zero and the spatial derivatives are evaluated finitely in the standard way:

$$p_z(i) = \frac{p(i) - p(i-1)}{\Delta z} \tag{4.27}$$

$$p_{zz}(i) = \frac{p(i+1) - 2p(i) + p(i-1)}{(\Delta z)^2} \tag{4.28}$$

for the i^{th} element, where $p = A$ or ϕ. Two methods of implementing Equations 4.22 and 4.23 are investigated: 1) with a single fixed $S_{e,0}$ for all depths and Δz equal to the separation of the depth of the reference saturation and the depths of interest, and 2) with a sequential approach, updating $S_{e,0}$ at each vertical step and fixing Δz to the vertical step size. Both implementations are applied top-down, starting from $z = 0$ m, and bottom-up, starting from $z = -0.5$ m. The first method involves setting a fixed "initial" saturation level $S_{e,0} = 1$ at depth $z = -0.5$ m below the top boundary for the bottom-up approach and $S_{e,0} = 0.447$, extracted from the FE model results, at $z = 0$ for the top-down approach. The spatial derivatives of A and ϕ are evaluated locally for each vertical step and Δz was stepped in increments of ± 1 cm. The second method makes use of a sequential approach with $\Delta z = \pm 1$ cm fixed and a continuously updating $S_{e,0} = S_e(i-1)$ for the i^{th} step. For each vertical step, $S_{e,0}$ is based on the estimate from the previous step but is limited to physically meaningful values $0 \leq S_e \leq 1$ to prevent runaway results. In the first vertical step in this sequential implementation, $S_{e,0} = 1$ for the bottom up approach and $S_{e,0} = 0.447$ for the top-down.

Secondly, we test the capabilities of the developed methodology in predicting the vertical saturation profile when positive and negative percolation rates are present. We verify that Equation 4.23 (stemming from the imaginary portion isolated in Equation 4.32) does not result in reliable estimates for the no-flux case, and thus focus on Equation 4.22. Here, A' and ϕ' are evaluated at each depth based on A and ϕ evaluated one periodic cycle (1 day) prior:

$$p'(t) = \frac{p(t) - p(t - \Delta t)}{\Delta t} \tag{4.29}$$

where $p = A$ or ϕ, $\Delta t = 1$ day, and t refers to the time of saturation profile estimation. Finally, the mass balance mean velocity estimate (Equation 4.25) is introduced to the top-down, sequential implementation of Equation 4.22 as discussed above. In general, the choice of differentiation evaluation methods (Equations 4.27–4.29), Δt, and Δz, as well as the velocity estimation method, may affect results (Anderson, 1995) and thus future studies may seek to investigate alternative numerical methods such as local polynomial fits to multiple data points. As a means for testing the developed semi-analytical model, the chosen method is sufficient as it represents a fundamental and widely-used numerical method for evaluating derivatives. Δt values are limited only by the sampling frequency and record length of the temperature time-series while the lower limit of Δz will be governed by the sensor spacing.

4.3.3 Results and discussion

Figure 4.5 displays the results of the implementation of Equations 4.22 and 4.23 by the above discussed methods for the no-flux case. The method of implementation has a pronounced effect on the results and it is clear that the S_e expression Equation 4.23 (dashed lines in Figure 4.5), derived by isolating the imaginary part of Equation 4.32, does not predict the saturation behaviour as accurately as that derived from the real part (Equation 4.22).

The local behaviour of A and ϕ and their derivatives at a given depth has a more pronounced effect in the fixed $S_{e,0}$ case (*b, c, f & g* in Figure 4.5). This is due to the greater sensitivity of the constructed β_2 term to larger Δz, as well as due to $C_{v,e}$, which depends on $S_{e,0}$, being prescribed a fixed value for all depths. The sequential implementations (*d, e, h & i* in Figure 4.5) more accurately predict the true saturation level. As with the fixed $S_{e,0}$ implementation, Equation 4.23 performs poorly; however, Equation 4.22 estimates the true S_e with <2% error for both the top-down (Figure 4.5*i*) and bottom-up (4.5*e*) approach over the entire depth range. By implementing the equations sequentially, the $S_{e,0}$ term and, subsequently, $C_{v,e}$ are updated at each step, allowing for errors to be minimized.

Equations 4.22 and 4.23 make use of different sets of derivatives of the sinusoidal temperature signal amplitude and phase. Both forms depend on A, ∇A, and $\nabla\phi$, but Equation 4.22 also depends on A' and $\nabla^2 A$, while Equation 4.23 also depends on ϕ' and $\nabla^2\phi$. Thus, there are two models: $S_e(A, \nabla A, \nabla^2 A, A', \nabla\phi)$, which we have shown can accurately predict effective saturation; and $S_e(A, \nabla A, \nabla\phi, \nabla^2\phi, \phi')$, which failed to accurately predicted effective saturation in the implementations investigated here. The assumption of local stability of phase behaviour in the derivation appears to be more sensitive than the assumption of amplitude stability. While the term $\nabla\phi$ appears in both Equations 4.22 and 4.23, the second spatial derivative $\nabla^2\phi$ appears only in Equation 4.23 which suggests that local stability of this sensitive term is easily violated. Analogies can be made with the heat-tracing seepage velocity

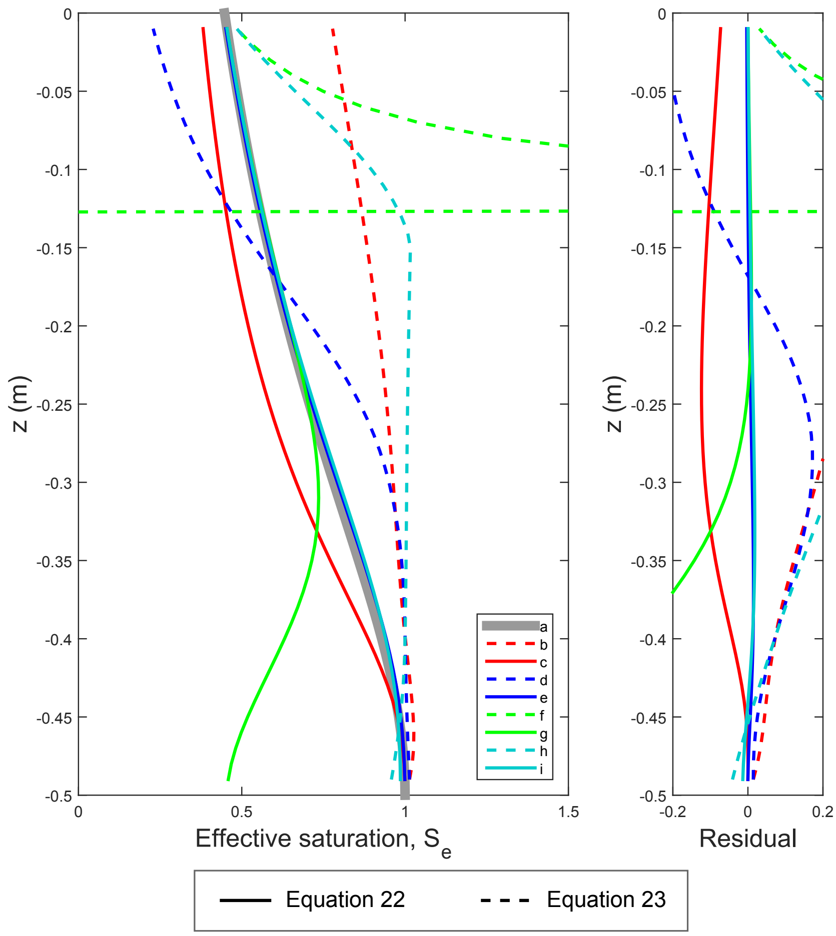

Fig. 4.5: Water saturation level, S_e, and the residual as estimated by Equations 4.22 (solid lines) and 4.23 (dashed lines) using various implementation methods. *a)* the true S_e from the fully-coupled finite element model; *b and c)* the method applied in an upwards direction with constant $S_{e,0} = 1$ based on the known value at $z = -0.5$ m and non-constant $\Delta z > 0$; *d and e)* the method applied sequentially in an upwards direction with $S_{e,0}$ based on the estimated value from the previous depth and $\Delta z = 0.01$m; *f and g)* the method applied in an downwards direction with constant $S_{e,0} < 1$ based on the known value at $z = 0$ m and non-constant $\Delta z < 0$; *h and i)* the method applied sequentially in an downwards direction with $S_{e,0}$ based on the estimated value from the previous depth and $\Delta z = -0.01$m

equations developed by Hatch et al. (2006). The phase-based velocity equation (6b in their work) is insensitive to the sign of the phase term, much like it is in Equation 4.22 and it has been observed that phase-based velocity equations do not perform as well as amplitude-based ones (Rau et al., 2010, Lautz, 2010, Jensen and Engesgaard, 2011, Roshan et al., 2012, Cuthbert and Mackay, 2013). As Equation 4.23, which depends on $\nabla^2\phi$, but not $\nabla^2 A$, performs poorer than Equation 4.22, this same phenomenon may also manifest itself in the vadose zone heat-tracing method presented here.

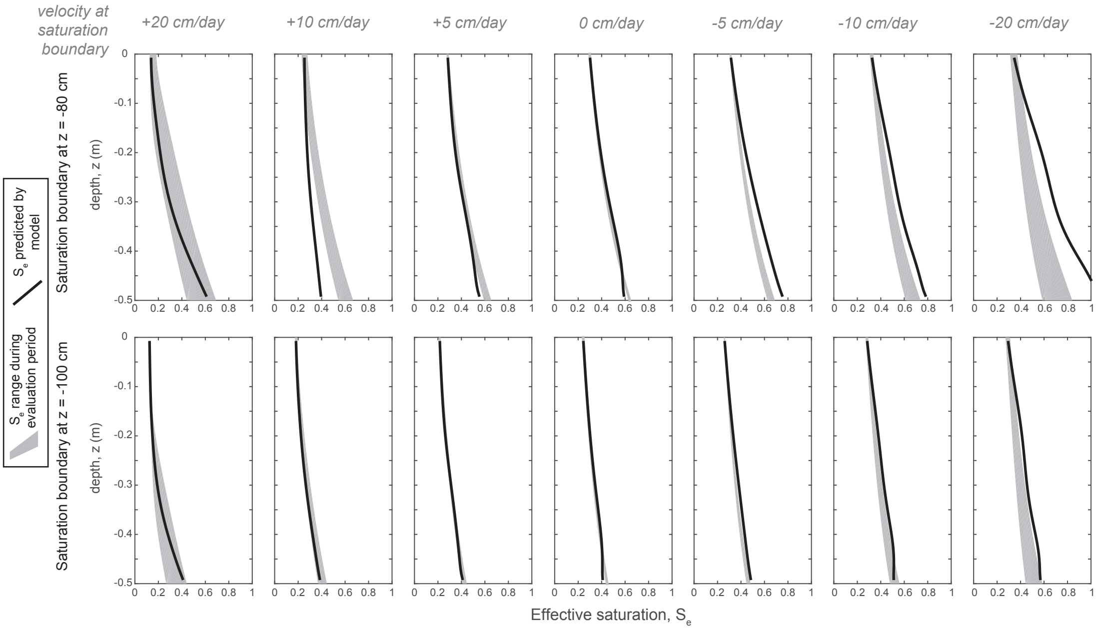

Fig. 4.6: Comparison of S_e from FE model output and from Equation 4.22 applied top-down with $S_{e,0}$ updated at each step. The grey shading indicates the range of values observed during the one-day period used for the evaluation.

As the sequential implementation of Equation 4.22 results in <2% error in the no-flow case, this method is further tested with the hydraulically transient example cases. The mass-balance velocity estimate method (Equation 4.25) is based on a single independent saturation measurement at $z = 0$ cm at a given time t and at $t-1$ day, so the analysis is restricted to the top-down case which corresponds to curve i in Figure 4.5. The method is tested at seven velocities and at two saturation boundary (water table) depths, -80 cm and -100 cm. The results (Figure 4.6) show that the method's agreement with the FE data is best at lower saturation levels and lower fluxes. Agreement between the saturation profile in the finite element model and that predicted by the method developed here is seen for all velocities except -20 cm/day when the saturation boundary is at -100 cm, and is also seen for $+5$ cm/day when the boundary is at -80 cm. As water velocity obeys a non-linear dependence on saturation level in the variably saturated zone, the simple mass balance treatment used here to estimate v may introduce error into the method at higher percolation rates. The actual velocity profiles for the example cases investigated in Figure 4.6 generally experience higher velocities at higher saturation levels when subjected to a given change in hydraulic head. This contributes to disagreement between the model and the FE data. Additionally, some of the discrepancy may stem from the violation of assumptions of local equilibrium. As fluxes in the unsaturated zone increase, these assumptions introduce greater error into the $S_e(A, \phi)$ profile calculations as there will be larger gradients of thermal properties and of velocity. Finally, because the calculations exploit the 1 day^{-1} frequency temperature oscillation which is dominant in natural systems, there will be a smoothing effect when transient conditions are experienced. In saturated zone heat tracing (e.g., Hatch et al., 2006, McCallum et al., 2012, Luce et al., 2013, Halloran et al., 2016d, and Chapter 3), transient hydraulic conditions have been shown to introduce thermal non-stationarity which affects velocity calculations (Rau et al., 2015). Here, transience in saturation rather than in water flux likely introduces non-stationarity.

4.3.4 Application considerations

The developed equations require saturation to be known at a given point in space. This is related to the non-uniqueness of saturation as a function of thermal diffusivity (Figure 4.2). A Monte Carlo sensitivity analysis was performed by allowing ϵ, v, $S_{e,0}$, k_{dry}, and k_{sat} to vary with a normal distribution around the true values with selected standard deviations (Figure 4.7). The simulation was performed on each parameter individually, as well as on all the parameters together (including and excluding $S_{e,0}$), for the first step in the top-down sequential implementation of Equation 4.22 (*i* in Figure 4.5) to show the relative importance of accurate measurements of the various parameters. The analysis shows, unsurprisingly, that an accurate determination of the value of $S_{e,0}$ has a large influence on subsequent estimates of S_e. Thus, in future applications of the developed method to field data, consideration will need to be given to ensure that saturation is known independently at one point or more along a temperature probe array installation. While installing a temperature probe column or coiled

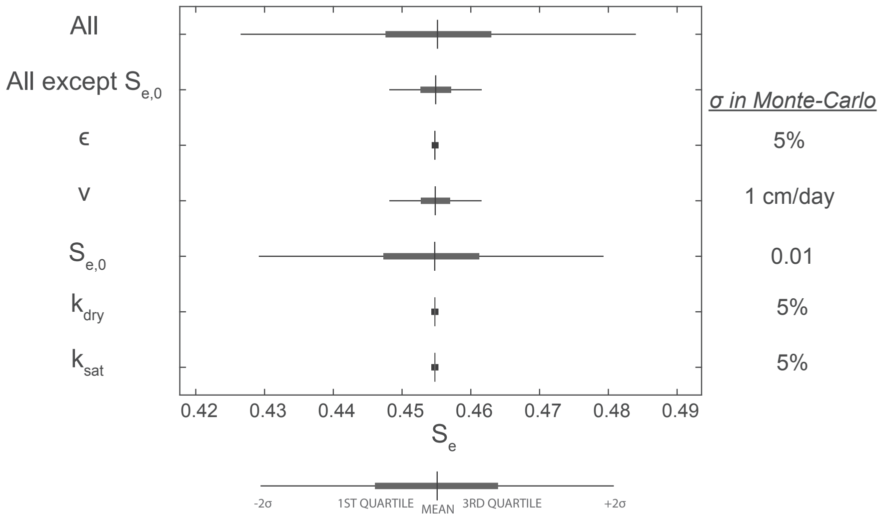

Fig. 4.7: The effects of uncertainty in physical parameters on the estimation of S_e. The error bars indicate the ±25% and ±47.7% (i.e., 2σ in the Gaussian distribution) uncertainties introduced by the stated error for each parameter. These error bars are indicative of the importance of accuracy in the measurements of each parameter. These values were determined in a $\Delta z = -1$ cm "top-down" implementation of Equation 4.22 (see Figure 4.5*i*) using a Gaussian distribution with the indicated standard deviations (σ) for each parameter in a Monte-Carlo simulation ($N = 1000$). For the "all" and "all except S_e" box plots, the parameters were treated as independent from one another.

FO-DTS to below the water table would ensure temperature measurements in the saturated zone and hence a known saturation level, our suggested velocity calculation method requires a saturated measurement. Thus the independent S_e measurement could be carried out by installing a moisture probe (TDR/TDT or other) or by making periodic surface measurements near the top of the soil profile. Knowledge of hydraulic head behaviour at the location could also be used to constrain velocity, although this would require deeper instrumentation installation. In cases where velocity estimates are impracticable, the developed method could still be employed for periods with stable hydraulic conditions.

If saturation can be reasonably estimated at one point, then Equation 4.22 provides a method for evaluating the vertical saturation profile from historical data, so long as there are more than three discrete temperature measurement points over depth, the minimum required to evaluate $\frac{\partial^2 A}{\partial z^2}$ and $\frac{\partial^2 \phi}{\partial z^2}$, although more temperature time-series will enable more accurate and detailed estimates. The model could also be used to estimate effective saturation in studies with periodic artificial heating or cooling where the dominant signal is not of a 1-day period. Note that the current model, and indeed all heat-tracing models in both the vadose zone and saturated zone, are best suited to steady-state hydraulic conditions (Rau et al., 2015) and only to depths where the relevant signal (in the case investigated here, $P = 1$ day) is strong enough to be measured accurately. Nonetheless, as the majority of our model derivation is in three dimensions, and sinusoidal temporal behaviour of temperature can allow the reconstruction of any signal via Fourier analysis, the model could find further use as a tool for thermal analysis of the shallow vadose zone. However, the weaker and higher-frequency non-diurnal signals will not penetrate as deep, compromising their use where measurement noise plays a role (Halloran et al., 2015a). As demonstrated (Figure 4.6), agreement between the method and data is best when lower levels of flux ($\lesssim$10 cm/day) are present or when the zone of interest is at a low saturation level. Thus, in locations where there are relatively stable hydraulic conditions or where the water table is $>$1 m below the surface, the developed method should be able to accurately predict subsurface saturation where material parameters are well constrained.

4.4 Concluding remarks

Effective saturation is a crucial control parameter for many hydraulic, biological and chemical processes. While it can be measured directly on a sub-meter scale via electromagnetic methods (Capacitance probes, TDR/TDT etc.) (Vereecken et al., 2008), these probes are ill-suited for distributed or fine-scale measurements and are not suitable for high-salinity environments. Temperature-based methods for estimating groundwater discharge and recharge rates are becoming widely used (Anderson, 2005, Constantz, 2008, Rau et al., 2014). A main advantage of temperature is that it is relatively straightforward to measure accurately and cost-effectively. Furthermore, it is a property that is routinely measured and of interest in many vadose zone and SW-GW interaction studies. The model and methodology outlined here further underscore the potential of temperature as a soil moisture tracer.

The proposed model, developed from the advection-conduction-dispersion equation and the thermal conductivity model of Côté and Konrad (2005), represents the first closed-form equations for the calculation of effective saturation from passive temperature measurements. It also includes a means for the integration of flux estimates which will allow it to be used during periods of subsurface percolation. Some previous studies (e.g., Béhaegel et al., 2007, Steele-Dunne et al., 2010) have assumed diffusion-only heat transport processes and have treated the physics in a simplistic way, although such an approach may yield valid results in steady-state hydraulic conditions. A rigorous comparison, under varied hydraulic and thermal conditions, of passive heat-tracing methods would embody an interesting future study. By comparing Equation 4.21 with the SW-GW flux heat-tracing equations developed by Stallman (1965), Hatch et al. (2006), McCallum et al. (2012), and Luce et al. (2013) one observes that the unsaturated zone introduces a greater level of complexity due to the highly non-linear dependence of thermal properties on effective saturation. Nonetheless, the proposed model can be used to estimate effective saturation profiles with reasonable accuracy as demonstrated. Various implementations of the equations were investigated and we conclude that the sequential implementation (i.e., with $S_{e,0}$ equal to the value calculated at the previous depth) of Equation 4.22 offers the most accurate predictions of effective saturation. We further tested the model under transient hydraulic conditions with the top-down sequential implementation that accurately reconstructed the soil water curve in the stable case and integrated a mass-balance estimate of velocity. These results showed good agreement between the predicted and true saturation estimates for lower levels of flux and when the water table was 50 cm below the depth range of interest. We envision this equation being used in applications where temperature time-series have been measured and estimates of effective saturation are needed at specific locations. This will likely include historic data which, when combined with other data (hydraulic head or, ideally, a single independent measurement of S_e) to constrain the saturation boundary and velocity, will profit from these methods to estimate S_e profiles. Finally, we hope that the derivation outlined in this work will inspire other researchers to develop methodologies and carry out field tests that further exploit the readily-measured parameter of temperature to study physical processes in the vadose zone.

Symbol	Definition and units
∇	del operator
$_z$	vertical partial derivative, $\frac{\partial}{\partial z}$ (subscript)
$_{zz}$	second vertical partial derivative, $\frac{\partial^2}{\partial z^2}$ (subscript)
$'$	temporal partial derivative, $\frac{\partial}{\partial t}$
$\Im$	imaginary part
$\Re$	real part
i	$\sqrt{-1}$
α_{vG}	van Genuchten constitutive relation constant (m^{-1})
θ_r	residual liquid volume fraction (unitless)
ϵ	porosity (unitless)
κ_c	Côté and Konrad (2005) parameter (unitless)
τ	decay constant (m)
ϕ	phase (radians)
ω	angular frequency (radians s^{-1})
A	amplitude of temperature oscillation (°C)
C_v	volumetric heat capacity (J m^{-3} K^{-1})
D	thermal diffusivity (m^2 s^{-1})
P	period (s)
S_e	effective saturation (unitless)
T	temperature (°C)
k	thermal conductivity (W m^{-1} K^{-1})
k_r	normalised thermal conductivity (unitless)
m	van Genuchten constitutive relation constant (unitless)
t	time (s)
$\vec{v}$ or v	velocity (m s^{-1})
$\vec{x}$	spatial vector (m)
z	vertical coordinate (m)
$_e$	effective, total (subscript)
$_f$	water (subscript)
$_0$	reference value (subscript)
$_{dry}$	dry sediment (subscript)
$_{wet}$	saturated sediment (subscript)

Tab. 4.2: Definitions of mathematical operators, variables, and subscripts.

Acknowledgements

We acknowledge support from the *UNSW School of Civil and Environmental Engineering*, the *Gary Johnston fund*, and the *Fonds de recherche du Québec – Nature et technologies (FRQNT)* dossier 173538. We thank Editor Graham Sander and the four anonymous reviewers for their insightful comments that have helped to produce a greatly improved manuscript.

4.A Symbol definitions

Symbols are defined in Tables 4.2 and 4.3.

Symbol	Definition
B	$\kappa_c - 1$
F	$\kappa_c(k_{sat} - k_{dry})$
G	k_{dry}
H	$C_{v,e}A' + C_{f,e}\vec{v} \cdot \nabla A$
J	$\nabla^2 A - A(\nabla\phi)^2$
M	∇A
L	$C_{v,e}A(\omega_0 + \phi') + C_{v,f}A\vec{v} \cdot \nabla\phi$
P	$2\nabla A \cdot \nabla\phi + A\nabla^2\phi$
W	$A\nabla\phi$

Tab. 4.3: Definitions of constructed parameters. α parameters are defined in Equations 4.15 and Equation 4.16.

4.B Derivation of first-principles expressions for k_e

Given the advection-conduction-dispersion equation (Equation 4.1) and assuming a temperature solution in the form of Equation 4.3, we combine the two equations to arrive at:

$$\begin{aligned}&C_{v,e}\left(A' + iA(\omega_0 + \phi')\right)e^{i(\omega_0 t + \phi)} + C_{v,f}\left(\vec{v} \cdot \nabla A + iA\vec{v} \cdot \nabla\phi\right)e^{i(\omega_0 t + \phi)} = \\ &\nabla \cdot \left[k_e\left(\nabla A + A\nabla(i\phi)\right)e^{i(\omega_0 t + \phi)}\right]\end{aligned} \tag{4.30}$$

Evaluating the divergence operator on the RHS, we obtain:

$$\begin{aligned}&C_{v,e}\left(A' + iA(\omega_0 + \phi')\right)e^{i(\omega_0 t + \phi)} + C_{v,f}\left(\vec{v} \cdot \nabla A + iA\vec{v} \cdot \nabla\phi\right)e^{i(\omega_0 t + \phi)} = \\ &\left[\left(\nabla^2 A + 2\nabla A \cdot \nabla(i\phi) + A\nabla(i\phi) \cdot \nabla(i\phi) + iA\nabla^2(\phi)\right)k_e + \left(\nabla A + A\nabla(i\phi)\right) \cdot \nabla k_e\right]e^{i(\omega_0 t + \phi)}\end{aligned} \tag{4.31}$$

Dropping the $e^{i(\omega_0 t + \phi)}$ terms from Equation 4.31 and simplifying, we obtain:

$$\begin{aligned}&C_{v,e}\left(A' + iA(\omega_0 + \phi')\right) + C_{v,f}\left(\vec{v} \cdot \nabla A + iA\vec{v} \cdot \nabla\phi\right) = \\ &k_e\left(\nabla^2 A - A(\nabla\phi)^2 + i(2\nabla A \cdot \nabla\phi + A\nabla^2\phi)\right) + \nabla k_e \cdot \left(\nabla A + iA\nabla\phi\right)\end{aligned} \tag{4.32}$$

By separating the real and imaginary parts and noting that A, ϕ, $C_{v,e}$, $C_{v,f}$, and k_e, as well as their derivatives, are purely real, Equation 4.32 can be rearranged in to two expressions. The real part is:

$$C_{v,e}A' + C_{v,f}\vec{v}\cdot\nabla A = \nabla k_e \cdot \nabla A + k_e(\nabla^2 A - A(\nabla\phi)^2) \quad (4.33)$$

and the imaginary part is:

$$AC_{v,e}(\omega_0 + \phi') + C_{v,f}(A\vec{v}\cdot\nabla\phi) = A\nabla k_e \cdot \nabla\phi + k_e(2\nabla A\cdot\nabla\phi + A\nabla^2\phi) \quad (4.34)$$

By rearranging these equations, we arrive at Equations 4.4 and 4.5. We note that in this appendix only the assumption of cyclic temperature behaviour has been made. Other assumptions (empirical k_e model, constant values of constructed α terms over Δz range, and homogeneous porous material) are documented where they occur in Section 4.2.3.

4.C Proof of validity of $\ln(\ldots)$ solution

In Equation 4.19, the $\ln(\ldots)$ solution is only valid when $\alpha_2^2 - 4\alpha_1\alpha_3 \geq 0$. The proof of this is presented here:
As per definitions: $\alpha_1 = H - JG$, $\alpha_2 = 2B(H-JG) - JF$, and $\alpha_3 = B^2(H-JG) - JFB$. $\alpha_2^2 - 4\alpha_1\alpha_3 \overset{?}{\geq} 0$
$[4B^2\alpha_1^2 - 4BJF\alpha_1 + J^2F^2] - 4\left[B^2\alpha_1^2 + BJF\alpha_1\right] \overset{?}{\geq} 0$
$J^2F^2 \overset{?}{\geq} 0$
J and $F \in \Re \therefore \alpha_2^2 - 4\alpha_1\alpha_3 \geq 0$

5. THERMAL REGIME OF A HIGHLY TRANSIENT, VARIABLY SATURATED SYSTEM

This chapter has been prepared for submission as a journal article:
L.J.S. Halloran, M.S. Andersen, and G.C. Rau (in preparation). "Heat transport dynamics in a tidally-driven variably saturated streambed."

Abstract

Temperature and moisture content in the variably saturated subsurface are two of the most important physical parameters that govern a variety of geochemical and biological processes. While progress has been made in extending the applicability of heat tracing to variably saturated conditions, highly transient systems such as intertidal streambeds remain a challenge due to non-linear coupling of non-stationary processes which complicates the heat transport calculations. Here, we present distributed temperature and discrete saturation depth profiles in a transect encompassing an intertidal section of a homogeneous sandy streambed. Thermal properties of the sediment were measured and the soil water retention curve was quantified using a centrifuge. Additionally, a fully-coupled thermal-hydraulic finite element (FE) model was developed taking into account the saturation dependence of thermal conductivity and this model was constrained by surface field data. Spectral analysis of the temperature measurements reveals the rapid decay of the tidally-driven temperature forcing within the top $\sim$30 cm of sediment. FE modelling reveals the complexity and transience of the shallow heat transport processes and quantifies the temporal evolution of water saturation and temperature throughout the domain. While the maximum depth of the investigated variably saturated zone is shallow ($<$20 cm), we demonstrate the significance of considering saturation-dependent thermal conductivity when streambed heat fluxes and storage are quantified. This

approach and these results will improve modelling of subsurface biogeochemical processes that depend on temperature and saturation levels.

5.1 Introduction

Sediment moisture content and temperature are arguably two of the most important physical parameters affecting many biological and geochemical processes in the vadose zone that are of interest in hydrology (e.g., van de Griend et al., 1985, Berndtsson et al., 1996, Jackson, 2002, Robinson et al., 2009, Vereecken et al., 2010, Stewart et al., 2013, Nimick et al., 2011) and soil science (e.g., Brandt, 1992, Davidson and Janssens, 2006, Bolten et al., 2010, Guntiñas et al., 2012, Perreault et al., 2013). For example, dependence on temperature and moisture content is observed in growth and transport of bacteria in the variably saturated subsurface (e.g. Russell et al., 2012), which is the habitat with the highest density of prokaryotes in particular (Or et al., 2007). Physical and chemical processes such as soil respiration (e.g., Lloyd and Taylor, 1994) and chemical volatilisation (e.g. Cohen and Ryan, 1989) are also strongly dependent on temperature and water saturation and thus modelling of these types of processes requires estimates of both parameters.

Temperature is a routinely recorded parameter that can now be measured at centimetre-scale spatial resolution using coiled fibre-optic distributed temperature sensing (FO-DTS) (e.g., Vogt et al., 2012, Briggs et al., 2012b, Halloran et al., 2016d, and Chapter 3) or, at a resolution of several centimetres, with arrays of small probes (e.g., Rau et al., 2012b, Bechkit et al., 2014). Fine-scale measurements of *in situ* moisture content at field sites present a greater challenge. Electromagnetic methods such as time-domain reflectometry (TDR) and transmissometry (TDT) offer accurate measurements of water content in a variety of conditions and their use is widespread (Robinson et al., 2003, Vereecken et al., 2008). However, where resolution on the $\lesssim$10 cm scale or where distributed measurements are desired, the cost of measuring the moisture content to an acceptable degree of spatial resolution or coverage using these probes can be prohibitive. The probes also fail in environments with high pore water electrical conductivity, limiting their use in coastal, estuarine, or saline arid zone applications. Their installation is also intrusive and can modify the hydraulic properties of the subsurface.

The use of heat-as-a-tracer in surface water and groundwater investigations has seen a large amount of interest over the past decade (e.g., Anderson, 2005, Constantz, 2008, Rau et al., 2014, Halloran et al., 2016b, and Chapter 2) and some promising investigations using heat tracing techniques in the variably saturated zone have recently been undertaken (Béhaegel et al., 2007, Sayde et al., 2010, Steele-Dunne et al., 2010, Krzeminska et al., 2012, Ciocca et al., 2012, Bechkit et al., 2014, Falocchi et al., 2015, Halloran et al., 2016c, and Chapter 4). For most passive methods that use natural temperature fluctuations, temporal resolution will be limited to one day when using the dominant diurnal signal. Active methods may offer better temporal resolution, but introduce another level of complexity in field installations and may be limited in applications at small spatial scales. In order to accurately estimate sub-diel time-scale dynamics and estimate moisture content within a metre-scale zone of interest, another approach is needed.

Tidally-affected streams offer an ideal setting for studying highly transient hydraulic and thermal processes and for testing the limits of modelling approaches based on surface measurements. The intertidal zone is also of interest to ecologists who seek to understand eutrophication and nutrient processes, as well as contaminant loading fluxes and degradation, and their ecological effects (e.g., Valiela et al., 1997, Bowen et al., 2007). Temperature measurements have been used to investigate SW-GW exchange in tidal rivers (Henderson et al., 2009, Bianchin et al., 2010) and intertidal zones (Befus et al., 2013). However, these studies dealt exclusively with saturated conditions where thermal properties can be considered constant. As processes in the intertidal zone are often affected by partially drained domains, an understanding of variably saturated conditions is important for appropriate assessments. Coupled modelling of variable-saturation thermal and hydraulic processes can be used to provide a better understanding of these dynamics in intertidal zones and, by extension, improve models of other temperature- and saturation-dependent processes.

Here, we investigate thermal and hydraulic processes in a tidally-affected variably-saturated shallow streambed by using field measurements and finite element (FE) modelling. Tidally-affected streams pose challenges for existing field and numerical methods as they are highly transient, have variably saturated zones, and may experience high salinity. The studied location (Acworth and Dasey, 2003, Acworth et al., 2006, Sadat-Noori et al., 2015, Sanders et al., 2015) exemplifies the type of system where established analytical heat-tracing and moisture content estimation methods break down due to the non-stationarity of the processes (Rau et al., 2015) and the intermittently high pore water electrical conductivity. Thus, fine vertical resolution data from coiled FO-DTS and discrete temperature measurements can be used to compare the streambed penetration depths of cyclic temperature signals attributable to tidal and diurnal mechanisms.

We also present a fully-coupled thermal and hydraulic model of a 2-D transect encompassing the intertidal zone of a natural streambed. We constrain our model with measurements of surface water and air temperature and surface water level, as well as with measured thermal and hydraulic properties. Further, we compare the model results with subsurface time-series measurements of temperature and variable sediment moisture to understand limitations of the approach. The moisture results are used to demonstrate that the highly non-linear dependence of thermal conductivity on saturation (e.g., Côté and Konrad, 2005, Lu et al., 2007, Halloran et al., 2016c, and Chapter 4) must be considered when near-surface temperature- and moisture-dependent phenomena such as heat fluxes are quantified. Additionally, frequency-domain time-series analysis techniques are used to compare the relative strengths and penetration depths of tidal and diurnal temperature signals in the streambed.

5.2 Methodology

We conducted *in situ* field measurements of temperature and moisture content in the bed of a tidally-forced stream. The temperature measurements are analysed to determine the relative effects of diurnal heating and tidal influences. The thermal and hydraulic behaviour of the system is simulated in a coupled Richards' equation/heat transport 2-D FE model. Measured and modelled data are compared with one another to reveal and quantify the limitations when variably saturated conditions are neglected. The moisture content predicted by the FE model is used to make improved estimates of vertical heat flux and energy storage. First, we report the details of the field measurements. This is followed by the modelling approach and by the determination of parameters required to model a variably saturated system.

5.2.1 Field measurements

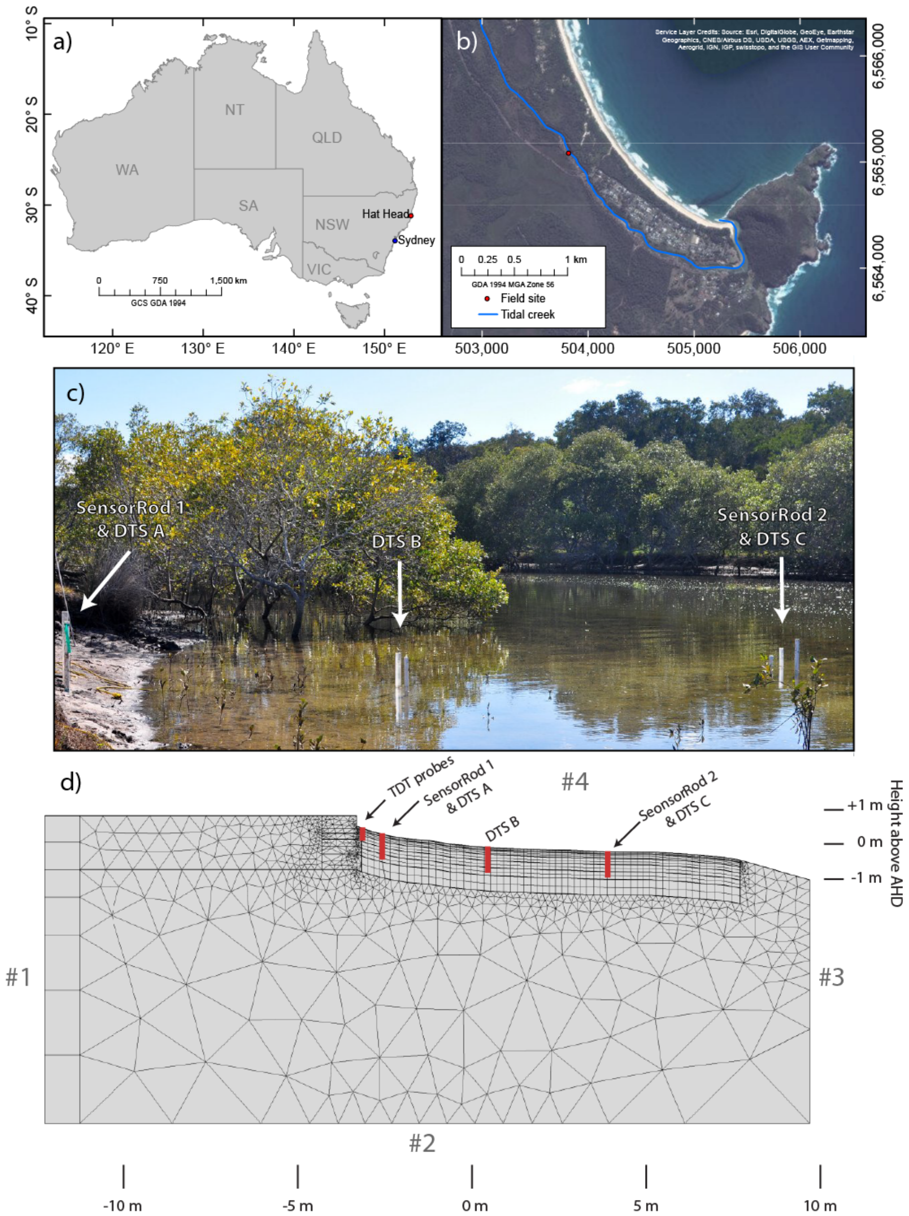

Fig. 5.1: a & b) Location of the field site at Korogoro Creek, Hat Head, NSW, Australia; c) The investigated transect viewed looking north; d) The modelled cross-section showing the finite element mesh with numbered boundaries and the relative locations of the temperature probes and the sediment moisture probes. The elevation relative to AHD is also shown.

The field site on Korogoro Creek at Hat Head (NSW, Australia) (Figure 5.1), approx. 2.6 km upstream from the Pacific Ocean, was chosen because the local surface water level is tidally-affected and the near-surface sediment consists of well-sorted sand (Acworth and Dasey, 2003). The site is exposed to the complex behaviour of diurnal thermal and tidal water level fluctuations and, consequently, highly transient water and heat flow conditions. These site characteristics do not lend themselves to established analytical heat-tracing methods (e.g., Keery et al., 2007, Hatch et al., 2006, McCallum et al., 2012, Luce et al., 2013). It is thus an ideal area to develop a coupled thermal-hydraulic FE modelling approach, alternative time-series analysis methods, and the use of vertical high-resolution temperature profiles to quantify the shallow thermal regime. Field work was carried out at Korogoro Creek Between May 12-19, 2014.

Vertical temperature profiles were recorded at three locations in the studied transect (Figure 5.1c & d). Both discrete sensors and coiled FO-DTS were employed. Temperature probe arrays (SensorRods) (Naranjo and Turcotte, 2015) containing iButton probes at separations of 0.0, 7.5, 20, 37.5, 57.5, and 80 cm (relative to the top sensor) were installed in two locations using a pointed drive head and downwards force. Both SensorRods were installed with the top sensor even with the sediment-water/air interface and no net change in sediment level was noted during the measurement period.

Temperature profiles were also recorded by coiled FO-DTS (e.g., Vogt et al., 2012, Halloran et al., 2016d, and Chapter 3) (Figure 5.1c & d) with a vertical resolution of $\sim$8.7 mm. The coiled sections of each of the three coiled installations were $\sim$100 cm in height. A pipe with non-recoverable pointed drive-head was used to create a guide bore for the FO-DTS coils during installation. Lengths of fibre-optic cable ($\sim$ 25 m each) connecting the Sensornet Oryx FO-DTS acquisition unit and the coils to one another were placed in a continuously agitated and cooled calibration bath with an accurate temperature reference to provide a two-point calibration for each coil. The SensorRods logged regularly at 5 minute intervals and the FO-DTS recorded at 10 minute intervals with the notable presence of multiple gaps of 15-200 minutes duration due to intermittent cuts to the power generator.

The surface water level and temperature were recorded at 15 and 5 minute intervals, respectively. The surface water temperature was recorded with a fully submerged Xylem EXO-2 probe along the transect. Air temperature measurements were obtained from the nearest weather station $\sim$20 km to the west at Kempsey, NSW (Australian BoM Site 059007). The surface water level was measured relative to the Australian Height Datum (AHD) at a location $\sim$1.8 km downstream on Korogoro Creek (Manly Hydraulics Lab Site 206465) and reached a minimum of -49.2 and maximum of 96.6 cm during the measurement period.

Sediment moisture measurements were recorded using Acclima Digital TDT sensors. Due to the periodic high salinity of the surface water caused by the tidal movement of brackish water in the creek, sediment moisture measurements could only be obtained when the net fluid electric conductivity (EC) was lower than a cut-off level of 1 S/m as implemented in the probe. The sensors were buried at heights of 45.9, 41.8, 36.0 and 31.5 cm relative to the AHD (depths of 2.0, 6.1, 11.9, 16.4 cm relative to the local sediment surface) at a distance of $\sim$60 cm from the FO-DTS coil A and SensorRod 1 along the transect (Figure 5.1d). The installation of the TDT probes required significant digging, and hence disturbance, of the creek sediments.

5.2.2 Time-series analysis

As our dataset includes both regularly and irregularly sampled data, a selection of methods are employed to determine the components of the signals. For regularly sampled data such as those from the SensorRods, the temporal evolution of different frequency components can be quantified using synchrosqueezing (Daubechies et al., 2011), an empirical mode decomposition-like tool (Huang et al., 1998) specifically designed for non-linear and non-stationary data. This can allow for the disentanglement of multiple components in a signal whose amplitudes may vary independently in time.

Fourier and wavelet time-series analysis methods are ill-suited for our FO-DTS data which has gaps due to interruptions to the mobile power source. For these irregularly sampled data, we employ the *Lomb-Scargle* periodogram (Lomb, 1976) to evaluate the power spectrum. Also known as least-squares spectral analysis, this technique allows for the calculation of the amplitudes of the various frequency components and returns a significance value so that ill-defined values can be excluded. As in other frequency-analysis methods, this occurs when signal-to-noise ratios are lower, such as observed in deeper installations where the surface boundary-driven signal is greatly attenuated.

5.2.3 Coupled thermal-hydraulic finite element modelling

Definitions and units of mathematical variables and their subscripts are found in Table 5.1, except where explicitly stated in the text.

5.2.3.1 Hydraulics of the variably saturated zone

We assume here that intertidal sediments do not undergo any significant deformation during a tidal cycle and thus consider only hydraulic and thermal processes while ignoring poromechanic physics. The behaviour of moisture flow in porous media under variably saturated conditions can be described by the mixed form of Richards' equation (Richards, 1931, Celia et al., 1990):

$$\frac{\partial \theta}{\partial t} - \nabla \cdot (K_e(H_p)\nabla H_p) - \frac{\partial K_e}{\partial z} = 0 \tag{5.1}$$

where θ is volumetric water content; t, time; K_e, effective hydraulic conductivity; H_p, pressure head; and z, the vertical coordinate. This equation is highly non-linear due to the dependence of hydraulic and material properties on saturation level and pressure. The van Genuchten soil water retention curve (SWRC) equations allow for the analytical definition of hydraulic properties at negative pressures $H_p < 0$ (van Genuchten, 1980) (i.e., unsaturated conditions):

$$\theta = \theta_r + S_e(\epsilon - \theta_r) \tag{5.2}$$

$$S_e = \frac{1}{(1 + |\alpha H_p|^{\frac{1}{1-m}})^m} \tag{5.3}$$

$$C_m = \frac{\alpha m}{1-m}(\epsilon - \theta_r) S_e{}^{\frac{1}{m}} (1 - S_e{}^{\frac{1}{m}})^m \tag{5.4}$$

$$K_e = K_{sat} K_r = K_{sat} S_e{}^l \left[1 - (1 - S_e{}^{\frac{1}{m}})^m\right]^2 \tag{5.5}$$

where $theta_r$ is residual moisture content; S_e, effective saturation; ϵ, porosity; C_m, specific moisture capacity; K_{sat}, saturated hydraulic conductivity; and K_r, relative permeability. In the case where $H_p \geq 0$, it is assumed that $\theta = \epsilon$, $S_e = 1$, $C_m = 0$, and $K_r = 1$ and these expressions reduce to the Darcy equation.

The parameters α, m, and l, usually referred to as the van Genuchten

Symbol	Definition and units (SI)
α	Van Genuchten constitutive relation constant (m^{-1})
β^*	smoothing function (unitless)
θ	water content (unitless)
θ_r	residual liquid volume fraction (unitless)
ϵ	porosity (unitless)
κ_c	Côté and Konrad (2005) parameter (unitless)
ρ	density (kg m^{-3})
ω	angular velocity (s^{-1})
C_v	volumetric heat capacity (J m^{-3} K^{-1})
C_m	specific moisture capacity (m^{-1})
H	hydraulic head (m)
H_p	pressure head (m)
K	hydraulic conductivity (m s^{-1})
K_r	relative permeability (unitless)
L_c	coupling length scale (m)
S_e	Effective saturation (unitless)
T	temperature (°C)
g	acceleration due to gravity (m s^{-2})
h	heat transfer coefficient (W m^{-2} K^{-1})
k	thermal conductivity (W m^{-1} K^{-1})
k_r	normalized thermal conductivity (unitless)
l	Van Genuchten constitutive relation constant (unitless)
m	Van Genuchten constitutive relation constant (unitless)
$\hat{n}$	normal unit vector (unitless)
$\vec{q}$	Darcy velocity (m s^{-1})
q_T	heat flux (W m^{-2})
t	time (s)
$\vec{v}$	fluid velocity (m s^{-1})
$\vec{x}$	spatial vector (m)
z	vertical coordinate (m)
$_s$	sediment (Subscript)
$_w$	water (Subscript)
$_a$	air (Subscript)
$_e$	effective, total (Subscript)
$_{dry}$	dry sediment (Subscript)
$_{sat}$	saturated sediment (Subscript)
$_{SW}$	surface water (Subscript)

Tab. 5.1: Mathematical symbol definitions. Throughout, subscripts are used to differentiate between different domains, materials, etc.

constitutive relation constants, are material-dependent. Their values can be estimated via various pedotransfer functions that use neural networks or soil texture tables, or by direct measurement of the SWRC. A review of much of the work in this domain is found in Vereecken et al. (2010). Where further constraint is required in the SWRC model or when the hydraulic conductivity cannot be measured at different levels of saturation, $l = 0.5$ is generally assumed (Mualem, 1976, Schaap and van Genuchten, 2006). The base data – namely, measurements of water content as a function of matric potential or equivalent (negative) hydraulic head – can be obtained with a Tempe cell (e.g., Shouse et al., 1995, Leij et al., 1996), pressure cell (e.g., Wang and Benson, 2004, Nahlawi et al., 2007), or centrifuge (e.g., Khanzode et al., 2002, Šimunek and Nimmo, 2005, Han et al., 2010). Here, we employ the centrifuge method of SWRC measurement (Section 5.2.4.1).

5.2.3.2 Temperature dynamics of the variably saturated zone

The heat transport dynamics of the variably saturated zone are governed by the advection-conduction-dispersion heat equation (Nield and Bejan, 2013):

$$C_{v,e}(t,\vec{x})\frac{\partial T(t,\vec{x})}{\partial t} + C_{v,w}(t,\vec{x})\vec{v}\cdot\nabla T(t,\vec{x}) = \nabla\cdot\left[k_e(t,\vec{x})\nabla T(t,\vec{x})\right] \tag{5.6}$$

where $C_{v,e}$ is effective volumetric heat capacity; T, temperature; $C_{v,w}$, water volumetric heat capacity; and k_e, effective thermal conductivity. Effective volumetric heat capacity, $C_{v,e}$, and thermal conductivity, k_e, are both dependent on moisture content. Volumetric heat capacity has a linear relationship with effective saturation level, S_e:

$$C_{v,e} = \epsilon S_e C_{v,w} + (1-\epsilon)C_{v,dry} \tag{5.7}$$

where $C_{v,dry}$ is the volumetric heat capacity of the dry sediment. Although a third component, air, is present, its volumetric heat capacity is negligible compared to those of the sediment and the water. The effective thermal conductivity, k_e, of porous sediment has a non-linear dependence on water content, due in part to capillary and adsorptive forces, that has been studied by many (e.g., Penner et al., 1975, Johansen, 1975, Ghuman and Lal, 1985, Tarnawski and Leong, 2000, Côté and Konrad, 2005, Lu et al., 2007). Two values, the saturated and dry thermal conductivity (k_{sat} and k_{dry}), are readily measured from sediment samples and the general dependence of k_e on S_e takes the empirical form (Johansen, 1975, Kersten, 1949):

$$k_e = k_{dry} + (k_{sat} - k_{dry})k_r \tag{5.8}$$

where k_r is the normalised thermal conductivity. For sandy materials such as the intertidal zone sediments at the Korogoro Creek field site, a sharper increase in k_e is generally observed at low S_e (Smits et al., 2010). The model of Côté and Konrad (2005) has been shown to accurately predict the thermal conductivity of many sands and it is the model we employ in this study:

$$k_r = \frac{\kappa_c S_e}{1 + (\kappa_c - 1)S_e} \tag{5.9}$$

where κ_c is an empirical model parameter. The coupling of hydraulic and thermal physical processes occurs via the strong dependence of the thermal parameters on water content, as well as through the velocity term in Equation 5.6.

5.2.3.3 Finite element solution and boundary conditions

The coupled equations 5.1-5.8 were solved using the FE modelling software package COMSOL Multiphysics v5 (e.g., Li et al., 2009, Wissmeier and Barry, 2010). Our model was constructed using the *Heat Transfer in Porous Media* and *Richards' Equation* modules with custom modifications to ensure correct treatment of $k_e(S_e)$ and $C_e(S_e)$. As vertical flow that reverses direction with the tidal cycle dominates this subsurface system, a 2-D cross-sectional model of the streambank was constructed using elevation measurements from the transect at Korogoro Creek. A convergent mesh was was applied to the modelling domain using a combination of rectangular and triangular elements (Figure 5.1d). The locations of the sediment moisture sensors and the discrete temperature probes in the SensorRods were explicitly defined as nodes so that the moisture content and temperature could be computed and compared with the measured values.

The model was executed with a 3-day run-up time (starting from May 11, 2014) with initial uniform temperature condition of 21.3 °C (average subsurface measured in the field) and the following hydraulic boundary conditions used (see

Figure 5.1d for boundary definitions):

$$\text{Boundaries 1 \& 3:} \quad \vec{q}\cdot\hat{n} = -K_e \frac{\partial H}{\partial x} \tag{5.10}$$

$$\text{Boundary 2:} \quad \vec{q}\cdot\hat{n} = 0 \tag{5.11}$$

$$\text{Boundary 4:} \quad \vec{q}\cdot\hat{n} = \begin{cases} \beta^*(|H - H_{SW}|)\frac{K_e}{k_r L_c}(H - H_{SW}), & H_{SW} \geq H \\ 0, & H_{SW} < H \end{cases} \tag{5.12}$$

where $\vec{q}$ is the Darcy velocity; $\hat{n}$, normal vector; H, hydraulic head; H_{SW}, the surface water level; L_c, coupling length; and β^*, a smoothing function. The thermal boundary conditions are:

$$\text{Boundaries 1, 2 \& 3:} \quad C_{v,e}\frac{\partial T}{\partial t} + C_{v,w}\vec{q}\cdot\nabla T = \nabla\cdot(k_e\nabla T) \tag{5.13}$$

$$\text{Boundary 4:} \quad k_e\hat{n}\cdot\nabla T = \begin{cases} h_{ww}(T_{SW} - T) & \text{if } y < H_{SW} \\ h_{wa}(T_a - T) & \text{if } y \geq H_{SW} \end{cases} \tag{5.14}$$

where T_{SW} is surface water temperature; T_a, air temperature; and h_{ww} and h_{wa}, heat transfer coefficients. $C_{v,e}$ and k_e are defined by Equations 5.7, 5.8, and 5.9.

Boundaries 1 and 3 ensure continuity of flow across the side boundaries and the modelled domain is large enough to ensure negligible non-horizontal flow at these boundaries. Boundary 2 is a simple no-flow boundary. All time-dependent dynamics in the modelled system are driven by $H_{SW}(t)$, $T_{SW}(t)$, and $T_a(t)$ in the boundary conditions of Boundary 4. Following the seepage face modelling approach of Chui and Freyberg (2009), where points on this boundary are below the surface water level, an inflow function, dependent on difference between the hydraulic head at the surface and the surface water level, is used for Boundary 4. The non-submerged regions are subjected to zero inflow conditions and conservation of mass is accounted for by allowing for variable saturation and seepage to the saturated zone. A smoothing function, β^*, which allows for a ramping up over 1 mm of hydraulic head difference, and a coupling length parameter, L_c, avoid numerical instability in zones transitioning from air-exposed to submerged (Chui and Freyberg, 2009). Thermally, boundary conditions 1–3 are consistent with their hydraulic counterparts, ensuring conservation of thermal energy. Thermal boundary 4 is subjected to heat transfer between the air and the surface when exposed and the water and the surface when submerged.

Parameter	Value	Source
α	6.58±0.20 m^{-1}	centrifuge measurements (Figure 5.2)
l	0.5	assumed (e.g., Schaap and van Genuchten, 2006)
m	0.754±0.023	centrifuge measurements (Figure 5.2)
θ_r	0.1046±0.028	centrifuge measurements (Figure 5.2)
ϵ	0.422±0.043	measurements of field samples
ρ_s	1551±16 kg m^{-1}	measurements of field samples
k_{dry}	0.277±0.018 W m^{-1} K^{-1}	measurements of field samples
k_{sat}	3.17±0.05 W m^{-1} K^{-1}	measurements of field samples
C_{dry}	1.27±0.03 ×10^{6} J m^{-3} K^{-1}	measurements of field samples
C_{wet}	2.78±0.04 ×10^{6} J m^{-3} K^{-1}	measurements of field samples
K_{sat}	9.21±2.26 m day^{-1}	field measurements (slug tests)
L_c	1 m	coupling length (Chui and Freyberg, 2009)
κ_c	3.55	value for sands (Côté and Konrad, 2005)

Tab. 5.2: Values of the hydraulic and thermal parameters used to solve equations 5.1-5.9 in the modelling domain. Uncertainties, where stated, are based on measurements of multiple samples. For definitions of the variables see Table 5.1.

5.2.4 Measurement of model parameters

5.2.4.1 Hydraulic parameters

In order to model the dynamics of the tidally-affected system using field measurements, Equations 5.1-5.5 require *a priori* knowledge of hydraulic parameters. Saturated hydraulic conductivity, k_{sat}, was estimated based on repeated slug test measurements at three locations along the transect (<75 cm from each of the FO-DTS coils), each performed at a depth of ~70 cm. A minimum of three tests were performed at each location and the resulting hydraulic head time-series as measured by pressure transducer probes were used to estimate K via the Hvorslev method (Hvorslev, 1951). The background fluctuation in hydraulic head due to the transient surface water boundary was assumed to be linear over the ~15 minutes of each test and was accounted for in the analysis. The average values and variance at each location were calculated and subsequently a final estimate (Table 5.2) was made via an inverse-variance-weighted average.

Centrifuges allow for accurate and relatively rapid measurement of the SWRC by decreasing the time needed for the variably saturated sediment sample to reach equilibrium for a given pressure. As the goal in our SWRC measurements is to estimate α and m via Equations 5.2 and 5.3, a conversion from the angular velocity or rotation rate to pressure head is needed. Following Nimmo (1990) and Šimunek and Nimmo (2005):

$$H_p(r,\omega) = \frac{\omega^2}{2g}(r^2 - r_0^2) = (5.5950 \times 10^{-4}\,\mathrm{m}^{-1})(r^2 - r_0^2)(\mathrm{RPM})^2 \tag{5.15}$$

where r is the distance of the sample from the centre of rotation, r_0 is the distance to the location with zero potential, and RPM (unitless) is the centrifuge rotation rate in rotations per minute.

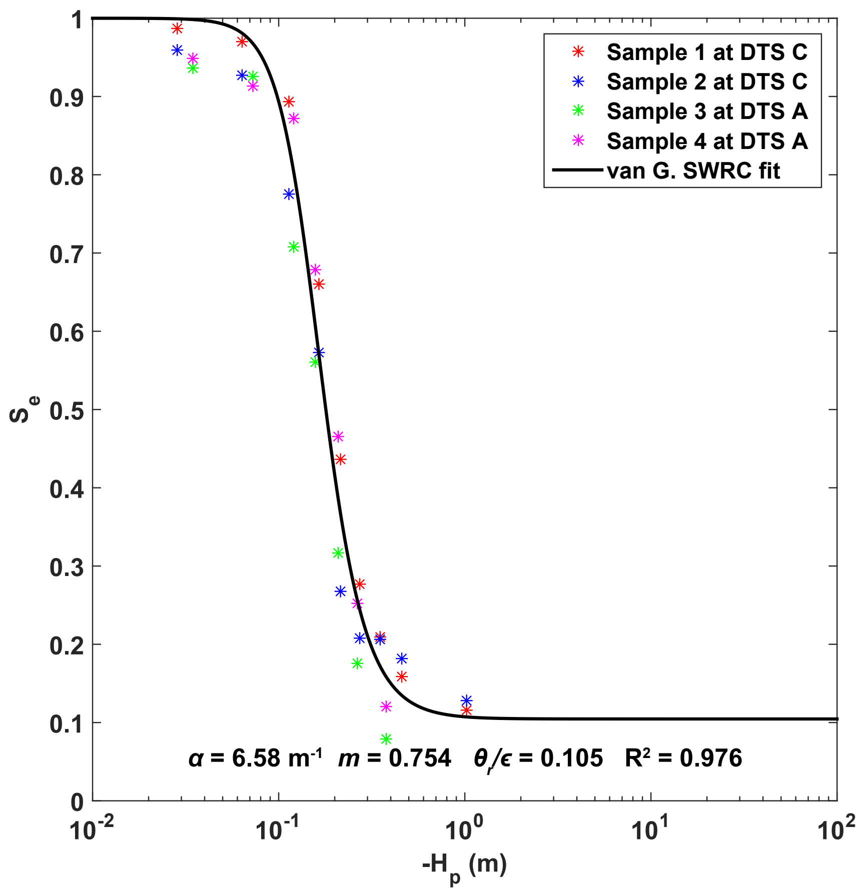

Fig. 5.2: The measured SWRC and fitted van Genuchten parameters (from Equations 5.2 and 5.3). A centrifuge technique (Nimmo, 1990, Šimunek and Nimmo, 2005) was used to measure the water retention curve of four sediment samples from the investigated transect, each from depths 20-30 cm relative to local surface.

The SWRC was measured by employing this centrifuge technique with four prepared sediment samples from the investigated transect. Oven-dried samples of ~65 g dry mass were placed into sample holders which had porous bases covered with filter paper. The total thickness of the samples was ~8.6 mm and thus r and r_0 were set to 145.0 and 149.3 mm in subsequent calculations. As the sample was thin, the variation in force through the sample was limited to ~5%. The samples were weighed to 10 mg precision and then completely saturated before allowing the excess water to drain under gravity with reproduction of previously-measured porosity confirmed by differential weighing. The samples were centrifuged in a Beckman-Coulter Allegra X-15R unit for 30 minutes for each spin rate step. The effluent and partially-saturated sample mass were recorded between spins and were used to calculate S_e; the equivalent pressure head was calculated by Equation 5.15. A least squares fit of Equations 5.2 and 5.3 was made to the data (Figure 5.2) to determine the van Genuchten parameters α, m and θ_r (Table 5.2) for use in the finite element model. Finally, a test to quantify organic content, which can induce hysteresis in the SWRC, was carried out by subjecting two samples to temperatures >500 °C for 5 hours in a muffle furnace. The test revealed negligible organic material of 0.33 and 0.44% for the two tested samples.

5.2.4.2 Thermal parameters

The thermal material properties of the sandy subsurface were determined from samples at three locations beside the FO-DTS coils in the transect, at depths to 30 cm, relative to the surface. The values of ρ and ϵ (Table 5.2) were evaluated through a combination of oven-drying, weighing, wetting, and volumetric measurements. Porosity determined from the measured wet and dry densities differed by <2 % from estimates based on the dry density and assuming a composition of 100 % silica ($\rho = 2.65$ g cm^{-3}), confirming the reliability of the measurement. To determine the values of k_{dry}, k_{sat}, $C_{v,dry}$ and $C_{v,sat}$ (Table 5.2), measurements of all samples were performed on oven-dried and on re-saturated material using a KD-2 thermal analyzer with a SH-1 probe from Decagon. Measurements were repeated a minimum of six times for each dry or wet sample, with a sample repeat time of 30 minutes.

5.3 Results and discussion

5.3.1 Tidal and diurnal drivers of streambed saturation and temperature

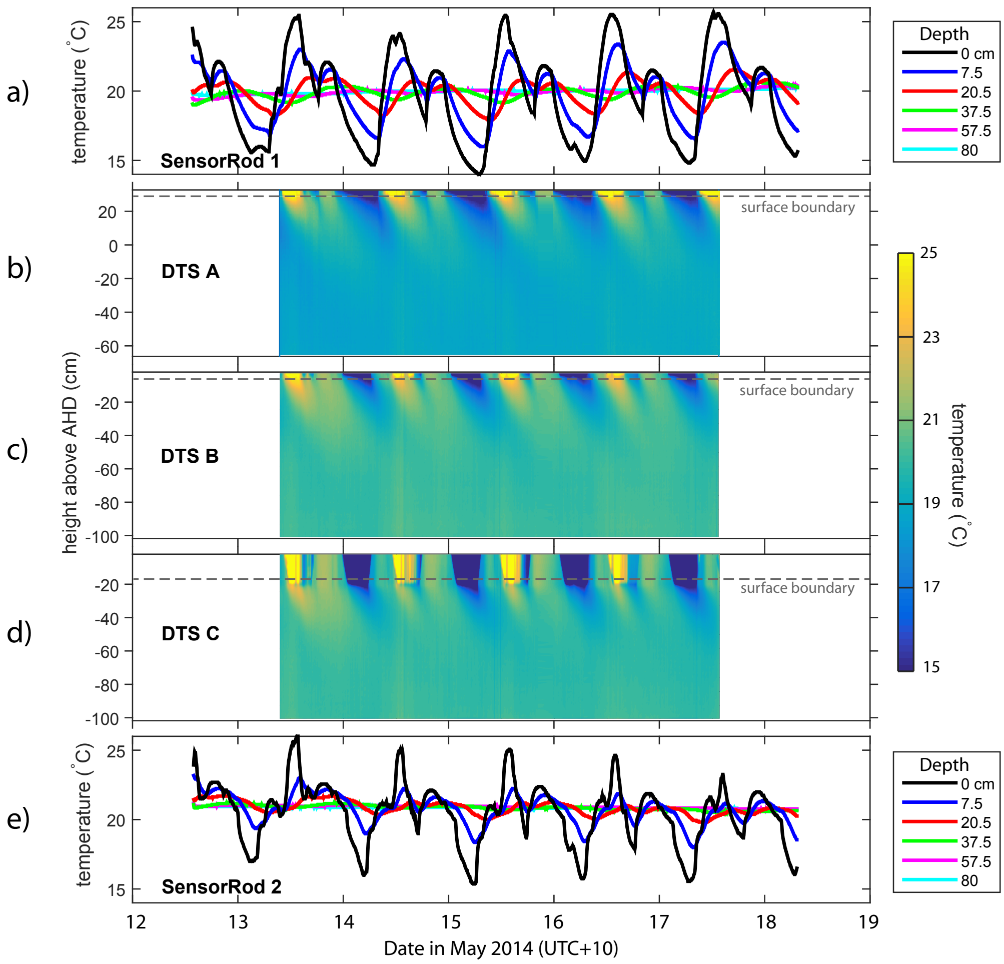

Fig. 5.3: a) Temperature of sensors in SensorRod 1; b) temperature profile of coiled DTS A; c) temperature profile of coiled DTS B; d) temperature profile of coiled DTS C; e) temperature of sensors in SensorRod 2.

Depth-profiles at three locations (Figure 5.1c & d) show the temporal variation of temperature (Figure 5.3). The SensorRod data shows the temperature at six discrete depths at the upper and lower locations, while the coiled FO-DTS shows a near-continuum temperature-depth profile at these and an intermediate location. The temperature profiles illustrate relatively abrupt changes in temperature compared to other published time-series (e.g., Rau et al., 2010, Vogt et al., 2012, Halloran et al., 2016d, and Chapter 3) due to the additional effect of the rising and falling tides. As the stream-ward location was submerged for longer durations, shorter periods of abrupt air-exposed temperature changes are seen in the records of DTS C and SensorRod 2. At the surface boundary, the recorded temperature ranges were 13.9–25.7, 13.8–25.8, and 14.4–26.1 °C for the locations of SensorRod 1/DTS A, DTS B, and SensorRod 2/DTS C, respectively. At depths $\gtrsim$30 cm, the average temperature is warmer by $\sim$1°C in the stream-ward location compared with the upper installations.

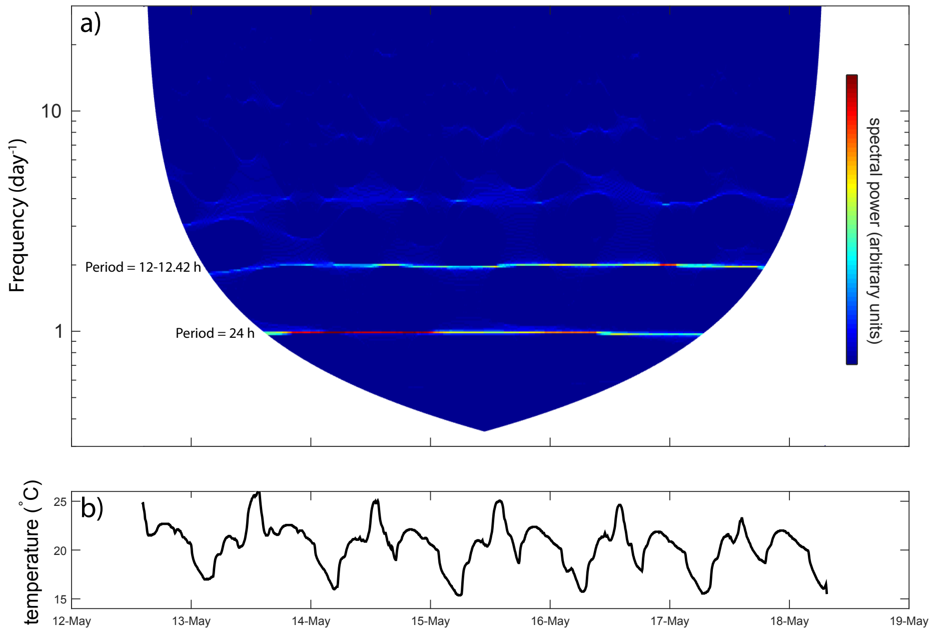

Fig. 5.4: a) Spectral analysis of temperature of record using the syncrosqueeze empirical mode decomposition-like tool (Daubechies et al., 2011). The input data (b) is taken from the uppermost sensor (at the surface boundary) in SensorRod 1.

The time-frequency spectrum calculated with the synchrosqueeze tool (Thakur et al., 2013) from the temperature sensor at the surface boundary in SensorRod 1 (Figure 5.4b) confirms the presence of two frequencies with periods of 24 h (rotation of the earth) and $\sim$12.4 h (dominant component of the tidal cycle) that dominate the thermal regime of the tidal creek. These can be attributed to a diurnal solar heating component and a semi-diurnal tidal component. The relative strength of these two components determines the depth to which surface-water infiltration plays a significant role in temperature dynamics.

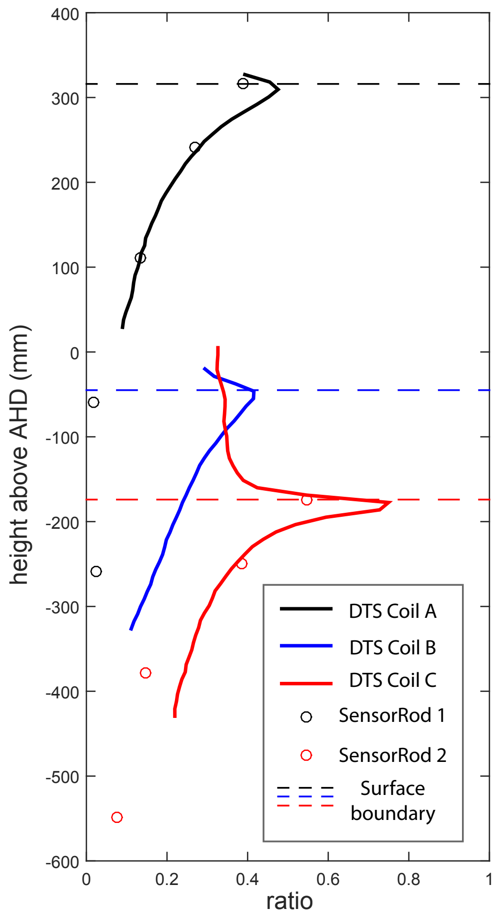

Fig. 5.5: Ratio of the power of the tidal component to the diurnal component of the temperature signal as calculated using the *Lomb-Scargle* periodogram (Lomb, 1976). The horizontal lines correspond to the height at which the coil is at the sediment-air/water boundary. Values in the deeper sections with significance values <0.5 in the *Lomb-Scargle* periodogram (due to the weaker temperature signal at depth) are ignored.

Spectral analysis of temperature time-series is important as it allows for the deconvolving of two separate phenomena attributable to advective heat transport via water flow and the primarily diffusive heat transport from the diurnal heating cycle. We employ the *Lomb-Scargle* periodogram (Lomb, 1976) to evaluate the power spectrum of our irregularly-sampled FO-DTS data. Using the complete data sets (Figure 5.3 b-d) and extracting the amplitude of the diurnal and semi-diurnal temperature components, the depth dependence of the ratio of these components can be calculated (Figure 5.5). For consistency, the same method is also applied to the SensorRod data. For each of the three locations, the ratio decreases with depth as the tidal semi-diurnal signal is attenuated more rapidly than the diurnal signal. This indicates that in this sand-dominated sediment with a variable surface water level, the thermal effects directly attributable to tides are only present to depths of $\sim$30 cm below the surface.

As the thermal and hydraulic properties of the sediment at Korogoro Creek have been measured (Table 5.2), it may be informative to compare these results to those from future measurements from other sites to understand the effects that thermal and hydraulic properties have on intertidal thermal regimes. For example, sediments that retain only a low level of saturation low tide will likely experience increased penetration depths of semi-diurnal thermal fluctuations. This would be due to a greater degree of advective heat transport and the larger temporal variations in thermal properties (e.g., Ju et al., 2011, Halloran et al., 2016c, and Chapter 4) caused by greater changes in water content, although other effects related to climate and tides will also play a role.

5.3.2 *Evaluation of spatio-temporal saturation and temperature dynamics*

The FE model was constrained by the following measured time-series: surface water level, surface water temperature, and air temperature. Figure 5.6 shows the temperature and moisture content outputs from the model. The shallow subsurface of the inter-tidal zone is subjected to two dominant forcings: 1) diurnal fluctuations (period of 24 h) that are purely thermal, and 2) semi-diurnal fluctuations (period of 12–12.42 h) that are both hydraulic and thermal. The variably saturated zone undergoes a cyclic saturation and desaturation process where the degree of change in moisture content is described by the *van Genuchten* SWRC (Equations 5.2–5.5) and the temperature dynamics by Equation 5.6. At the high and low tide extremes (Figure 5.7) thermal conditions differ significantly due to the contrasting thermal boundary conditions, saturation level, and water flow. When the domain is submerged, it is subjected to water inflow resulting in relatively homogeneous temperatures throughout the shallow sediments. Under low tide conditions, the temperature profile exhibits a characteristic shallow

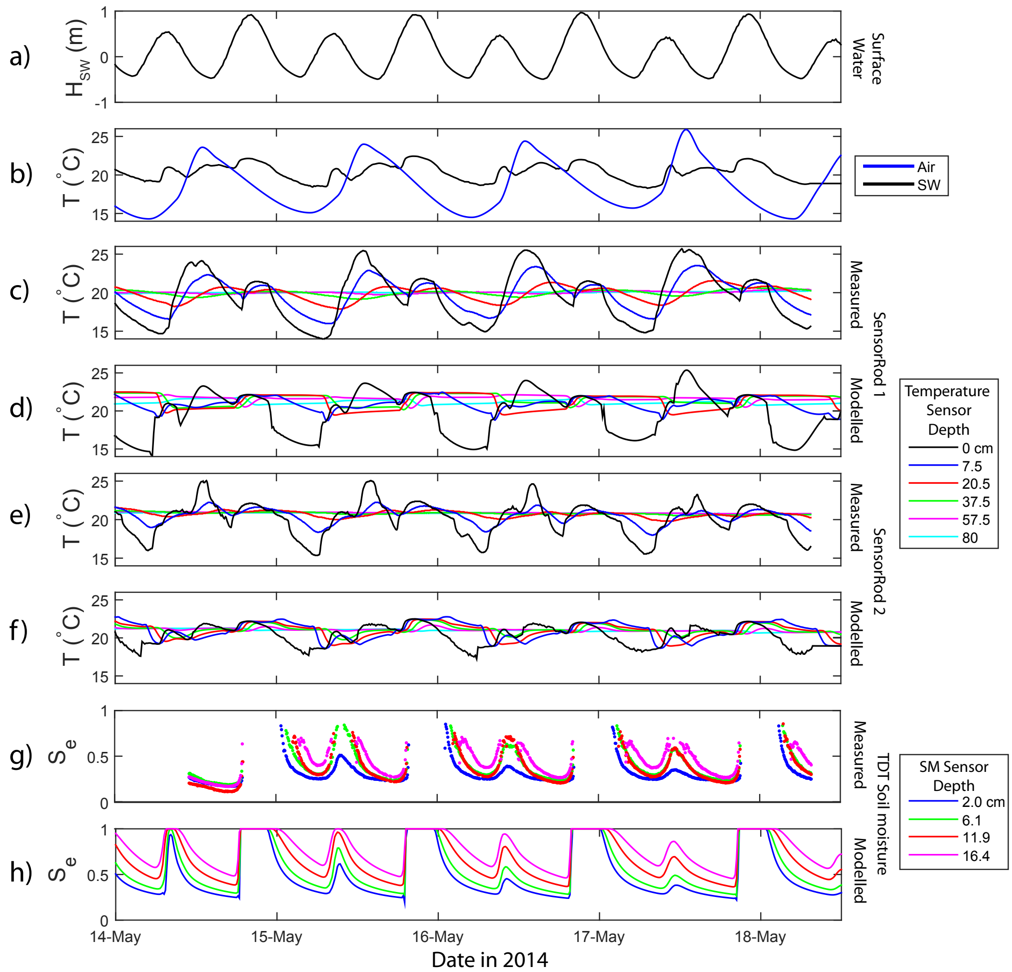

Fig. 5.6: a) Measured surface water level, relative to the AHD; b) air and surface water temperature; c) measured temperatures from SensorRod 1; d) temperature output for SensorRod 1 location from finite element model; e) measured temperatures from SensorRod 2; f) temperature output for SensorRod 2 location from finite element model; g) measured saturation level from buried TDT sensors; and h) modelled saturation output from the finite element model for the TDT sensor locations.

horizontal temperature banding, i.e. a shallow zone with significantly lower or higher temperatures that is dampened with depth.

The model provides an informative estimation of the temporal behaviour of effective saturation throughout the domain. At the location of the buried TDT probes, the effective saturation calculated by the model can be compared directly with the probe measurements (Figure 5.8). Varying degrees of agreement

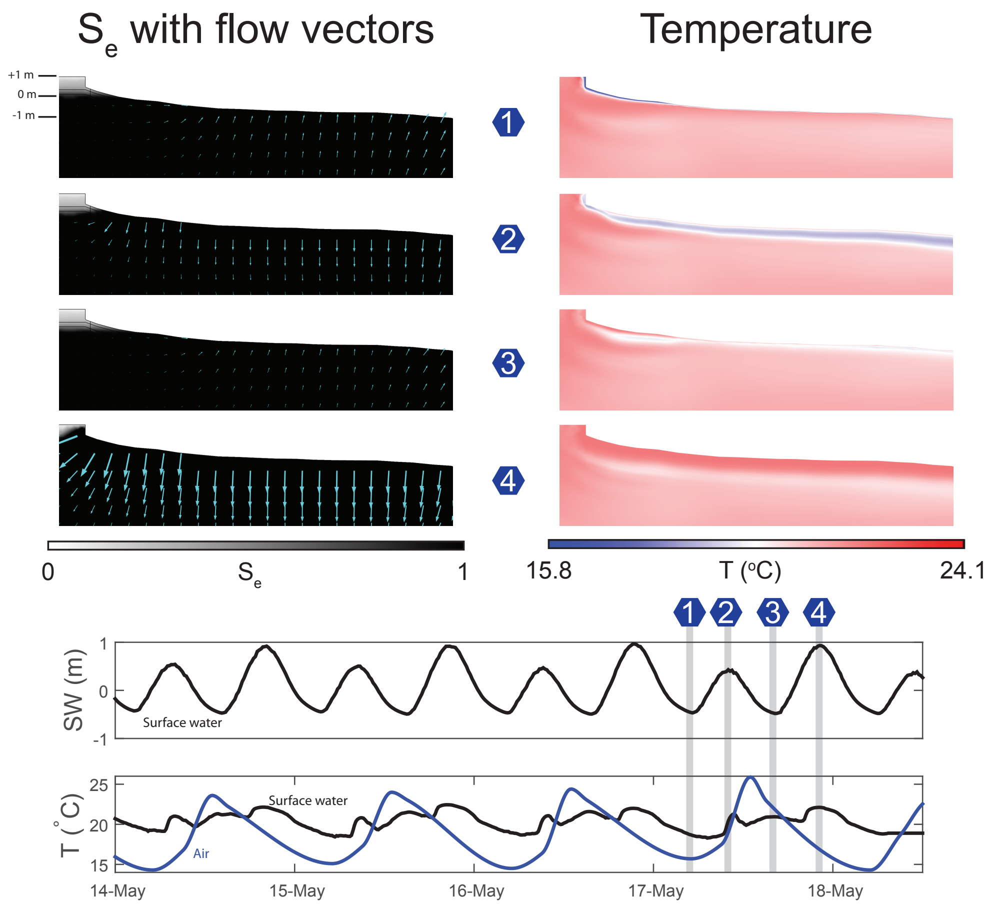

Fig. 5.7: Temperature, saturation and flow vector output in the domain of interest from the FE model. Modelling results are shown for high and low surface water level extremes over one tidal day. Only the upper portion of the investigated intertidal domain became unsaturated during low tide conditions.

between the modelled and measured moisture data S_e can be observed owing to several factors. Firstly, TDT probes are intrusive and their installation requires more significant disturbance of the subsurface than does a cylindrical temperature probe. This can alter the packing of the sediment and therefore its hydraulic properties. This is evident when comparing the first TDT-recorded S_e minimum with the second (Figure 5.6g), although it is not clear whether or not complete resaturation of the location does indeed return the subsurface properties to their original values. Secondly, the measured depth and deviation from horizontal installation of the TDT probes, whose measurements are anisotropic, has some uncertainty. The location of the sensors may have undergone a slight alteration after their installation as the first high-tide occurred. The similar records from the middle two sensors, measured to be ∼6 cm apart, are evidence of this as one would expect a more marked difference in minimum saturation at that separation. Thirdly, our FE model, which incorporates the *van Genuchten* model based on drying curves, does not account for possible hysteresis in the SWRC and associated delay in drainage and trapping of air when wetting up, although these effects should be minor for sands with low organic content. Additionally, vertical heterogeneity in the hydraulic properties may be a factor, although, based on our measurements and those of previous investigations at this location (Acworth and Dasey, 2003, Acworth et al., 2006), we expect relatively homogeneous conditions.

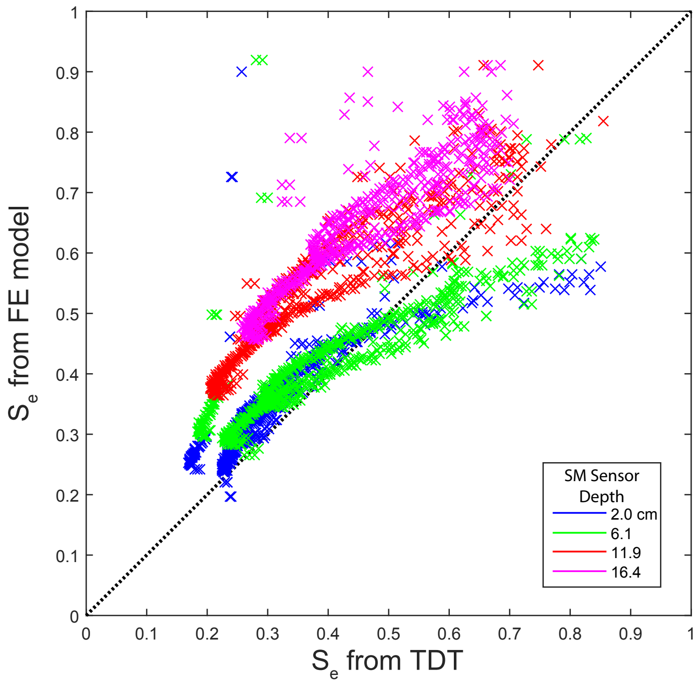

Fig. 5.8: Comparison of effective saturation at the TDT probe locations as calculated in the FE model and as measured by the probes. Not shown are data from time-steps at which the TDT probes failed due to high EC or at which uncertainty in sensor depth resulted in $S_e = 1$ for only the FE-derived values.

Finally, and perhaps most importantly, the 25% uncertainty in measured saturated hydraulic conductivity (Table 5.2) likely plays a role as it can introduce error to the model through Equation 5.5 which it scales linearly. The assumption of $l = 0.5$ in the *van Genuchten* model, as is common (Mualem, 1976, Schaap and van Genuchten, 2006), may also affect results as Equation 5.5 governs the rate of drainage as the surface water level decreases. While uncertainty in this equation would be inconsequential for a steady hydraulic state, the studied case is highly transient with the rate of change in the surface water level varying between approximately -10 and 10 m/day. As hydraulic conductivity is notoriously spatially variable even when conditions are saturated (e.g., Sudicky, 1986), the performance of models of coupled thermal-hydraulic processes in transient unsaturated conditions is likely to be greatly affected by uncertainty in its measurement.

These results show that while TDR/TDT probes may be an option when small-scale distributed saturation estimates in the near subsurface are the goal, care should be taken with their application. This is due in part to the drastic changes in EC (>4 S/m) that occur periodically in surface water in a tidal creek. A modelling approach based on surface measurements of temperature and water level, while certainly imperfect, can provide estimates of moisture content without any of the salinity- or disturbance-related limitations inherent to electromagnetic probes. Nonetheless, as the modelling approach illustrated here depends principally on the surface water boundary, thermal properties, and SWRC, the main advantage of the approach is to provide understanding of the process dynamics at play.

While the principal aim of the finite element model is to estimate the spatio-temporal behaviour of the shallow variably saturated streambed, we can also compare the modelled and measured temperatures at the discrete temperature sensor locations (Figure 5.6c–f). The model predicts the general behaviour of the temperature time-series, but a temporal offset in the arrival of the rising surface water level shows that small uncertainties in elevation measurements can affect the time-matching of the modelling results. The model appears to predict the temperature response at all depths more accurately when the probes are below the surface water level compared to surface air exposure of the probe location. This is partly due to the coarse air temperature record and the fact that the model does not include radiative heat transfer at the surface because of the spatial and temporal variability of insolation across the transect.

5.3.3 Heat transport and storage under variably saturated conditions

In coastal intertidal zones where there is a large swash zone, conductive heat balance calculations assuming saturated conditions (e.g., Befus et al., 2013) may be applicable. Nevertheless, in the case of a beach with a high hydraulic conductivity and swash zone that is significantly smaller than the intertidal zone (e.g., Russell et al., 2012) or in the case of the tidally-affected sandy streambed considered here (with no wave influence), unsaturated conditions develop regularly. Because of the strong, non-linear dependence of thermal conductivity, and consequently also thermal diffusivity, on water saturation (e.g., Côté and Konrad, 2005, Halloran et al., 2016c, and Chapter 4) the presence of unsaturated conditions will result in overestimation of heat transport. Here, we make use of the calculated S_e time-series from the finite element model to test the influence of variable saturation effects by estimating the conductive heat flux. The model confirms that at SensorRod 2 (lower in the in intertidal zone) there is negligible development of unsaturated conditions; however, at SensorRod 1, these conditions are present to depths <20.5 cm relative to the local surface with a minimum surface saturation level of 0.47.

Using *Fourier*'s Law for heat flux, q_T,

$$q_T(t) = k_e(S_e(t))\frac{dT(t)}{dz} \tag{5.16}$$

with saturation-dependent k_e (Equations 5.8 and 5.9), we calculate the vertical heat flux and total heat balance using the SensorRod temperatures at the upper and lower extremes of the studied transect. We define $q_T > 0$ as thermal energy being transferred to the subsurface (downwards) and use the $S_e(t)$ output of the finite element model at the sensor locations (Figure 5.6) as input for Equation 5.16. The result is shown in Figure 5.9 and illustrates that the effect of ignoring unsaturated conditions is a 5–15% overestimation of the magnitude of thermal energy storage (depending on which point in the final diurnal cycle is chosen) in this shallow and ephemeral unsaturated zone. While the maximum depth of the variably saturated zone is relatively shallow here (the bottom 4 sensors, ≥20.5 cm

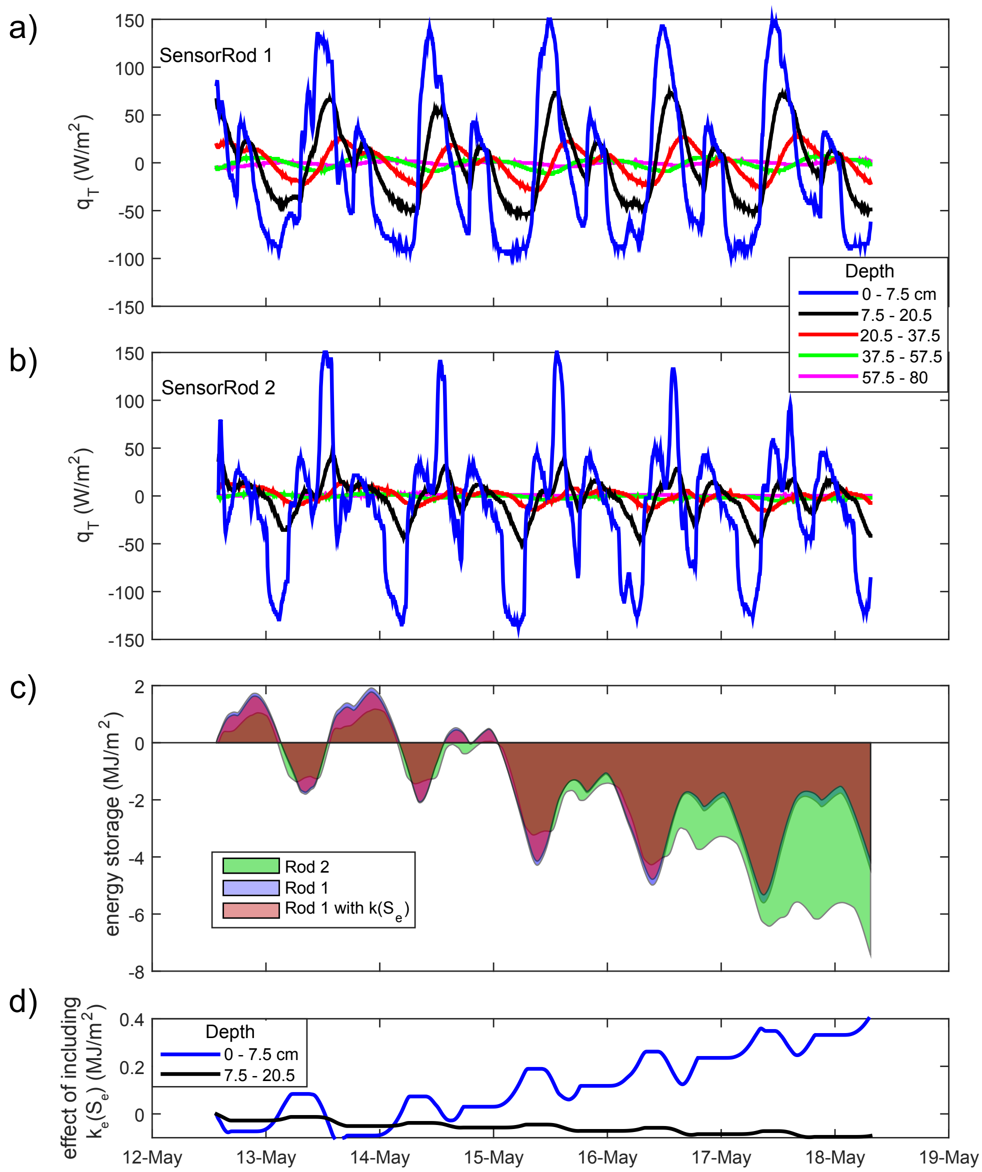

Fig. 5.9: Vertical heat flux at a) SensorRod 1 and b) SensorRod 2. The cumulative heat storage (c) between 0 to 80 cm depth at both rods is calculated. The effect of the inclusion of $k_e(S_e)$ in the calculation is shown only for SensorRod 1 as the other did not experience significant unsaturated conditions. As unsaturated conditions were experienced only in the upper 20.5 cm, the difference between the cumulative heat storage with and without unsaturated effects (d) is shown for the two shallowest intervals.

depth, remain saturated), the inclusion of the dependence of k_e on S_e still has a notable effect. Similar to the discussion of advective transport effects in Section

5.3.1, the effects on heat transport will be more pronounced when lower levels of saturation are experienced. Therefore, caution should be taken in streambed and streambank heat balance calculations when unsaturated conditions are present. An estimate of soil moisture content must be integrated into studies and used to inform thermal calculations. This may entail FE modelling or interpolated measurements with conventional electromagnetic probes, although these require disturbance of sediment and may be unreliable in coastal or estuarine zones for reasons previously outlined.

The coupled finite element modelling approach outlined here allows for estimates of S_e and T throughout a domain with minimal disturbance of the subsurface, although independent measurements of these quantities are important for understanding model limitations. Nonetheless, a combined field and FE modelling approach can, in turn, contribute to improvement in the evaluation of thermal (e.g., Wörman et al., 2012, Befus et al., 2013) and biogeochemical processes (e.g., Boulton, 1993, Greskowiak et al., 2005), among others. For example, the approach can be employed to model the evolution of contaminant degradation and transport (e.g., O'Carroll et al., 2013) or microbial growth and transport (e.g., Holden and Fierer, 2005). In both of these cases, characterisation of the soil moisture and temperature dependence of the relevant processes would be necessary, and a combination of field and modelling results could be used to constrain estimates.

5.4 Conclusions

Investigating thermal regimes under variably saturated conditions poses many challenges due to the complexity and interconnectedness of the processes at play. We illustrate how saturation levels and heat fluxes can be obtained by joint interpretation of numerical models and field measurements in the superficially simple case of an intertidal zone with uniform sediment and cyclic surface water levels. We constructed a finite-element model with coupled hydraulic and thermal physics and used continuous surface measurements of temperature and surface water level to constrain it. The thermal properties were measured using heat-pulse probes and the SMRC was evaluated using a centrifuge method (Šimunek and Nimmo, 2005) that performed very well for the sandy sediment at our field site.

The relative strength of the diurnal solar-driven temperature forcing and that of the tidal forcing was evaluated using high spatial resolution coiled FO-DTS measurements. This revealed that the cyclic thermal effects attributable to tidal forcings were only present to depths of $\sim$30 cm. As noted, many geochemical and biological processes in the variably saturated zone, such as transport phenomena and microbial processes, are strongly dependent on moisture content and temperature (e.g., Cohen and Ryan, 1989, Russell et al., 2012). An understanding of the mechanisms of variation in these parameters is important in the analysis and modelling of such processes.

Using measured temperature and sediment moisture time-series from a transect perpendicular to Korogoro Creek, we evaluated the performance of a FE modelling approach and found that the dynamics of moisture content can be estimated to reasonable accuracy, although temperature prediction capabilities, which relied on coarser air temperature data, did not perform as well. As TDR/TDT probes require soil disturbance and are affected by high salinity, the finite element modelling approach explored here offers the advantage of being able to estimate sediment moisture throughout the entire tidally-affected domain, although highly transient processes are more prone to error stemming from the measurements contributing to the *van Genuchten* model. Nevertheless, model results can subsequently be used to improve other types of calculations and can provide estimates where other methods may fail.

Using the moisture content modelling results, the effect of ignoring thermal conductivity's strong dependence on saturation level in calculating near-surface heat storage was found to be an overestimation by 5–15% for the monitored duration. While this is a small amount, these effects will be much more pronounced when lower saturation levels occur, such as in zones with a larger tidal range and in sediments with a higher hydraulic conductivity than that analysed here. Thus, future thermal regime investigations should take into account the strong, non-linear dependence of thermal transport on saturation level and must consider the variably saturated zone.

While much development of heat-tracing has been undertaken over the past decade, only a small portion of it is applicable to the vadose zone (Rau et al., 2014) and no current analytical method is sufficient for highly transient variably-saturated systems such as tidally-affected streams. Future research involving variably saturated conditions and thermal calculations will benefit from using a coupled thermal-hydraulic modelling approach in conjunction with field measurements. This work can serve as a useful guide to the treatment of coupled thermal and hydraulic physics for the rapidly expanding interest in understanding processes that occur in variably saturated conditions.

Acknowledgements

Funding for equipment was provided in part by the Australian Government *National Collaborative Research Infrastructure Strategy Program* (NCRIS). We acknowledge the support of the *UNSW School of Civil and Environmental Engineering*, the *Fonds de recherche du Québec – Nature et technologies (FRQNT)* (173538), the *Gary Johnston fund* at UNSW, and the *National Centre for Groundwater Research and Training* (NCGRT). The authors thank Evan Jensen, Filip Vrcelj & Kurt Booth of UNSW; Mahmood Sadat-Noori of Southern Cross University; and Marianne Laurin for their valuable assistance with field measurements. Additionally, we are grateful for the aid of Richard Crane and Dayna McGeeney with the centrifuge measurements.

6. SUMMARY AND CONCLUSIONS

6.1 Overview

Both temperature and soil moisture are important control parameters for a variety of near subsurface processes. The variably saturated subsurface presents challenges due to the complex, coupled, non-linear thermal and hydraulic processes that govern the dynamics of the system. In this thesis, various facets of this domain have been explored. The previous chapters have reviewed and consolidated a large body of knowledge, developed novel methodological approaches, and advanced fundamental understanding. Specifically, heat and water transport in the variably saturated subsurface was investigated by four primary approaches:

- Review of the current state of research into heat-tracing and thermal processes in the variably saturated subsurface (Chapter 2)

- Development and testing of a matrix method that can be used to delineate subsurface conditions and to compare and analyse heat-tracing methods (Chapter 3)

- Development and verification of a semi-analytical model to determine soil moisture content from natural temperature variations in the shallow subsurface (Chapter 4)

- Investigation of the thermal regime of a highly transient, variably-saturated streambed system using a combination of field measurements and numerical modelling (Chapter 5)

6.2 Summary and discussion

In Chapter 2, the current state of research on heat-tracing in variably saturated conditions was extensively reviewed. Research in this domain has been accelerating over the past decade as the advantages of temperature as a proxy for hydraulic processes have become better understood. The relevant thermal and hydraulic physics of variably saturated porous media, including important empirical models for the dependence of thermal conductivity on water saturation, were detailed in this chapter. Heat-tracing methods applicable to the vadose zone can be split into two types: active-heating and passive. While active heating methods may offer better temporal resolution than passive ones, using natural temperature variations as a basis offers lesser experimental complexity and minimal thermal disturbance of the natural system. Furthermore, natural temperature variations may themselves be of interest for many studies due to the dependencies of many geochemical and ecological processes on temperature. The growing body of passive and active-heating methods applicable to unsaturated conditions, including that developed in Chapter 4 (Halloran et al., 2016c), was examined in depth.

Vadose zone thermal regime studies that fuse hydraulic and thermal physics were also discussed in Chapter 2. Studies in the shallow vadose zone, including the tidal streambed study of Chapter 5 (Halloran et al., 2016a), were reviewed, as were studies of the deep vadose zone. Relevant practical considerations for heat-tracing in variably saturated conditions include temperature measurement equipment and numerical modelling packages. The benefits and disadvantages of many point-in-space (discrete) temperature probes and those of fibre-optic distributed temperature sensing (FO-DTS), which is employed here in a coiled configuration in Chapters 3 (Halloran et al., 2016d) and 5 (Halloran et al., 2016a), were outlined. Finally, a discussion of future directions for research in this domain – many of which build directly on the work of Chapters 3-5 – revealed many exciting opportunities.

A matrix method with a variety of applications to heat-tracing was developed and demonstrated in Chapter 3 (Halloran et al., 2016d). The method offers a novel way to visualise vertical column temperature measurements and associated derived quantities such as vertical water flow rates. The utility of the approach is greatest when applied to high vertical resolution temperature measurements, such as those obtained with coiled FO-DTS (e.g., Vogt et al., 2010, Briggs et al., 2012b, Halloran et al., 2016a, and Chapter 5). By using pair-by-pair calculations from temperature records to produce a detailed matrix, the spatial information in the dataset can be analysed in a variety of ways. Subsets of the temperature measurement or other derived data with fixed upper or lower sensor positions, or fixed sensor separation, can be readily selected from the matrices for further analysis. To demonstrate several functions of the method, the approach was applied to datasets from a field coiled FO-DTS installation and from realistic scenarios synthesised using numerical models. Three common saturated zone heat-tracing analytical equations (Hatch et al., 2006, McCallum et al., 2012) were compared using the matrices. The Hatch et al. (2006) method that uses temperature amplitude was found to give the most realistic estimates of vertical flow rates. The effects of temperature sensor separation were also analysed using the coiled FO-DTS dataset and the experimental trade-off between noisy velocity estimates and fine spatial resolution was detailed. These effects are highly dependent on the local subsurface, thus it is difficult to make broad recommendations for all systems based on this analysis. Nonetheless, as field studies may have limits on the number or the duration of FO-DTS deployments, this type of analysis can be used to optimise sensor spacing for discrete temperature sensor array installations (e.g. Rau et al., 2010, Bianchin et al., 2010). Finally, the effects of contrasting layers, non-vertical flow, and unsaturated conditions on velocity estimates were evaluated with output from coupled thermal-hydraulic finite element numerical models. This revealed signatures imparted to the matrices by common subsurface conditions and showed the need for vadose zone-specific methods when unsaturated conditions are present.

The derivation of a novel heat-tracing model for the estimation of water saturation profiles in the shallow subsurface was presented in Chapter 4. This semi-analytical approach melds the full advection-conduction-dispersion equation with the widely-used Côté and Konrad (2005) thermal conductivity–saturation empirical relationship for porous media and uses the phase and amplitude of cyclic temperature signals as inputs. Two equations, stemming from the imaginary and real components in the mathematical derivation, were derived. These equations rely on assumptions of locally stable phase and amplitude behaviour which, in practise, can be constrained with fine spatial resolution temperature data (e.g., using coiled FO-DTS as in Chapters 3 and 5). One of these (Equation 4.22) was found to predict saturation profiles to within 2% for zero water flow cases when employing a vertically sequential (step-by-step) implementation. Further tests of this model and implementation showed that the method can accurately reproduce saturation profiles under transient hydraulic conditions. These tests were performed at a wide range of saturation levels and with both upwards and downwards percolation up to 20 cm/day. The results illustrated that the variation of saturation with depth could be accurately reproduced under the effects of water percolation rates up to 10 cm/day. In general, temperature-based estimates of water saturation become more difficult under the effect of percolation or at higher levels of saturation (see Chapter 2 and, e.g., Steele-Dunne et al., 2010, Krzeminska et al., 2012) and thus the developed methodology had advantages over other approaches. Like all heat-tracing methods, thermal parameter measurements of the porous media are required in order to apply the developed method. While an independent estimate of saturation at a single point is required, it avoids the assumption of uniform thermal diffusivity throughout the domain and also includes explicit treatment of velocity, which is a clear advantage over other methods (e.g., Béhaegel et al., 2007, Steele-Dunne et al., 2010, Krzeminska et al., 2012). This developed method improves on the growing body of passive unsaturated zone heat-tracing (Section 2.3.1) as it is applicable to the entire saturation range, includes percolation effects, and avoids the problem of non-uniqueness in the inverse thermal diffusivity-saturation function. Although the passive heat-tracing approach simplifies field deployments and allows for the true ambient temperature – which itself is often of interest – to be measured, it is not applicable to situations with highly transient water fluxes, such as the tidal streambed studied in Chapter 5.

The beds and banks of tidal streams – and, more generally, the intertidal zone – exemplify the type of highly transient system where non-stationary components dominate subsurface temperature signals and thus where passive heat tracing methods fail (Rau et al., 2015). A section of the streambed of the tidally-affected Korogoro Creek in Hat Head, NSW, Australia was instrumented with temperature and soil moisture probes. A fully coupled thermal-hydraulic finite element model was used in conjunction with this field data to study and quantify the thermal regime of the system and to test the capabilities of the modelling approach in accurately predicting soil moisture throughout the domain. As the TDT soil moisture probes were intermittently affected by high pore water electrical conductivity and their installation required significant disturbance of the subsurface, a combined field measurement and finite element modelling approach presents notable advantages. By coupling Richards' equation (Richards, 1931) with the thermal physics governing variably saturated porous media this technique was used to evaluate soil moisture and temperature throughout the domain based primarily on surface measurements of air and surface water temperature and surface water level. Using a variety of modern techniques including the centrifuge SWRC approach of Šimunek and Nimmo (2005), great care was taken to obtain accurate measurements of the many hydraulic and thermal parameters required to model the system. Although the unsaturated zone was shallow and intermittent in the studied domain, variable saturation, as demonstrated, needs to be taken into account in order to quantify physical, ecological or geochemical processes such as heat flux correctly. Frequency-domain techniques (Lomb, 1976, Daubechies et al., 2011) were also used to evaluate the relative penetration depths of periodic heating imparted by tidal and diurnal cycles. The introduced approach obviously does not replace field measurements, but does demonstrate how modelling the thermal and hydraulic physics of a highly transient and variably saturated system with measurements of surface forcings can improve spatio-temporal understanding of coupled thermo-hydraulic processes in the subsurface with fewer measurements.

6.3 Outlook for future research

This doctoral thesis demonstrates that heat-as-a-tracer is a rapidly advancing field of research and its connection and application to variably saturated conditions is still at a relatively early stage of development. A variety of future research ideas that connect heat-transport and the vadose zone have been detailed in Section 2.6. These are directly connected to the results of Chapters 3–5. Opportunities, supported by the advances detailed in this thesis, exist in this domain. Here, specific lines of research that will build on the work presented in this thesis are presented.

6.3.1 Comparison of passive methods

Methods for the determination of soil moisture profiles from temperature measurements have the potential to make a large impact on studies of the variably saturated shallow subsurface, including investigations of SW-GW interaction where unsaturated conditions are intermittently present. Thus, a full examination and comparison of the passive heat-tracing method developed in Chapter 4 (Halloran et al., 2016c) and other methods (Béhaegel et al., 2007, Steele-Dunne et al., 2010, Bechkit et al., 2014, Dong et al., 2015b,a) is a logical next step. The implementation of the various methods in both a field and modelling context will help establish which methods are best suited to various conditions. Such a study should investigate multiple aspects of the effectiveness of these methods, namely: *a)* accuracy in reproducing thermal profiles in both hydraulically stable and transient conditions, *b)* limits on accuracy caused by non-stationary signals (i.e., changes in water flux), *c)* performance of the methods over a large range of saturation (i.e., from field capacity to fully saturated), and *d)* effects of various soil textural classes on the performance of the methods. The matrix method developed in Chapter 3 (Halloran et al., 2016d) would aid in comparing the effects of heterogeneous conditions or other assumption violations on soil moisture profiles predicted by passive heat-tracing methods.

Some of the main difficulties encountered by passive heat-tracing for soil moisture estimation are related to conditions of active percolation and the non-uniqueness of soil moisture as a function of thermal diffusivity (Figures 2.2 and 4.2). The method developed in Chapter 4 (Halloran et al., 2016c) includes both the full analytical heat-transport equation and a velocity estimation technique. At high levels of saturation associated with a shallow water table, it has been shown to accurately reproduce vertical saturation profiles when percolation rates up to $\sim$10 cm/day are present (Section 4.3). It would therefore be useful to test other methods against this type of scenario with variable percolation rate and a wide range of water saturation to compare limits on applicability. Furthermore, both field and numerical data would help in the characterisation and comparison of the effects of heterogeneity and measurement noise on the various methods. Such a study would ideally be carried out as a collaboration involving developers of multiple methods due to their familiarity with the implementation of the algorithms.

6.3.2 Dual measurement of hydraulic and thermal properties

As outlined in Section 2.6, the measurement, characterisation, and archiving of the hydraulic and thermal parameters of a large variety of sediments would greatly improve our understanding of coupled thermal-hydraulic processes in variably saturated conditions. Such characterisation would aid modelling and numerical applications in vadose zone hydrology, as well as in other field such as geotechnical engineering. This would be a large project that would likely be contributed to by many publications focusing on specific textural classes of soils (e.g., sandy loams, fine sands, etc.). Specifically, a database of measurements of the following parameters would be ideal:

- thermal conductivity of saturated, dry, and, if possible, partially saturated sediment
- volumetric or specific heat capacity
- dry density
- porosity
- saturated hydraulic conductivity
- van Genuchten SWRC parameters

Other secondary measurements such as grain size distribution and organic content could also be included. The database would be similar to the ROSETTA database (Schaap et al., 2001, Schaap, 2002), but with the addition of thermal parameters. The new database could indeed build on published results should the previously measured samples be available for additional analysis.

Analysis of interdependencies of thermal and hydraulic parameters would potentially establish robust empirical relationships such as a dependency of thermal conductivity on van Genuchten parameters over a wide range of conditions. Novel mathematical formulations and characterisation would aid future modelling studies of coupled thermo-hydro processes in variably saturated porous media by reducing data requirements and allowing for reasonable estimates to be made based on new empirical or statistical models. While such a database would ideally incorporate results from previously published research, almost no full characterisations of all of the aforementioned parameters in variably saturated sediments exist, with the exception of the measurements presented in Chapter 5 (Halloran et al., 2016a).

6.3.3 Thermal regimes in the variably saturated subsurface

To date, the bulk of thermal regime studies have dealt exclusively with saturated conditions. As 87% of global land cover is permanently or intermittently unsaturated (Latham et al., 2014), unsaturated conditions are an unavoidable complexity that needs to be incorporated into studies of a wide variety of temperature-dependent physical, geochemical, and biological processes (Chapter 2). Magnitudes and propagation depths of natural thermal signals and interdependencies of moisture content and heat transport will have implications for these processes and thus their quantification is of interest. Heat balance studies (e.g., Allan and Soden, 2008, Menberg et al., 2013) will benefit from a robust treatment of variably saturated conditions and the saturation-dependent thermal parameters involved. At field scales, the modelling approach of Chapter 5 (Halloran et al., 2016a) will help constrain sub-daily variations in temperature and soil moisture, while simpler methodologies may be applicable at longer temporal scales. Finally, with the potential for changes to local hydrological conditions by climate change, landuse change, or other direct anthropogenic action, characterisation of VZ thermal regimes and temperature- and saturation-dependent geochemical and ecological phenomena would establish a basis for predicting long-term effects of climate and anthropogenic drivers on temperatures and soil moisture levels.

6.4 Concluding statement

In the subsurface, thermal and hydraulic physics are interdependent. Due to the dependence of many geochemical, ecological and physical processes on both temperature and soil moisture, accurate quantification and understanding of these processes is crucial. Moreover, as temperature is a robust and readily measured quantity, methods for exploiting it to quantify hydraulic phenomena are appealing. In this thesis, knowledge has been significantly advanced through the analysis, comparison, development, and testing of heat-tracing approaches. Furthermore, a deeper understanding of coupled thermal-hydraulic processes in the variably saturated subsurface has been gained. Although thermal processes in conjunction with variable saturation present many interesting challenges due to the complexity and non-linearity of the physical framework, the heat-tracing approaches presented in this thesis will aid future studies in the variably saturated subsurface.

BIBLIOGRAPHY

Acworth, R. I. and Dasey, G. R. (2003). Mapping of the hyporheic zone around a tidal creek using a combination of borehole logging, borehole electrical tomography and cross-creek electrical imaging, New South Wales, Australia. *Hydrogeology Journal*, 11(3):368–377, doi:10.1007/s10040-003-0258-4.

Acworth, R. I., Hughes, C. E., and Turner, I. L. (2006). A radioisotope tracer investigation to determine the direction of groundwater movement adjacent to a tidal creek during spring and neap tides. *Hydrogeology Journal*, 15(2):281–296, doi:10.1007/s10040-006-0085-5.

Al Bitar, A., Leroux, D., Kerr, Y. H., Member, S., Merlin, O., Richaume, P., Sahoo, A., and Wood, E. F. (2012). Evaluation of SMOS Soil Moisture Products Over Continental U . S . Using the SCAN / SNOTEL Network. *IEEE Transactions on Geoscience and Remote Sensing*, 50(5):1572–1586.

Allan, R. P. and Soden, B. J. (2008). Atmospheric Warming and the Amplification of Precipitation Extremes. *Science*, 321(5895):1481–1484, doi:10.1126/science.1160787.

Andersen, M. S. and Acworth, R. I. (2009). Stream-aquifer interactions in the Maules Creek catchment, Namoi Valley, New South Wales, Australia. *Hydrogeology Journal*, 17(8):2005–2021, doi:10.1007/s10040-009-0500-9.

Andersen, M. S., Rutlidge, H., Eberhard, S., Halloran, L. J. S., Neilson, B. T., Rau, G. C., Li, C., Salma, A., Chen, J., Moll, C., Murphy, C., Cuthbert, M. O., and Baker, A. (2015). Mapping groundwater discharge and water chemistry in a perennial stream in northern New South Wales. In IAH/NCGRT, editor, *Australian Groundwater Conference*, page 161, Canberra, ACT, Australia.

Anderson, J. (1995). *Computational Fluid Dynamics: The Basics with Applications*. McGraw Hill.

Anderson, M. P. (2005). Heat as a ground water tracer. *Ground Water*, 43(6):951–68, doi:10.1111/j.1745-6584.2005.00052.x.

Andreasen, M., Andreasen, L. A., Jensen, K. H., Sonnenborg, T. O., and Bircher, S. (2013). Estimation of Regional Groundwater Recharge Using Data from a Distributed Soil Moisture Network. *Vadose Zone Journal*, 12(3), doi:10.2136/vzj2013.01.0035.

Anibas, C., Schneidewind, U., Vandersteen, G., Joris, I., Seuntjens, P., and Batelaan, O. (2016). From streambed temperature measurements to spatial-temporal flux quantification: using the LPML method to study groundwater-surface water interaction. *Hydrological Processes*, 30(2):203–216, doi:10.1002/hyp.10588.

Assouline, S., Tyler, S. W., Selker, J. S., Lunati, I., Higgins, C. W., and Parlange, M. B. (2013). Evaporation from a shallow water table: Diurnal dynamics of water and heat at the surface of drying sand. *Water Resources Research*, 49(7):4022–4034, doi:10.1002/wrcr.20293.

Aufleger, M., Conrad, M., Perzlmaier, S., and Porras, P. (2005). Improving a fiber optics tool for monitoring leakage. *Hydro Review Worldwide*, 13(4):18–23.

Bahr, J. M., Hart, D. J., and Leaf, A. T. (2011). Distributed temperature sensing (DTS) as a hydrostratigraphic characterization tool. Technical report, Wisconsin Department of Natural Resources.

Balland, V. and Arp, P. A. (2005). Modeling soil thermal conductivities over a wide range of conditions. *Journal of Environmental Engineering and Sciences*, 4(6):549–558, doi:10.1139/S05-007.

Barry, D., Parlange, J.-Y., Sander, G., and Sivapalan, M. (1993). A class of exact solutions for Richards' equation. *Journal of Hydrology*, 142(1-4):29–46, doi:10.1016/0022-1694(93)90003-R.

Barry-Macaulay, D., Bouazza, A., Wang, B., and Singh, R. (2015). Evaluation of soil thermal conductivity models. *Canadian Geotechnical Journal*, 52(11):1892–1900, doi:10.1139/cgj-2014-0518.

Basinger, J. M., Kluitenberg, G. J., Ham, J. M., Frank, J. M., Barnes, P. L., and Kirkham, M. B. (1997). Laboratory Evaluation of the Dual-Probe Heat-Pulse Method for Measuring Soil Water Content. *Vadose Zone Journal*, 2:389–399, doi:10.2113/2.3.389.

Bear, J. (1979). *Hydraulics of Groundwater*. McGraw-Hill, New York.

Bechkit, M. A. (2011). *Sur la détermination de la teneur en eau et de l'infiltration à partir de mesures passives de la température du sol*. PhD thesis, L'Université Pierre et Marie Curie.

Bechkit, M. A., Flageul, S., Guerin, R., and Tabbagh, A. (2014). Monitoring soil water content by vertical temperature variations. *Ground water*, 52(4):566–72, doi:10.1111/gwat.12090.

Becker, M. W., Bauer, B., and Hutchinson, A. (2013). Measuring Artificial Recharge with Fiber Optic Distributed Temperature Sensing. *Ground Water*, 51(5):670–878, doi:10.1111/j.1745-6584.2012.01006.x.

Befus, K. M., Cardenas, M. B., Erler, D. V., Santos, I. R., and Eyre, B. D. (2013). Heat transport dynamics at a sandy intertidal zone. *Water Resources Research*, 49(6):3770–3786, doi:10.1002/wrcr.20325.

Béhaegel, M., Sailhac, P., and Marquis, G. (2007). On the use of surface and ground temperature data to recover soil water content information. *Journal of Applied Geophysics*, 62(3):234–243, doi:10.1016/j.jappgeo.2006.11.005.

Beliaev, A. Y. and Hassanizadeh, S. M. (2001). A Theoretical Model of Hysteresis and Dynamic Effects in the Capillary Relation for Two-phase Flow in Porous Media. *Transport in Porous Media*, 43:487–510, doi:10.1023/A:1010736108256.

Bell, J. (1987). Neutron probe practice. 3rd ed. Hydrology Report 19. Technical report, Institute of Hydrology, Wallingford, UK.

Beltrami, H., Smerdon, J. E., Pollack, H. N., and Huang, S. (2002). Continental heat gain in the global climate system. *Geophysical Research Letters*, 29(8):1167, doi:10.1029/2001GL014310.

Berndtsson, R., Nodomi, K., Yasuda, H., Persson, T., Chen, H., and Jinno, K. (1996). Soil water and temperature patterns in an arid desert dune sand. *Journal of Hydrology*, 185(1-4):221–240, doi:10.1016/0022-1694(95)02987-7.

Bianchin, M., Smith, L., and Beckie, R. (2010). Quantifying hyporheic exchange in a tidal river using temperature time series. *Water Resources Research*, 46(7):1–21, doi:10.1029/2009WR008365.

Bircher, S., Skou, N., Jensen, K. H., Walker, J. P., and Rasmussen, L. (2012). A soil moisture and temperature network for SMOS validation in Western Denmark. *Hydrology and Earth System Sciences*, 16(5):1445–1463, doi:10.5194/hess-16-1445-2012.

Blasch, K. W., Ferré, T. P. A., Hoffmann, J. P., and Fleming, J. B. (2006). Relative contributions of transient and steady state infiltration during ephemeral streamflow. *Water Resources Research*, 42(8):W08405, doi:10.1029/2005WR004049.

Blöschl, G. and Sivapalan, M. (1995). Scale issues in hydrological modelling: A review. *Hydrological Processes*, 9:251–290, doi:10.1002/hyp.3360090305.

Blume, T., Krause, S., Meinikmann, K., and Lewandowski, J. (2013). Upscaling lacustrine groundwater discharge rates by fiber-optic distributed temperature sensing. *Water Resources Research*, 49(12):7929–7944, doi:10.1002/2012WR013215.

Bolten, J. D., Crow, W. T., Zhan, X., Jackson, T. J., and Reynolds, C. A. (2010). Evaluating the Utility of Remotely Sensed Soil Moisture Retrievals for Operational Agricultural Drought Monitoring. *IEEE Journal of Selected Topics in Applied Earth Observations and Remote Sensing*, 3(1):57–66, doi:10.1109/JSTARS.2009.2037163.

Boulton, A. J. (1993). Stream Ecology and Surface-Hyporheic Hydrologic Exchange: Implications, Techniques and Limitations. *Australian Journal of Maritime Freshwater Research*, 44:553–64.

Bowen, J. L., Kroeger, K. D., Tomasky, G., Pabich, W. J., Cole, M. L., Carmichael, R. H., and Valiela, I. (2007). A review of land-sea coupling by groundwater discharge of nitrogen to New England estuaries: Mechanisms and effects. *Applied Geochemistry*, 22(1):175–191, doi:10.1016/j.apgeochem.2006.09.002.

Brandt, S. (1992). Zero vs. conventional tillage and their effects on crop yield and soil moisture. *Canadian Journal of Plant Science*, 688(July):679–688, doi:10.4141/cjps92-084.

Bredehoeft, J. and Papadopulos, I. S. (1965). Rates of vertical groundwater movement estimated from earth's thermal profile. *Water Resources Research*, 1(2):325.

Briggs, M. A., Lautz, L. K., and Mckenzie, J. M. (2012a). A comparison of fibre-optic distributed temperature sensing to traditional methods of evaluating groundwater inflow to streams. *Hydrological Processes*, 26(9):1277–1290, doi:10.1002/hyp.8200.

Briggs, M. A., Lautz, L. K., McKenzie, J. M., Gordon, R. P., and Hare, D. K. (2012b). Using high-resolution distributed temperature sensing to quantify spatial and temporal variability in vertical hyporheic flux. *Water Resources Research*, 48(2):1–16, doi:10.1029/2011WR011227.

Bristow, K. L. (1998). Measurement of thermal properties and water content of unsaturated sandy soil using dual-probe heat-pulse probes. *Agricultural and Forest Meteorology*, 89(2):75–84, doi:10.1016/S0168-1923(97)00065-8.

Bristow, K. L., White, R. D., and Kluitenberg, G. J. (1994). Comparison of single and dual probes for measuring soil thermal properties with transient heating. *Australian Journal of Soil Research*, 32(3):447, doi:10.1071/SR9940447.

Brookfield, A. E., Sudicky, E. A., Park, Y. J., and Conant, B. (2009). Thermal transport modelling in a fully integrated surface/subsurface framework. *Hydrological Processes*, 23(15):2150–2164, doi:10.1002/hyp.7282.

Brooks, R. and Corey, A. (1964). Hydraulic properties of porous media. Technical report, Colorado State University.

Brunner, P. and Simmons, C. T. (2012). HydroGeoSphere: A Fully Integrated, Physically Based Hydrological Model. *Ground Water*, 50(2):170–176, doi:10.1111/j.1745-6584.2011.00882.x.

Caissie, D., Kurylyk, B. L., St-Hilaire, A., El-Jabi, N., and MacQuarrie, K. T. B. (2014). Streambed temperature dynamics and corresponding heat fluxes in small streams experiencing seasonal ice cover. *Journal of Hydrology*, 519:1441–1452, doi:10.1016/j.jhydrol.2014.09.034.

Campbell, G. S. (1985). *Soil physics with BASIC: Transport models for soil-plant systems.* Elsevier B.V., Netherlands.

Campbell, G. S., Calissendorff, C., and Williams, J. H. (1991). Probe for Measuring Soil Specific Heat Using A Heat-Pulse Method. *Soil Science Society of America Journal*, 55(1):291, doi:10.2136/sssaj1991.03615995005500010052x.

Cardenas, M. B. (2010). Thermal skin effect of pipes in streambeds and its implications on groundwater flux estimation using diurnal temperature signals. *Water Resources Research*, 46(3):1–12, doi:10.1029/2009WR008528.

Cardenas, M. B. and Wilson, J. L. (2007). Thermal regime of dune-covered sediments under gaining and losing water bodies. *Journal of Geophysical Research*, 112:G04013, doi:10.1029/2007JG000485.

Carslaw, H. and Jaeger, J. (1959). *Conduction of heat in solids*. Clarendon Press, Oxford, U.K., 2 edition.

Celia, M., Bouloutas, E., and Zarba, R. (1990). A general mass-conservative numerical solution for the unsaturated flow equation. *Water Resources Research*, 26(7):1483–1496, doi:10.1029/WR026i007p01483.

Chanasyk, D. S. and Naeth, M. A. (1996). Field measurement of soil moisture using neutron probes. *Canadian Journal of Soil Science*, 76(3):317–323, doi:10.4141/cjss96-038.

Chen, S. X. (2008). Thermal conductivity of sands. *Heat and Mass Transfer*, 44(10):1241–1246, doi:10.1007/s00231-007-0357-1.

Chew, C. C., Small, E. E., Larson, K. M., and Zavorotny, V. U. (2014). Effects of Near-Surface Soil Moisture on GPS SNR Data: Development of a Retrieval Algorithm for Soil Moisture. *IEEE Transactions on Geoscience and Remote Sensing*, 52(1):537–543, doi:10.1109/TGRS.2013.2242332.

Chin, S., Primerov, N., and Thévenaz, L. (2012). Sub-centimeter spatial resolution in distributed fiber sensing based on dynamic brillouin grating in optical fibers. *IEEE Sensors Journal*, 12(1):189–194, doi:10.1109/JSEN.2011.2126568.

Chui, T. F. M. and Freyberg, D. L. (2009). Implementing Hydrologic Boundary Conditions in a Multiphysics Model. *Journal of Hydrologic Engineering*, 14(12):1374–1377, doi:10.1061/(ASCE)HE.1943-5584.0000113.

Chung, S.-O. and Horton, R. (1987). Soil heat and water flow with a partial surface mulch. *Water Resources Research*, 23(12):2175–2186, doi:10.1029/WR023i012p02175.

Ciocca, F., Lunati, I., Van de Giesen, N., and Parlange, M. B. (2012). Heated Optical Fiber for Distributed Soil-Moisture Measurements: A Lysimeter Experiment. *Vadose Zone Journal*, 11(4), doi:10.2136/vzj2011.0199.

Cohen, Y. and Ryan, P. A. (1989). Chemical transport in the top soil zone - the role of moisture and temperature gradients. *Journal of Hazardous Materials*, 22(3):283–304, doi:10.1016/0304-3894(89)80002-0.

COMSOL (2014). *COMSOL Multiphysics User's Guide*. 5.0 edition.

Constantz, J. (2008). Heat as a tracer to determine streambed water exchanges. *Water Resources Research*, 44:1–20, doi:10.1029/2008WR006996.

Constantz, J., Marisa, H., and Grace, W. (2003a). Comparison of heat and bromide as ground water tracers near streams. *Ground Water*, 41(5):647, doi:10.1111/j.1745-6584.2003.tb02403.x.

Constantz, J., Naranjo, R. C., Niswonger, R. G., Allander, K., Neilson, B. T., Rosenberry, D., Smith, D. W., Rosecrans, C. Z., and Stonestrom, D. A. (2016). <scp>G</scp> roundwater exchanges near a channelized versus unmodified stream mouth discharging to a subalpine lake. *Water Resources Research*, doi:10.1002/2015WR017013.

Constantz, J., Tyler, S. W., and Kwicklis, E. (2003b). Temperature-Profile Methods for Estimating Percolation Rates in Arid Environments. *Vadose Zone Journal*, 2(1):12–24, doi:10.2136/vzj2003.0012.

Cosenza, P., Guérin, R., and Tabbagh, A. (2003). Relationship between thermal conductivity and water content of soils using numerical modelling. *European Journal of Soil Science*, 54(3):581–588, doi:10.1046/j.1365-2389.2003.00539.x.

Côté, J. and Konrad, J.-M. (2005). A generalized thermal conductivity model for soils and construction materials. *Canadian Geotechnical Journal*, 42(2):443–458, doi:10.1139/t04-106.

Curtis, A. and Kyle, P. (2011). Geothermal point sources identified in a fumarolic ice cave on Erebus volcano, Antarctica using fiber optic distributed temperature sensing. *Geophysical Research Letters*, 38(16):L16802, doi:10.1029/2011GL048272.

Cuthbert, M. O. and Mackay, R. (2013). Impacts of nonuniform flow on estimates of vertical streambed flux. *Water Resources Research*, 49(1):19–28, doi:10.1029/2011WR011587.

Cuthbert, M. O., Mackay, R., Durand, V., Aller, M.-F., Greswell, R., and Rivett, M. (2010). Impacts of river bed gas on the hydraulic and thermal dynamics of the hyporheic zone. *Advances in Water Resources*, 33(11):1347–1358, doi:10.1016/j.advwatres.2010.09.014.

Dahiya, R., Ingwersen, J., and Streck, T. (2007). The effect of mulching and tillage on the water and temperature regimes of a loess soil: Experimental findings and modeling. *Soil and Tillage Research*, 96(1-2):52–63, doi:10.1016/j.still.2007.02.004.

Dakin, J., Pratt, D., Bibby, G., and Ross, J. (1985). Distributed Optical Fibre Raman Temperature Sensor Using a Semiconductor Light Source and Detector. *Electronics Letters*, 21(13):569–570, doi:10.1111/mono.12024.

Daniels, D., Gunton, D., and Scott, H. (1988). Introduction to subsurface radar. *Radar Signal Process.*, 135:278–320.

Darcy, H. (1858). *Les fontaines publiques de la ville de Dijon: exposition et application*. Victor Dalmont., Paris.

Daubechies, I., Lu, J., and Wu, H. T. (2011). Synchrosqueezed wavelet transforms: An empirical mode decomposition-like tool. *Applied and Computational Harmonic Analysis*, 30(2):243–261, doi:10.1016/j.acha.2010.08.002.

Davidson, E. A. and Janssens, I. A. (2006). Temperature sensitivity of soil carbon decomposition and feedbacks to climate change. *Nature*, 440(7081):165–173, doi:10.1038/nature04514.

de Vries, D. (1952). *Mededelingen van de Landbouwhogeschool te Wageningen*. PhD thesis.

de Vries, D. (1963). Thermal properties of soils. In Van Wijk, W., editor, *Physics of Plant Environment*, pages 210–235. North-Holland Publishing Company, Amsterdam.

de Vries, D. and Peck, A. J. (1958). On the cylindrical probe method of measuring thermal conductivity with special reference to soils. *Australian Journal of Physics*, 11(2):255–271.

Dingman, S. (2002). *Physical hydrology*. Prentice-Hall, Upper Saddle River, NJ, 2 edition.

Domenico, P. A. and Schwartz, F. W. (1998). *Physical and chemical hydrogeology*. Wiley, NYC.

Donazzi, F., Occhini, E., and Seppi, A. (1979). Soil thermal and hydrological characteristics in designing underground cables. *Proceedings of the Institution of Electrical Engineers*, 126(6):506, doi:10.1049/piee.1979.0119.

Dong, J., Steele-Dunne, S. C., Judge, J., and van de Giesen, N. (2015a). A particle batch smoother for soil moisture estimation using soil temperature observations. *Advances in Water Resources*, 83:111–122, doi:10.1016/j.advwatres.2015.05.017.

Dong, J., Steele-Dunne, S. C., Ochsner, T. E., and van de Giesen, N. (2015b). Determining soil moisture by assimilating soil temperature measurements using the Ensemble Kalman Filter. *Advances in Water Resources*, 86:340–353, doi:10.1016/j.advwatres.2015.08.011.

Dong, Y., McCartney, J. S., and Lu, N. (2015c). Critical Review of Thermal Conductivity Models for Unsaturated Soils. *Geotechnical and Geological Engineering*, 33(2):207–221, doi:10.1007/s10706-015-9843-2.

Doucette, R. and Peterson, E. W. (2014). Identifying water sources in a karst aquifer using thermal signatures. *Environmental Earth Sciences*, doi:10.1007/s12665-014-3387-2.

Dowman, C. E., Ferré, T. P. A., Hoffmann, J. P., Rucker, D. F., and Callegary, J. B. (2003). Quantifying Ephemeral Streambed Infiltration from Downhole Temperature Measurements Collected Before and After Streamflow. *Vadose Zone Journal*, 2(4):595–601, doi:10.2113/2.4.595.

Duque, C., Muller, S., Sebok, E., Haider, K., and Engesgaard, P. (2015). Estimating groundwater discharge to surface waters using heat as a tracer in low flux environments: the role of thermal conductivity. *Hydrological Processes*, 30(3):383–395, doi:10.1002/hyp.10568.

El-Kadi, A. I. (2001). Modeling hydrocarbon biodegradation in tidal aquifers with water-saturation and heat inhibition effects. *Journal of Contaminant Hydrology*, 51(1-2):97–125, doi:10.1016/S0169-7722(01)00119-X.

Entekhabi, D., Njoku, E. G., O'Neill, P., Kellogg, K. H., Crow, W. T., Edelstein, W. N., Entin, J., Goodman, S. D., Jackson, T. J., Johnson, J. T., Kimball, J. S., Piepmeier, J. R., Koster, R. D., Martin, N., McDonald, K., Moghaddam, M., Moran, M. S., Reichle, R., Shi, J., Spencer, M., Thurman, S. W., Tsang, L., and van Zyl, J. J. (2010). The Soil Moisture Active Passive (SMAP) Mission. *Proceedings of the IEEE*, 98(5):704–716, doi:10.1109/JPROC.2010.2043918.

Evensen, G. (2003). The Ensemble Kalman Filter: Theoretical formulation and practical implementation. *Ocean Dynamics*, 53(4):343–367, doi:10.1007/s10236-003-0036-9.

Falocchi, M., Barontini, S., and Ranzi, R. (2015). A parametrization of a steady periodic solution of the Fourier equation to model soil temperature dynamics. *Journal of Geophysical Research: Earth Surface*, 120(9):1784–1802, doi:10.1002/2015JF003664.

Farouki, O. (1981). Thermal properties of soils. Technical report, US Army corp of Engineers: Cold Regions Research and Engineering Laboratory, Hanover, NH.

Farouki, O. (1982). Cold Regions Research and Engineering Laboratory Report 82-8: Evaluation of methods for calculating soil thermal conductivity. Technical report, US Corps of Army Engineers, Hanover, NH.

Ferguson, G. and Bense, V. (2011). Uncertainty in 1D Heat-Flow Analysis to Estimate Groundwater Discharge to a Stream. *Ground Water*, 49(3):336–347, doi:10.1111/j.1745-6584.2010.00735.x.

Findlay, S. (1995). Importance of surface-subsurface exchange in stream ecosystems: the hyporheic zone. *Limnology and oceanography*, 40(1):159–164, doi:10.4319/lo.1995.40.1.0159.

Franz, T. E., Zreda, M., Rosolem, R., and Ferré, T. P. A. (2013). A universal calibration function for determination of soil moisture with cosmic-ray neutrons. *Hydrology and Earth System Sciences*, 17(2):453–460, doi:10.5194/hess-17-453-2013.

Ghanbarian-Alavijeh, B., Liaghat, A., Huang, G., and van Genuchten, M. T. (2010). Estimation of the van Genuchten Soil Water Retention Properties from Soil Textural Data. *Pedosphere*, 20(4):456–465, doi:10.1016/S1002-0160(10)60035-5.

Ghuman, B. and Lal, R. (1985). Thermal conductivity, thermal diffusivity, and thermal capacity of some Nigerian soils. *Soil Science*, 139(1):74–80.

Goto, M., Matsukura, N., and Hagiwara, Y. (2005). Heat transfer characteristics of warm water flow with cool immiscible droplets in a vertical pipe. *Experimental Thermal and Fluid Science*, 29(3):371–381, doi:10.1016/j.expthermflusci.2004.05.006.

Greskowiak, J., Prommer, H., Massmann, G., Johnston, C. D., Nützmann, G., and Pekdeger, A. (2005). The impact of variably saturated conditions on hydrogeochemical changes during artificial recharge of groundwater. *Applied Geochemistry*, 20(7):1409–1426, doi:10.1016/j.apgeochem.2005.03.002.

Guntiñas, M. E., Leirós, M. C., Trasar-Cepeda, C., and Gil-Sotres, F. (2012). Effects of moisture and temperature on net soil nitrogen mineralization: A laboratory study. *European Journal of Soil Biology*, 48:73–80, doi:10.1016/j.ejsobi.2011.07.015.

Halloran, L. J. S., Andersen, M. S., and Rau, G. C. (2016a). Heat transport dynamics in a tidally-driven variably saturated streambed. *(in preparation)*.

Halloran, L. J. S., Rau, G. C., and Andersen, M. S. (2016b). Heat as a tracer to quantify processes and properties in the vadose zone: A review. *(under review)*.

Halloran, L. J. S., Rau, G. C., Andersen, M. S., Roshan, H., and Acworth, R. I. (2015a). Natural temperature variations and soil moisture content in the vadose zone. In *Australian Groundwater Conference*, page 231, Canberra. IAH/NCGRT.

Halloran, L. J. S., Roshan, H., Rau, G. C., and Andersen, M. S. (2016c). Calculating water saturation from passive temperature measurements in near-surface sediments: Development of a semi-analytical model. *Advances in Water Resources*, 89:67–79, doi:10.1016/j.advwatres.2016.01.007.

Halloran, L. J. S., Roshan, H., Rau, G. C., Andersen, M. S., and Acworth, R. I. (2016d). Improved spatial delineation of streambed properties and water fluxes using distributed temperature sensing. *Hydrological Processes*, doi:10.1002/hyp.10806.

Halloran, L. J. S., Roshan, H., Rau, G. C., Cuthbert, M. O., Andersen, M. S., and Acworth, R. I. (2015b). Soil moisture content estimation from passive temperature measurements. In *European Geosciences Union General Assembly*, page 1312, Vienna, Austria. EGU.

Han, X.-W., Shao, M.-A., and Horton, R. (2010). Estimating van Genuchten Model Parameters of Undisturbed Soils Using an Integral Method. *Pedosphere*, 20(1):55–62, doi:10.1016/S1002-0160(09)60282-4.

Harley, M. D., Turner, I. L., Short, A. D., and Ranasinghe, R. (2011). Assessment and integration of conventional, RTK-GPS and image-derived beach survey methods for daily to decadal coastal monitoring. *Coastal Engineering*, 58(2):194–205, doi:10.1016/j.coastaleng.2010.09.006.

Hatch, C. E., Fisher, A. T., Revenaugh, J. S., Constantz, J., and Ruehl, C. (2006). Quantifying surface water-groundwater interactions using time series analysis of streambed thermal records: Method development. *Water Resources Research*, 42(10):1–14, doi:10.1029/2005WR004787.

Hausner, M. B., Suárez, F., Glander, K. E., van de Giesen, N., Selker, J. S., and Tyler, S. W. (2011). Calibrating single-ended fiber-optic Raman spectra distributed temperature sensing data. *Sensors*, 11(11):10859–79, doi:10.3390/s111110859.

Hausner, M. B., Wilson, K. P., Gaines, D. B., and Tyler, S. W. (2012). Interpreting seasonal convective mixing in Devils Hole, Death Valley National Park, from temperature profiles observed by fiber-optic distributed temperature sensing. *Water Resources Research*, 48(5), doi:10.1029/2011WR010972.

Healy, R. W. (2008). Simulating Water, Solute, and Heat Transport in the Subsurface with the VS2DI Software Package. *Vadose Zone Journal*, 7(2):632, doi:10.2136/vzj2007.0075.

Hecht-Méndez, J., Molina-Giraldo, N., Blum, P., and Bayer, P. (2010). Evaluating MT3DMS for Heat Transport Simulation of Closed Geothermal Systems. *Ground Water*, 48(5):741–756, doi:10.1111/j.1745-6584.2010.00678.x.

Heitman, J. L., Basinger, J. M., Kluitenberg, G. J., M, H. J., Frank, J. M., Barnes, P. L., and Ham, J. M. (2002). Field Evaluation of the Dual-Probe Heat-Pulse Method for Measuring Soil Water Content. *Vadose Zone Journal*, 2(4):552–560, doi:10.2113/2.4.552.

Henderson, R. D., Day-Lewis, F. D., and Harvey, C. F. (2009). Investigation of aquifer-estuary interaction using wavelet analysis of fiber-optic temperature data. *Geophysical Research Letters*, 36(6):L06403, doi:10.1029/2008GL036926.

Holden, P. A. and Fierer, N. (2005). Microbial Processes in the Vadose Zone. *Vadose Zone Journal*, 4(1):1, doi:10.2136/vzj2005.0001.

Hopmans, J. W., Šimunek, J., and Bristow, K. L. (2002). Indirect estimation of soil thermal properties and water flux using heat pulse probe measurements: Geometry and dispersion effects. *Water Resources Research*, 38(1):7–1–7–14, doi:10.1029/2000WR000071.

Hsieh, P. A., Wingle, W., and Healy, R. W. (2000). Water-Resources Investigations Report 99-4130: VS2DI - A Graphical Software Package for Simulating Fluid Flow and Solute or Energy Transport in Variably Saturated Porous Media. Technical report, USGS, Lakewood, CO.

Hu, G., Zhao, L., Wu, X., Li, R., Wu, T., Xie, C., Qiao, Y., Shi, J., Li, W., and Cheng, G. (2016). New Fourier-series-based analytical solution to the conduction-convection equation to calculate soil temperature, determine soil thermal properties, or estimate water flux. *International Journal of Heat and Mass Transfer*, 95:815–823, doi:10.1016/j.ijheatmasstransfer.2015.11.078.

Huang, N. E., Shen, Z., Long, S. R., Wu, M. C., Shih, H. H., Zheng, Q., Yen, N.-C., Tung, C. C., and Liu, H. H. (1998). The empirical mode decomposition and the Hilbert spectrum for nonlinear and non-stationary time series analysis. *Proceedings of the Royal Society A: Mathematical, Physical and Engineering Sciences*, 454(1971):903–995, doi:10.1098/rspa.1998.0193.

Hughes, B. J. D. and Sanford, W. E. (2004). SUTRA-MS: A Version of SUTRA Modified to Simulate Heat and Multiple-Solute Transport. Technical report, USGS, Reston, VA.

Huisman, J. A., Hubbard, S. S., Redman, J. D., and Annan, A. P. (2003). Measuring Soil Water Content with Ground Penetrating Radar: A Review. *Vadose Zone Journal*, 2(4):476, doi:10.2136/vzj2003.4760.

Hvorslev, M. (1951). Time lag and soil permeability in groundwater observations. Technical report, US Army Corps Engrs Waterways Experiment Station.

Jackson, T. J. (2002). Remote sensing of soil moisture: Implications for groundwater recharge. *Hydrogeology Journal*, 10(1):40–51, doi:10.1007/s10040-001-0168-2.

Jensen, J. K. and Engesgaard, P. (2011). Nonuniform Groundwater Discharge across a Streambed: Heat as a Tracer. *Vadose Zone Journal*, 10(1):98, doi:10.2136/vzj2010.0005.

Johansen, Ø. (1975). *Thermal conductivity of soils*. PhD thesis, University of Trondheim, Trondheim, Norway.

Johnson, A. N., Boer, B. R., Woessner, W. W., Stanford, J. A., Poole, G. C., Thomas, S. A., and O'Daniel, S. J. (2005). Evaluation of an Inexpensive Small-Diameter Temperature Logger for Documenting Ground Water-River Interactions. *Ground Water Monitoring and Remediation*, 25(4):68–74, doi:10.1111/j.1745-6592.2005.00049.x.

Ju, Z., Ren, T., and Hu, C. (2011). Soil Thermal Conductivity as Influenced by Aggregation at Intermediate Water Contents. *Soil Science Society of America Journal*, 75(1):26, doi:10.2136/sssaj2010.0050N.

Kalbus, E., Reinstorf, F., and Schirmer, M. (2006). Measuring methods for groundwater, surface water and their interactions: a review. *Hydrology and Earth System Sciences Discussions*, 3(4):1809–1850, doi:10.5194/hessd-3-1809-2006.

Kaviany, M. (1995). *Principles of Heat Transfer in Porous Media*. Springer, NYC, 2 edition.

Keery, J., Binley, A., Crook, N., and Smith, J. W. (2007). Temporal and spatial variability of groundwaterâĂŞsurface water fluxes: Development and application of an analytical method using temperature time series. *Journal of Hydrology*, 336(1-2):1–16, doi:10.1016/j.jhydrol.2006.12.003.

Kellner, E. and Hubbart, J. (2015). Agricultural and forested land use impacts on floodplain shallow groundwater temperature regime. *Hydrological Processes*, 30(4):625–636, doi:10.1002/hyp.10645.

Kerr, Y. H., Waldteufel, P., Wigneron, J.-P., Martinuzzi, J.-M., Font, J., and Berger, M. (2001). Soil Moisture Retrieval from Space: The Soil Moisture and Ocean Salinity (SMOS) Mission. *IEEE Transactions on Geoscience and Remote Sensing*, 39(8):1729–1735, doi:10.1109/36.942551.

Kersten, M. (1949). Laboratory research for the determination of the thermal properties of soils. Technical report, Univ. of Minnesota, Minneapolis.

Khanzode, R. M., Vanapalli, S. K., and Fredlund, D. G. (2002). Measurement of soil-water characteristic curves for fine-grained soils using a small-scale centrifuge. *Canadian Geotechnical Journal*, 39(5):1209–1217, doi:10.1139/t02-060.

Kipp Jr, K. (1987). USGS Water Resources Investigations Report 86-4095: HST3D - A Computer Code for Simulation of heat and solute transport in 3-D GW Flow Systems. Technical report, USGS, Denver, CO.

Kirkland, M. R., Hills, R. G., and Wierenga, P. (1992). Algorithms for solving Richards' equation for variably saturated soils. *Water Resources Research*, 28(8):2049–2058, doi:10.1029/92WR00802.

Kodešová, R., Fér, M., Klement, A., Nikodem, A., Teplá, D., Neuberger, P., and Bureš, P. (2014). Impact of various surface covers on water and thermal regime of Technosol. *Journal of Hydrology*, 519:2272–2288, doi:10.1016/j.jhydrol.2014.10.035.

Kosugi, K. (1996). Lognormal distribution model for unsaturated soil hydraulic properties. *Water Resources Research*, 32(9):2697–2703, doi:10.1029/96WR01776.

Krzeminska, D. M., Steele-Dunne, S. C., Bogaard, T. A., Rutten, M. M., Sailhac, P., and Geraud, Y. (2012). High-resolution temperature observations to monitor soil thermal properties as a proxy for soil moisture condition in clay-shale landslide. *Hydrological Processes*, 26(14):2143–2156, doi:10.1002/hyp.7980.

Kurylyk, B. L., MacQuarrie, K. T. B., and McKenzie, J. M. (2014). Climate change impacts on groundwater and soil temperatures in cold and temperate regions: Implications, mathematical theory, and emerging simulation tools. *Earth-Science Reviews*, 138:313–334, doi:10.1016/j.earscirev.2014.06.006.

Kurylyk, B. L. and Watanabe, K. (2013). The mathematical representation of freezing and thawing processes in variably-saturated, non-deformable soils. *Advances in Water Resources*, 60:160–177, doi:10.1016/j.advwatres.2013.07.016.

Land, L. A. and Paull, C. K. (2001). Thermal gradients as a tool for estimating groundwater advective rates in a coastal estuary: White Oak River, North Carolina, USA. *Journal of Hydrology*, 248(1-4):198–215, doi:10.1016/S0022-1694(01)00405-X.

Larson, K. M., Small, E. E., Gutmann, E. D., Bilich, A. L., Braun, J. J., and Zavorotny, V. U. (2008). Use of GPS receivers as a soil moisture network for water cycle studies. *Geophysical Research Letters*, 35:L24405, doi:10.1029/2008GL036013.

Latham, J., Cumani, R., Rosati, I., and Bloise, M. (2014). FAO Global Land Cover (GLC-SHARE) Beta-Release 1.0 Database. Technical report, FAO Land and Water Division, Rome.

Lautz, L. K. (2010). Impacts of nonideal field conditions on vertical water velocity estimates from streambed temperature time series. *Water Resources Research*, 46(1):1–14, doi:10.1029/2009WR007917.

Leach, J. A. and Moore, R. D. (2011). Stream temperature dynamics in two hydrogeomorphically distinct reaches. *Hydrological Processes*, 25(5):679–690, doi:10.1002/hyp.7854.

Leij, F., Alves, W., van Genuchten, M. T., and Williams, J. (1996). *The UNSODA unsaturated soil hydraulic database: user's manual*. US EPA, Cincinnati, OH.

Li, Q., Ito, K., Wu, Z., Lowry, C. S., and Loheide, S. P. (2009). COMSOL multiphysics: A novel approach to ground water modeling. *Ground Water*, 47(4):480–487, doi:10.1111/j.1745-6584.2009.00584.x.

Liu, G., Knobbe, S., and Butler, Jr., J. (2013). Resolving centimeter-scale flows in aquifers and their hydrostratigraphic controls. *Geophysical Research Letters*, 40(6):1098–1103, doi:10.1002/grl.50282.

Liu, X. (2011). Evaluation of the Heat-Pulse Technique for Measuring Soil Water Content with Thermo-TDR Sensor. *Procedia Environmental Sciences*, 11(2008):1234–1239, doi:10.1016/j.proenv.2011.12.185.

Lloyd, J. J. and Taylor, J. A. (1994). On the temperature dependence of soil respiration. *Functional Ecology*, 8(3):315–323, doi:10.2307/2389824.

Lomb, N. R. (1976). Least-squares frequency analysis of unequally spaced data. *Astrophysics and Space Science*, 39(2):447–462, doi:10.1007/BF00648343.

Lowry, C. S., Walker, J. F., Hunt, R. J., and Anderson, M. P. (2007). Identifying spatial variability of groundwater discharge in a wetland stream using a distributed temperature sensor. *Water Resources Research*, 43(10):W10408, doi:10.1029/2007WR006145.

Lu, S., Ren, T., Gong, Y., and Horton, R. (2007). An Improved Model for Predicting Soil Thermal Conductivity from Water Content at Room Temperature. *Soil Science Society of America Journal*, 71(1):8, doi:10.2136/sssaj2006.0041.

Luce, C. H., Tonina, D., Gariglio, F. P., and Applebee, R. (2013). Solutions for the diurnally forced advection-diffusion equation to estimate bulk fluid velocity and diffusivity in streambeds from temperature time series. *Water Resources Research*, 49:1–19, doi:10.1029/2012WR012380.

Lunt, I. A., Hubbard, S. S., and Rubin, Y. (2005). Soil moisture content estimation using ground-penetrating radar reflection data. *Journal of Hydrology*, 307(1-4):254–269, doi:10.1016/j.jhydrol.2004.10.014.

Mahmood, R. (1996). Scale issues in soil moisture modelling: problems and prospects. *Progress in Physical Geography*, 20(3):273–291, doi:10.1177/030913339602000302.

Maier, F., Schaffer, M., and Licha, T. (2015). Determination of temperatures and cooled fractions by means of hydrolyzable thermo-sensitive tracers. *Geothermics*, 58:87–93, doi:10.1016/j.geothermics.2015.09.005.

Masselink, G., Kroon, A., and Davidson-Arnott, R. (2006). Morphodynamics of intertidal bars in wave-dominated coastal settings – A review. *Geomorphology*, 73(1-2):33–49, doi:10.1016/j.geomorph.2005.06.007.

Matheswaran, K., Blemmer, M., Rosbjerg, D., and Boegh, E. (2014). Seasonal variations in groundwater upwelling zones in a danish lowland stream analyzed using distributed temperature sensing (dts). *Hydrological Processes*, 28(3):1422–1435, doi:10.1002/hyp.9690.

McCallum, A. M., Andersen, M. S., Rau, G. C., and Acworth, R. I. (2012). A 1-D analytical method for estimating surface water-groundwater interactions and effective thermal diffusivity using temperature time series. *Water Resources Research*, 48(11):W11532, doi:10.1029/2012WR012007.

McCumber, M. C. and Pielke, R. A. (1981). Simulation of the effects of surface fluxes of heat and moisture in a mesoscale numerical model: 1. Soil layer. *Journal of Geophysical Research*, 86(C10):9929, doi:10.1029/JC086iC10p09929.

Menberg, K., Bayer, P., Zosseder, K., Rumohr, S., and Blum, P. (2013). Subsurface urban heat islands in German cities. *Science of the Total Environment*, 442:123–133, doi:10.1016/j.scitotenv.2012.10.043.

Michael, H. A., Mulligan, A. E., and Harvey, C. F. (2005). Seasonal oscillations in water exchange between aquifers and the coastal ocean. *Nature*, 436(7054):1145–1148, doi:10.1038/nature03935.

Moradkhani, H., Hsu, K.-L., Gupta, H. V., and Sorooshian, S. (2005). Uncertainty assessment of hydrologic model states and parameters: Sequential data assimilation using the particle filter. *Water Resources Research*, 41(5):17, doi:10.1029/2004WR003604.

Mori, Y., Hopmans, J. W., Mortensen, A. P., and Kluitenberg, G. J. (2003). Multi-Functional Heat Pulse Probe for the Simultaneous Measurement of Soil Water Content, Solute Concentration, and Heat Transport Parameters. *Vadose Zone Journal*, 2(4):561, doi:10.2136/vzj2003.0561.

Mori, Y., Hopmans, J. W., Mortensen, A. P., and Kluitenberg, G. J. (2005). Estimation of Vadose Zone Water Flux from Multi-Functional Heat Pulse Probe Measurements. *Soil Science Society of America Journal*, 69(3):599, doi:10.2136/sssaj2004.0174.

Mualem, Y. (1976). A new model for predicting the hydraulic conductivity of unsaturated porous media. *Water Resources Research*, 12(3), doi:10.1029/WR012i003p00513.

Nahlawi, H., Bouazza, A., and Kodikara, J. (2007). Characterisation of geotextiles water retention using a modified capillary pressure cell. *Geotextiles and Geomembranes*, 25(3):186–193, doi:10.1016/j.geotexmem.2006.12.001.

Naranjo, R. C. and Turcotte, R. (2015). A new temperature profiling probe for investigating groundwater-surface water interaction. *Water Resources Research*, 51(9):7790–7797, doi:10.1002/2015WR017574.

Nield, D. A. and Bejan, A. (2013). Chapter 2: Heat Transfer Through a Porous Medium. In *Convection in Porous Media*, pages 31–47. Springer, New York, NY.

Nimick, D. A., Gammons, C. H., and Parker, S. R. (2011). Diel biogeochemical processes and their effect on the aqueous chemistry of streams: A review. *Chemical Geology*, 283(1-2):3–17, doi:10.1016/j.chemgeo.2010.08.017.

Nimmo, J. R. (1990). Experimental testing of transient unsaturated flow theory at low water content in a centrifugal field. *Water Resources Research*, 26(9):1951–1960, doi:10.1029/WR026i009p01951.

Noborio, K. (2001). Measurement of soil water content and electrical conductivity by time domain reflectometry: A review. *Computers and Electronics in Agriculture*, 31:213–237.

Noborio, K., McInnes, K. J., and Heilman, J. L. (1996). Measurements of soil water content, heat capacity, and thermal conductivity. *Soil Science*, 161(1):22–28.

O'Carroll, D., Sleep, B. E., Krol, M., Boparai, H., and Kocur, C. (2013). Nanoscale zero valent iron and bimetallic particles for contaminated site remediation. *Advances in Water Resources*, 51:104–122, doi:10.1016/j.advwatres.2012.02.005.

Ochsner, T. E., Horton, R., and Ren, T. (2001). A New Perspective on Soil Thermal Properties. *Soil Science Society of America Journal*, 65(6):1641, doi:10.2136/sssaj2001.1641.

Onderka, M., Banzhaf, S., Scheytt, T., and Krein, A. (2013). Seepage velocities derived from thermal records using wavelet analysis. *Journal of Hydrology*, 479:64–74, doi:10.1016/j.jhydrol.2012.11.022.

Or, D., Smets, B. F., Wraith, J. M., Dechesne, A., and Friedman, S. P. (2007). Physical constraints affecting bacterial habitats and activity in unsaturated porous media - a review. *Advances in Water Resources*, 30(6-7):1505–1527, doi:10.1016/j.advwatres.2006.05.025.

Paniconi, C., Troch, P. A., van Loon, E. E., and Hilberts, A. G. J. (2003). Hillslope-storage Boussinesq model for subsurface flow and variable source areas along complex hillslopes: 2. Intercomparison with a three-dimensional Richards equation model. *Water Resources Research*, 39(11), doi:10.1029/2002WR001730.

Penner, E., Johnston, G. H., and Goodrich, L. E. (1975). Thermal Conductivity Laboratory Studies of Some Mackenzie Highway Soils. *Canadian Geotechnical Journal*, 12(3):271–288, doi:10.1139/t75-033.

Perreault, S., Chokmani, K., Nolin, M. C., and Bourgeois, G. (2013). Validation of a Soil Temperature and Moisture Model in Southern Quebec, Canada. *Soil Science Society of America Journal*, 77(2):606, doi:10.2136/sssaj2012.0311.

Perzlmaier, S., Auñeger, M., and Conrad, M. (2004). Distributed fiber optic temperature measurements in hydraulic engineering: Prospects of the heat-up method. In *Proceedings of the 72nd ICOLD Annual Meeting Workshop on Dam Safety Problems and Solutions-Sharing Experience, 16-22 May*, Seoul, Korea. Korean National Commitee on Large Dams.

Perzlmaier, S., Straer, K., Strobl, T., and Auñeger, M. (2006). Integral seepage monitoring on open channel embankment dams by the DFOT heat pulse method. In *Proceedings of the 74th Annual Meeting, International Commitee on Large Dams*, Barcelona, Spain.

Pollack, H. N. and Smerdon, J. E. (2004). Borehole climate reconstructions: Spatial structure and hemispheric averages. *Journal of Geophysical Research D: Atmospheres*, 109(11):1–9, doi:10.1029/2003JD004163.

Pryor, R. W. (2011). *Multiphysics Modeling Using COMSOL: A First Principles Approach*. Jones and Bartlett, Sudbury, MA.

Ramakrishna, A., Tam, H. M., Wani, S. P., and Long, T. D. (2006). Effect of mulch on soil temperature, moisture, weed infestation and yield of groundnut in northern Vietnam. *Field Crops Research*, 95:115–125, doi:10.1016/j.fcr.2005.01.030.

Rao, Y. and Huang, S. (2008). Applications of Fiber Optic Sensors. In Yin, S., Ruffin, P., and Yu, F., editors, *Fiber Optic Sensors*, chapter 10, pages 397–434. CRC Press, Boca Raton, FL, 2 edition.

Rau, G. C., Andersen, M. S., and Acworth, R. I. (2012a). Experimental investigation of the thermal dispersivity term and its significance in the heat transport equation for flow in sediments. *Water Resources Research*, 48(3):1–21, doi:10.1029/2011WR011038.

Rau, G. C., Andersen, M. S., and Acworth, R. I. (2012b). Experimental investigation of the thermal time-series method for surface water-groundwater interactions. *Water Resources Research*, 48(3):W03530, doi:10.1029/2011WR011560.

Rau, G. C., Andersen, M. S., McCallum, A. M., and Acworth, R. I. (2010). Analytical methods that use natural heat as a tracer to quantify surface water- groundwater exchange, evaluated using field temperature records. *Hydrogeology Journal*, 18:1093–1110, doi:10.1007/s10040-010-0586-0.

Rau, G. C., Andersen, M. S., McCallum, A. M., Roshan, H., and Acworth, R. I. (2014). Heat as a tracer to quantify water flow in near-surface sediments. *Earth-Science Reviews*, 129:40–58, doi:10.1016/j.earscirev.2013.10.015.

Rau, G. C., Cuthbert, M. O., McCallum, A. M., Halloran, L. J. S., and Andersen, M. S. (2015). Assessing the accuracy of 1-D analytical heat tracing for estimating near-surface sediment thermal diffusivity and water flux under transient conditions. *Journal of Geophysical Research: Earth Surface*, 120(8):1551–1573, doi:10.1002/2015JF003466.

Raymond, J., Therrien, R., Gosselin, L., and Lefebvre, R. (2011). Numerical analysis of thermal response tests with a groundwater flow and heat transfer model. *Renewable Energy*, 36(1):315–324, doi:10.1016/j.renene.2010.06.044.

Read, T., Bour, O., Bense, V., Le Borgne, T., Goderniaux, P., Klepikova, M. V., Hochreutener, R., Lavenant, N., and Boschero, V. (2013). Characterizing groundwater flow and heat transport in fractured rock using fiber-optic distributed temperature sensing. *Geophysical Research Letters*, 40:2055–2059, doi:10.1002/grl.50397.

Reiter, M. (2001). Using precision temperature logs to estimate horizontal and vertical groundwater flow components. *Water Resources Research*, 37(3):663–674, doi:10.1029/2000WR900302.

Reiter, M. (2004). Continuous Temperature Logging in Air across the Deep Vadose Zone. *Vadose Zone Journal*, 3:982–989, doi:10.2113/3.3.982.

Reiter, M., Costain, J. K., and Minier, J. (1989). Heat flow data and vertical groundwater movement, examples from southwestern Virginia. *Journal of Geophysical Research*, 94(B9):12423, doi:10.1029/JB094iB09p12423.

Ren, T., Kluitenberg, G. J., and Horton, R. (2000). Determining Soil Water Flux and Pore Water Velocity by a Heat Pulse Technique. *Soil Science Society of America Journal*, 64(2):552–560, doi:10.2136/sssaj2000.642552x.

Richards, L. (1931). Capillary Conduction of Liquids Through Porous Mediums. *Journal of Applied Physics*, 1:318, doi:10.1063/1.1745010.

Robinson, C., Gibbes, B., and Li, L. (2006). Driving mechanisms for groundwater flow and salt transport in a subterranean estuary. *Geophysical Research Letters*, 33(3):L03402, doi:10.1029/2005GL025247.

Robinson, D. A., Campbell, C. S., Hopmans, J. W., Hornbuckle, B. K., Jones, S. B., Knight, R., Ogden, F., Selker, J. S., and Wendroth, O. (2008). Soil Moisture Measurement for Ecological and Hydrological Watershed-Scale Observatories: A Review. *Vadose Zone Journal*, 7(1):358, doi:10.2136/vzj2007.0143.

Robinson, D. A., Jones, S. B., Wraith, J. M., Or, D., and Friedman, S. P. (2003). A Review of Advances in Dielectric and Electrical Conductivity Measurement in Soils Using Time Domain Reflectometry. *Vadose Zone Journal*, 2(1996):444–475, doi:10.2136/vzj2003.4440.

Robinson, D. A., Lebron, I., Kocar, B., Phan, K., Sampson, M., Crook, N., and Fendorf, S. (2009). Time-lapse geophysical imaging of soil moisture dynamics in tropical deltaic soils: An aid to interpreting hydrological and geochemical processes. *Water Resources Research*, 45(4), doi:10.1029/2008WR006984.

Ronan, A., Prudic, D. E., Thodal, C. E., and Constantz, J. (1998). Field study and simulation of diurnal temperature effects on infiltration and variably saturated flow beneath an ephemeral stream. *Water Resources Research*, 34(9):2137–2153, doi:10.1029/98WR01572.

Roshan, H., Rau, G. C., Andersen, M. S., and Acworth, R. I. (2012). Use of heat as tracer to quantify vertical streambed flow in a two-dimensional flow field. *Water Resources Research*, 48(10):1–16, doi:10.1029/2012WR011918.

Roshan, H., Young, M., Andersen, M. S., and Acworth, R. I. (2014). Limitations of fibre optic distributed temperature sensing for quantifying surface water groundwater interactions. *Hydrology and Earth System Sciences Discussions*, 11(7):8167–8190, doi:10.5194/hessd-11-8167-2014.

Rosolem, R., Shuttleworth, W. J., Zreda, M., Franz, T. E., Zeng, X., and Kurc, S. A. (2013). The Effect of Atmospheric Water Vapor on Neutron Count in the Cosmic-Ray Soil Moisture Observing System. *Journal of Hydrometeorology*, 14(5):1659–1671, doi:10.1175/JHM-D-12-0120.1.

Rousseau, M., Di Pietro, L., Angulo-Jaramillo, R., Tessier, D., and Cabibel, B. (2004). Preferential Transport of Soil Colloidal Particles: Physicochemical Effects on Particle Mobilization. *Vadose Zone Journal*, 3(1):247–261, doi:10.2136/vzj2004.2470.

Russell, T. L., Yamahara, K. M., and Boehm, A. B. (2012). Mobilization and transport of naturally occurring enterococci in beach sands subject to transient infiltration of seawater. *Environmental Science and Technology*, 46(11):5988–5996, doi:10.1021/es300408z.

Saar, M. O. (2011). Review: Geothermal heat as a tracer of large-scale groundwater flow and as a means to determine permeability fields. *Hydrogeology Journal*, 19(1):31–52, doi:10.1007/s10040-010-0657-2.

Sadat-Noori, M., Santos, I. R., Sanders, C. J., Sanders, L. M., and Maher, D. T. (2015). Groundwater Discharge into an Estuary Using Spatially Distributed Radon Time Series and Radium Isotopes. *Journal of Hydrology*, 528:703–719, doi:10.1016/j.jhydrol.2015.06.056.

Saito, H., Simunek, J., and Mohanty, B. (2006). Numerical Analysis of Coupled Water, Vapor, and Heat Transport in the Vadose Zone. *Vadose Zone Journal*, 5:784–800, doi:10.2136/vzj2006.0007.

Sanders, C. J., Santos, I. R., Maher, D. T., Sadat-Noori, M., Schnetger, B., and Brumsack, H. (2015). Dissolved iron exports from an estuary surrounded by coastal wetlands: Can small estuaries be a significant source of Fe to the ocean? *Marine Chemistry*, 176:75–82, doi:10.1016/j.marchem.2015.07.009.

Sass, J., Lachenbruch, A., Dudley, W., Priest, S., and Monroe, R. (1988). Temperature, thermal conductivity, and heat flow near Yucca Mountain, Nevada: Some tectonic and hydrologic implications (USGS Open-file Report 87-649). Technical report, USGS, Denver, CO.

Sayde, C., Buelga, J. B., Rodríguez Sinobas, L., El Khoury, L., English, M., van de Giesen, N., and Selker, J. S. (2014). Mapping variability of soil water content and flux across 1-1000 m scales using the Actively Heated Fiber Optic method. *Water Resources Research*, 50(9):7302–7317, doi:10.1002/2013WR014983.

Sayde, C., Gregory, C., Gil-Rodriguez, M., Tufillaro, N., Tyler, S. W., van de Giesen, N., English, M., Cuenca, R., and Selker, J. S. (2010). Feasibility of soil moisture monitoring with heated fiber optics. *Water Resources Research*, 46(6):1–8, doi:10.1029/2009WR007846.

Schaap, M. G. (2002). Rosetta v1.2: A computer program for estimating soil hydraulic parameters with hierarchical pedotransfer functions. Technical report, University of Arizona.

Schaap, M. G., Leij, F., and van Genuchten, M. T. (2001). Rosetta: a Computer Program for Estimating Soil Hydraulic Parameters With Hierarchical Pedotransfer Functions. *Journal of Hydrology*, 251(3-4):163–176, doi:10.1016/S0022-1694(01)00466-8.

Schaap, M. G. and van Genuchten, M. T. (2006). A Modified Mualem-van Genuchten Formulation for Improved Description of the Hydraulic Conductivity Near Saturation. *Vadose Zone Journal*, 5(1):27, doi:10.2136/vzj2005.0005.

Schmidt, C., Conant, B., Bayer-Raich, M., and Schirmer, M. (2007). Evaluation and field-scale application of an analytical method to quantify groundwater discharge using mapped streambed temperatures. *Journal of Hydrology*, 347(3-4):292–307, doi:10.1016/j.jhydrol.2007.08.022.

Schofield, R. K. (1935). The pF of the water in soil. In *Transactions of 3rd International Congress of Soil Science, Volume 2*.

Schornberg, C., Schmidt, C., Kalbus, E., and Fleckenstein, J. H. (2010). Simulating the effects of geologic heterogeneity and transient boundary conditions on streambed temperatures - Implications for temperature-based water flux calculations. *Advances in Water Resources*, 33(11):1309–1319, doi:10.1016/j.advwatres.2010.04.007.

Schrefler, B. (2002). Mechanics and thermodynamics of saturated/unsaturated porous materials and quantitative solutions. *Applied Mechanics Reviews*, 55(4):351, doi:10.1115/1.1484107.

Sebok, E., Duque, C., Kazmierczak, J., Engesgaard, P., Nilsson, B., Karan, S., and Frandsen, M. (2013). High-resolution distributed temperature sensing to detect seasonal groundwater discharge into Lake Vaeng, Denmark. *Water Resources Research*, 49(9):5355–5368, doi:10.1002/wrcr.20436.

Selker, J. S., Thévenaz, L., Huwald, H., Mallet, A., Luxemburg, W. M. J. ., van de Giesen, N., Stejskal, M., Zeman, J., Westhoff, M. C., and Parlange, M. B. (2006a). Distributed fiber-optic temperature sensing for hydrologic systems. *Water Resources Research*, 42(12):1–8, doi:10.1029/2006WR005326.

Selker, J. S., van de Giesen, N., Westhoff, M. C., Luxemburg, W. M. J. ., and Parlange, M. B. (2006b). Fiber optics opens window on stream dynamics. *Geophysical Research Letters*, 33(24):L24401, doi:10.1029/2006GL027979.

Shan, C. and Bodvarsson, G. (2004). An analytical solution for estimating percolation rate by fitting temperature profiles in the vadose zone. *Journal of Contaminant Hydrology*, 68(1-2):83–95, doi:10.1016/S0169-7722(03)00126-8.

Shija, N. and MacQuarrie, K. T. B. (2014). Numerical Simulation of Active Heat Injection and Anomalous Seepage near an Earth Dam-Concrete Interface. *International Journal of Geomechanics*, 15(5):1–11, doi:10.1061/(ASCE)GM.1943-5622.0000432.

Shiozawa, S. and Campbell, G. S. (1990). Soil thermal conductivity. *Remote Sensing Reviews*, 5(1):301–310, doi:10.1080/02757259009532137.

Shouse, P., Russell, W., Burden, D., Selim, H., Sisson, J., and van Genuchten, M. T. (1995). Spatial variability of soil water retention functions in a silt loam soil. *Soil Science*, 159(1):1–11.

Simpson, M. J. and Clement, T. P. (2003). Comparison of finite difference and finite element solutions to the variably saturated flow equation. *Journal of Hydrology*, 270:49–64, doi:10.1016/S0022-1694(02)00294-9.

Šimunek, J. and Bradford, S. a. (2008). Vadose Zone Modeling: Introduction and Importance. *Vadose Zone Journal*, 7(2):581, doi:10.2136/vzj2008.0012.

Šimunek, J. and Nimmo, J. R. (2005). Estimating soil hydraulic parameters from transient flow experiments in a centrifuge using parameter optimization technique. *Water Resources Research*, 41(4), doi:10.1029/2004WR003379.

Šimunek, J. and van Genuchten, M. T. (2008). Modeling Nonequilibrium Flow and Transport Processes Using HYDRUS. *Vadose Zone Journal*, 7(2):782, doi:10.2136/vzj2007.0074.

Sleep, B. E., Sehayek, L., and Chien, C. C. (2000). Modeling wells in variably saturated soil with wellbore fluid gravity segregation. *Advances in Water Resources*, 23(7):689–697, doi:10.1016/S0309-1708(00)00005-1.

Smits, K. M., Sakaki, T., Limsuwat, A., and Illangasekare, T. H. (2010). Thermal Conductivity of Sands under Varying Moisture and Porosity in Drainage-Wetting Cycles. *Vadose Zone Journal*, 9(1):172, doi:10.2136/vzj2009.0095.

Soto, M. A., Ramírez, J. A., and Thévenaz, L. (2016). Intensifying the response of distributed optical fibre sensors using 2D and 3D image restoration. *Nature Communications*, 7:10870, doi:10.1038/ncomms10870.

Splinter, K. D., Carley, J. T., Golshani, A., and Tomlinson, R. (2014). A relationship to describe the cumulative impact of storm clusters on beach erosion. *Coastal Engineering*, 83:49–55, doi:10.1016/j.coastaleng.2013.10.001.

Stafford, J. V. (1988). Remote, Non-contact of Soil Moisture and in-situ Measurement Content: a Review. *Journal of Agricultural Engineering Research*, 41:151–172, doi:10.1016/0021-8634(88)90175-8.

Stallman, R. (1965). Steady one-dimensional fluid flow in a semi-infinite porous medium with sinusoidal surface temperature. *Journal of Geophysical Research*, 70(12):2821–2827.

Steele-Dunne, S. C., Rutten, M. M., Krzeminska, D. M., Hausner, M. B., Tyler, S. W., Selker, J. S., Bogaard, T. A., and van de Giesen, N. (2010). Feasibility of soil moisture estimation using passive distributed temperature sensing. *Water Resources Research*, 46(3):1–12, doi:10.1029/2009WR008272.

Stephansson, O., Hudson, J. A., and Jing, L. (2004). *Coupled Thermo-Hydro-Mechanical-Chemical Processes in Geo-Systems Fundamentals , Modelling , Experiments and Applications*. Elsevier, Amsterdam.

Stephens, D. (1995). *Vadose zone hydrology*. CRC Press.

Stewart, R. D., Rupp, D. E., Najm, M. R. A., and Selker, J. S. (2013). Modeling effect of initial soil moisture on sorptivity and infiltration. *Water Resources Research*, 49(10):7037–7047, doi:10.1002/wrcr.20508.

Striegl, A. M. and Loheide II, S. P. (2012). Heated Distributed Temperature Sensing for Field Scale Soil Moisture Monitoring. *Ground Water*, 50(3):340–347, doi:10.1111/j.1745-6584.2012.00928.x.

Su, Z., Wen, J., Dente, L., Van Der Velde, R., Wang, L., Ma, Y., Yang, K., and Hu, Z. (2011). The tibetan plateau observatory of plateau scale soil moisture and soil temperature (Tibet-Obs) for quantifying uncertainties in coarse resolution satellite and model products. *Hydrology and Earth System Sciences*, 15(7):2303–2316, doi:10.5194/hess-15-2303-2011.

Suárez, F., Aravena, J. E., Hausner, M. B., Childress, A. E., and Tyler, S. W. (2011). Assessment of a vertical high-resolution distributed-temperature-sensing system in a shallow thermohaline environment. *Hydrology and Earth System Sciences*, 15(3):1081–1093, doi:10.5194/hess-15-1081-2011.

Sudicky, E. A. (1986). A natural gradient experiment on solute transport in a sand aquifer: Spatial variability of hydraulic conductivity and its role in the dispersion process. *Water Resources Research*, 22(13):2069–2082, doi:10.1029/WR022i013p02069.

Suzuki, S. (1960). Percolation measurements based on heat flow through soil with special reference to paddy fields. *Journal of Geophysical Research*, 65(9):463–466, doi:10.1029/JZ065i009p02883.

Tabbagh, A., Bendjoudi, H., and Benderitter, Y. (1999). Determination of recharge in unsaturated soils using temperature monitoring. *Water Resources Research*, 35(8):2439–2446, doi:10.1029/1999WR900134.

Tarnawski, V. and Leong, W. (2000). Thermal conductivity of soils at very low moisture content and moderate temperatures. *Transport in Porous Media*, 41:137–147, doi:10.1023/A:1006738727206.

Thakur, G., Brevdo, E., Fučkar, N. S., and Wu, H. T. (2013). The Synchrosqueezing algorithm for time-varying spectral analysis: Robustness properties and new paleoclimate applications. *Signal Processing*, 93(5):1079–1094, doi:10.1016/j.sigpro.2012.11.029.

Therrien, R., McLaren, R. G., Sudicky, E. A., and Panday, S. M. (2010). HydroGeoSphere: A three-dimensional numerical model describing fully-integrated subsurface and surface flow and solute transport. Technical report, Groundwater Simulations Group, University of Waterloo, Waterloo, ON.

Tindall, J., Kunkel, J., and Anderson, D. (1999). *Unsaturated zone hydrology for scientists and engineers*. Prentice-Hall, New Jersey.

Tocci, M. D., Kelley, C., and Miller, C. T. (1997). Accurate and economical solution of the pressure-head form of Richards' equation by the method of lines. *Advances in Water Resources*, 20(1):1–14, doi:10.1016/S0309-1708(96)00008-5.

Trefry, M. G. and Muffels, C. (2007). FEFLOW: A Finite-Element Ground Water Flow and Transport Modeling Tool. *Ground Water*, 45(5):525–528, doi:10.1111/j.1745-6584.2007.00358.x.

Turner, I. L. and Acworth, R. I. (2004). Field Measurements of Beachface Salinity Structure using Cross-Borehole Resistivity Imaging. *Journal of Coastal Research*, 203:753–760, doi:10.2112/1551-5036(2004)20[753:FMOBSS]2.0.CO;2.

Tyler, S. W., Selker, J. S., Hausner, M. B., Hatch, C. E., Torgersen, T., Thodal, C. E., and Schladow, S. G. (2009). Environmental temperature sensing using Raman spectra DTS fiber-optic methods. *Water Resources Research*, 45:W00D23, doi:10.1029/2008WR007052.

Valiela, I., Collins, G., Kremer, J., Lajtha, K., Geist, M., Seely, M., Brawley, J., and Sham, C. H. (1997). Nitrogen Loading from Coastal Watersheds to Receiving Estuaries: New Method and Application. *Ecological Applications*, 7(2):358–380, doi:10.1890/1051-0761(1997)007[0358:NLFCWT]2.0.CO;2.

van de Giesen, N., Steele-Dunne, S. C., Jansen, J., Hoes, O., Hausner, M. B., Tyler, S. W., and Selker, J. S. (2012). Double-ended calibration of fiber-optic Raman spectra distributed temperature sensing data. *Sensors*, 12(5):5471–85, doi:10.3390/s120505471.

van de Griend, A., Camillo, P., and Gurney, R. (1985). Discrimination of Soil Physical Parameters, Thermal Inertia, and Soil Moisture from Diurnal Surface Temperature Fluctuations. *Water Resources Research*, 21(7):997–1009, doi:10.1029/WR021i007p00997.

van Genuchten, M. T. (1980). A closed-form equation for predicting the hydraulic conductivity of unsaturated soils. *Soil Science Society of America Journal*, 44:892–898, doi:10.2136/sssaj1980.03615995004400050002x.

Vandersteen, G., Schneidewind, U., Anibas, C., Schmidt, C., Seuntjens, P., and Batelaan, O. (2015). Determining groundwater-surface water exchange from temperature-time series: Combining a local polynomial method with a maximum likelihood estimator. *Water Resources Research*, 51(2):922–939, doi:10.1002/2014WR015994.

Vereecken, H., Huisman, J. A., Bogena, H., Vanderborght, J., Vrugt, J. A., and Hopmans, J. W. (2008). On the value of soil moisture measurements in vadose zone hydrology: A review. *Water Resources Research*, 46(4):1–21, doi:10.1029/2008WR006829.

Vereecken, H., Weynants, M., Javaux, M., Pachepsky, Y., Schaap, M. G., and van Genuchten, M. T. (2010). Using Pedotransfer Functions to Estimate the van Genuchten-Mualem Soil Hydraulic Properties: A Review. *Vadose Zone Journal*, 9(4):795, doi:10.2136/vzj2010.0045.

Verhoef, A., van den Hurk, B. J., Jacobs, A. F., and Heusinkveld, B. G. (1996). Thermal soil properties for vineyard (EFEDA-I) and savanna (HAPEX-Sahel) sites. *Agricultural and Forest Meteorology*, 78(1-2):1–18, doi:10.1016/0168-1923(95)02254-6.

Vo, T. D., He, J., Magi, E., Collins, M. J., Clark, A. S., Ferguson, B. G., Xiong, C., and Eggleton, B. J. (2014). Chalcogenide fiber-based distributed temperature sensor with sub-centimeter spatial resolution and enhanced accuracy. *Optics express*, 22(2):1560–8, doi:10.1364/OE.22.001560.

Vogt, T., Schirmer, M., and Cirpka, O. A. (2012). Investigating riparian groundwater flow close to a losing river using diurnal temperature oscillations at high vertical resolution. *Hydrology and Earth System Sciences*, 16(2):473–487, doi:10.5194/hess-16-473-2012.

Vogt, T., Schneider, P., Hahn-Woernle, L., and Cirpka, O. A. (2010). Estimation of seepage rates in a losing stream by means of fiber-optic high-resolution vertical temperature profiling. *Journal of Hydrology*, 380(1-2):154–164, doi:10.1016/j.jhydrol.2009.10.033.

Wagner, V., Li, T., Bayer, P., Leven, C., Dietrich, P., and Blum, P. (2014). Thermal tracer testing in a sedimentary aquifer: field experiment (Lauswiesen, Germany) and numerical simulation. *Hydrogeology Journal*, 22(1):175–187, doi:10.1007/s10040-013-1059-z.

Wang, X. and Benson, C. (2004). Leak-Free Pressure Plate Extractor For Measuring the Soil Water Characteristic Curve. *Geotechnical Testing Journal*, 27(2):11392, doi:10.1520/GTJ11392.

Ward, A. S., Gooseff, M. N., and Singha, K. (2010). Imaging hyporheic zone solute transport using electrical resistivity. *Hydrological Processes*, 24(7):948–953, doi:10.1002/hyp.7672.

Wechsler, A. E. (1992). The Probe Method for Measurement of Thermal Conductivity. In Maglić, K. D., Cezairliyan, A., and Peletsky, V. E., editors, *Compendium of Thermophysical Property Measurement Methods: Vol. 2*, pages 161–185. Springer, New York.

Weiss, J. D. (2003). Using Fiber Optics to Detect Moisture Intrusion into a Landfill Cap Consisting of a Vegetative Soil Barrier. *Journal of the Air & Waste Management Association*, 53(9):1130–1148, doi:10.1080/10473289.2003.10466268.

Western, A. W., Grayson, R. B., and Blöschl, G. (2002). Scaling of Soil Moisture: A Hydrologic Perspective. *Annual Review of Earth and Planetary Sciences*, 30(1):149–180, doi:10.1146/annurev.earth.30.091201.140434.

Wissmeier, L. and Barry, D. (2010). Simulation Tool for Variably Saturated Flow Two- and Three- Dimensional Domains. *Environmental Modelling & Software*, 25(August):526–538, doi:10.1016/j.envsoft.2009.10.001.

Woodside, W. and Messmer, J. H. (1961). Thermal Conductivity of Porous Media. I. Unconsolidated Sands. *Journal of Applied Physics*, 32(9):1688, doi:10.1063/1.1728419.

Wörman, A., Riml, J., Schmadel, N., Neilson, B. T., Bottacin-Busolin, A., and Heavilin, J. E. (2012). Spectral scaling of heat fluxes in streambed sediments. *Geophysical Research Letters*, 39(23):2–7, doi:10.1029/2012GL053922.

Zeeman, M. J., Selker, J. S., and Thomas, C. K. (2015). Near-Surface Motion in the Nocturnal, Stable Boundary Layer Observed with Fibre-Optic Distributed Temperature Sensing. *Boundary-Layer Meteorology*, 154(2):189–205, doi:10.1007/s10546-014-9972-9.

Zreda, M., Desilets, D., Ferré, T. P. A., and Scott, R. L. (2008). Measuring soil moisture content non-invasively at intermediate spatial scale using cosmic-ray neutrons. *Geophysical Research Letters*, 35(21), doi:10.1029/2008GL035655.

Zreda, M., Shuttleworth, W. J., Zeng, X., Zweck, C., Desilets, D., Franz, T. E., and Rosolem, R. (2012). COSMOS: The cosmic-ray soil moisture observing system. *Hydrology and Earth System Sciences*, 16(11):4079–4099, doi:10.5194/hess-16-4079-2012.